ISTANBUL TECHNICAL UNIVERSITY ★ GRADUATE SCHOOL

FABRICATION AND CHARACTERIZATION OF NOVEL MEMBRANES FOR BATTERY SEPARATOR APPLICATIONS

M.Sc. THESIS

Ubey AHMETOGLU

Department of Nanoscience and Nanoengineering

Nanoscience and Nanoengineering Programme

MAY 2023

ISTANBUL TECHNICAL UNIVERSITY ★ GRADUATE SCHOOL

FABRICATION AND CHARACTERIZATION OF NOVEL MEMBRANES FOR BATTERY SEPARATOR APPLICATIONS

M.Sc. THESIS

Ubey AHMETOGLU
(513201024)

Department of Nanoscience and Nanoengineering

Nanoscience and Nanoengineering Programme

Thesis Advisor: Assoc. Prof. Dr. Ali KILIC

MAY 2023

ISTANBUL TEKNİK ÜNİVERSİTESİ ★ LİSANSÜSTÜ EĞİTİM ENSTİTÜSÜ

PİL SEPERATÖR UYGULAMALARI İÇİN YENİLİKÇİ MEMBRAN YAPILARIN ÜRETİMİ VE KARAKTERİZASYONU

YÜKSEK LİSANS TEZİ

Ubey AHMETOGLU
(513201024)

Nanobilim ve Nanomühendisliği Anabilim Dalı

Nanobilim ve Nanomühendisliği Programı

Tez Danışmanı: Doç. Dr. Ali KILIÇ

MAYIS 2023

Ubey Ahmetoğlu, a M.Sc. student of İTU Graduate School student ID 513201024, successfully defended the thesis entitled "FABRICATION AND CHARACTERIZATION OF NOVEL MEMBRANES FOR BATTERY SEPARATOR APPLICATIONS", which he prepared after fulfilling the requirements specified in the associated legislations, before the jury whose signatures are below.

Thesis Advisor :	**Assoc. Prof. Dr. Ali KILIC** Istanbul Technical University	.....
Jury Members :	**Prof. Ali Demir** Istanbul Technical University	.....
	Asst. Prof. Dr. Mehmet Durmuş Çalışır Recep Tayyip Erdoğan University	.....

Date of Submission : 03.05.2023
Date of Defense : 26/05/2023

To my precious family,

FOREWORD

This work is dedicated to those who fall, yet they stand, those who succeed after they fail and to those who do whatever it takes to push themselves forward. To the reader of this work hoping that it would guide him to new horizons in his field. To my thesis supervisor, Assoc. Prof. Dr. Ali Kılıç, whom without his guidance and patience, this work won't be done.

To my lab peer, and experiment friend, Melike Güngör, our future doctor who was with me through thick and thin of this work and helped me the most when needed. To my lab, TEMAG lab, and its priceless brigade. To all the nameless heroes that assisted the writing and conducting of this work. Writing words of gratitude to all of you is the least I can do. The limitless uncoditional support of my precious family was alway the first and final motivation for me in completing this work.

This work was supported by the Scientific Research Projects Coordination Unit (BAP) grants with the project ID: 43163. I also acknowledge the help of my dear friend Muhammed Yusufoglu for facilitiating elechtrochemical analysis experiments at Koc university. The support and contribution of Istanbul Technical University TEMAG Laboratory and AREKA Technology Ltd. Comp. (www.arekananofiber.com) are infinitely appreciated.

April 2023

Ubey AHMETOGLU
(Chemical Engineer)

TABLE OF CONTENTS

Page

ABBREVIATIONS

LiBs : Lithium ion batteries
NaBs : Sodium ion batteries
TIPS : Thermally Induced Phase Separation
MD : Machine Direction
TD : Transverse Direction
PE : Polyethylene
PP : Polypropylene
Na-ion : Sodium ion
Li-ion : Lithium ion
UHMWPE : Ultra High Molecular Weight Polyethylene
CA, CA-alg : Calcium Alginate
NA, Na-alg : Sodium alginate
TPU : Thermoplastic Polyurethane
LOI : Limiting Oxygen Index
UF : Ultra FIltration
MF : Micro Filtration
NF : Nano Filtration
RO : Reverse Osmosis
BFD : Block Flow Diagram
SSE : Single Screw Extruder
TSE : Twin Screw Extruder
PVC : Polyvinyl Chloride
S-L : Solid-liquid
L-L : Liquid-liquid
SLE : Solide Liquid Equilibrium
DOP : Dioctyl Phthalate
PMP : Polymethylpentene
DSC : Differential Scanning Calorimetry
EIS : Electrochemical Impedance Spectroscopy
SEM : Scanning Electron Microscopy
SEI : Solid Electrolyte Interface
PCL : Polycaprolactone
MTZ : Metronidazole
CIP : Ciprofloxacin
CNF : Carbon Nanofiber
GPE : Gel Polymer Electrolyte
EC : Ethylene Carbonate
DEC : Diethyl Carbonate
PC : Propylene Carbonate
$NaClO_4$: Sodium Perchlorate
DMF : Dimethylformamide

SYMBOLS

T	**:** Temperature
T_m	**:** Melting temperature
P	**:** Pressure
R	**:** Ideal gas constant
R_b	**:** Bulk resistance
R_{ct}	**:** Charge transfer resistance
Q	**:** Constant phase element
C	**:** Capacitance
i	**:** species
I_i, I_{tot}	**:** Total and fraction current
t_+	**:** transference number
ΔG, ΔG_{mix}	**:** Gibbs free energy
ΔH_{mix}, ΔH_u	**:** Enthalpy
ΔS_{mix}	**:** Entropy
$\emptyset_d$	**:** Polymer fraction
χ	**:** Flory-Hoggins interaction parameter
Z'	: Real resistance
Z''	**:** Imaginary resistance

LIST OF TABLES

Page

LIST OF FIGURES

Page

FABRICATION AND CHARACTERIZATION OF NOVEL MEMBRANES FOR BATTERY SEPARATOR APPLICATIONS

With the prospering industry of electrical mobility, the need for high performance batteries and energy sources is on the rise. The demand on efficient and safe batteries has exponentially increased. In general, batteries consist of three main critical components; anode, cathode and a separator. While anode and cathode are the active parts in charge and power generation, battery separators are the non-active insulative part. They are a porous structure that allows the passage of ions back and forth while they are made of inherently electrically insulative materials that prohibits the contact of the two poles preventing any short circuit possibility. Battery separators can be made of several materials and substances and carries several key properties. They can be made of any porous insulative material with defined pore size and porosity for their intended application. Along their porous structure, they should carry high chemical stability, strong integrity, and stability under elevating temperatures. Since there are various reactions occuring inside a battery which may lead to increase in the cell temperature, several approaches are used to fabricate battery separators with high thermal stability and flame retardancy. Among these approaches, coating the separator with inherently flame-retardant materials is a common method. Sodium alginate, as a natural polysaccharide, that shows significant flame retardancy performance when crosslinked with calcium. Cross-linked calcium alginate is reported to exhibit a limiting oxygen index (LOI) of 34.

Several polymers are used to fabricate the battery separator. Ultra-high molecular weight polyethylene (UHMWPE) is widely used in battery separator applications due to its high mechanical strength and chemical stability. Film casting is a process widely used to fabricate battery separators. In the wet process film casting, UHMWPE is melt-mixed with a low molecular weight diluent (also called porogen) and casted through a film die before its conveyed into stretching and extraction steps to obtain final porous membrane. Another type of common separators is the nanofiber based. They can be fabricated via several methods including centrifugal spinning, where a rotor is ejecting the polymeric solution into fibers while rotating at very high speeds. The aim of this thesis is to fabricate lithium and sodium ion battery separators with different fabrication methods and enhance their thermal performance by coating them with calcium alginate. Film casting and centrifugal spinning processes were used to obtain two different membrane structures from two different polymers.

In film casting process, UHMWPE was mixed with paraffin oil (PO) then melt extruded through a twin-screw extruder (TSE). 30% UHMWPE, 70% PO and 1% antioxidant mixture was prepared. The temperature of the 6 heating zones and die was held at 130, 140, 150, 160, 170, 180, and 180℃ respectively. The screw rotating speed was held constant at 35rpm. Melt blend was casted through a stripe die with a thickness of 3 mm. The obtained sheets were hot pressed at 180℃ and 8 tons of load for 8 minutes then cooled down to room temperature. Final film thickness obtained was in the range of 200-400μm. Optimization experiments were conducted on the samples to study the effect of different stretching ratios, the importance of extraction step order, the effect of the constrained and non constrained uniaxial stretching, and

the effect of heating distance between the sample and the stretching machine. It was found that the extraction of the oil after stretching led to a smaller and more uniform pore sizes in comparison to bigger pores formed when the oil was extracted before stretching. Heating of the samples in the stretching machine was done with open system using thermal irratiators. Distances of 13.5, 16.5, and 19.5cm were studied. Heaters caused the film to melt fastly and close the pores formed at close distances while at 19.5cm the heating wasn't enough to initiate any pores. The films are then stretched with a custom-made uniaxial stretching machine, where pore formation is initiated. Two stretching ratios were applied; 2×1.5 and 4×1.5. Higher stretching ratios showed closure of pores. The optimum parameters were found to be 1.5×2 constrained stretching ratio with 16.5 cm heating distance and 110℃ heating temperature. After that three Samples (S1, S2, and S3) were fabricated and hot pressed into three thicknesses of 280, 200, and 280μm. These samples are then stretched and annealed to obtain samples of three final thicknesses of 40, 60, and 80μm. Finally, these samples are immersed in n-hexane to extract the oil and obtain the desired porous structure and the final membrane. These membranes are then put in a coin cell configuration and tested for sodium ion (Na-ion) battery separator performance. The ionic conductivities of S1, S2, and S3 samples are 0.09, 0.48, and 0.04mS/cm^2 respectively. S2 sample showed better performance in comparison to other samples due to its higher porosity and uniform pore distribution.

Nanofibrous membrane on the other hand was fabricated from thermoplastic polyurethane (TPU) by centrifugal spinning process. TPU was dissolved in dimethylformamide (DMF)/acetone mixture and spun into nanofibers. Optimization of the process was done by altering the polymer concentration, solvent ratios, needle diameter (gauge), and rotating speeds. The optimum nanofibers were obtained at 10% TPU dissolved in 2:1 DMF/acetone ratio with 30G needle diameter and 13,000 rpm rotating speed. Obtained nanofibers were treated with sodium alginate which was then crosslinked with calcium chloride ($CaCl_2$). After Calcium Alginate (Ca-alg, CA) treatment, the samples were hot pressed at 120℃ and 8 tonnes of load for 2 minutes. Treatment with CA enhance the thermal performance of the separators. The obtained coated nanofibrous membranes are then put into coin cell configuration with 1M $LiPF_6$ and 1M $NaClO_4$ electrolytes and its performance were measured. These membranes were tested for sodium ion (Na-ion) and lithium ion (Li-ion) batteries. The nanofibrous membranes exhibited significant better performance when compared to the commercial Celgard 2500 polypropylene (PP) separator. The ionic conductivities of the neat TPU, pressed TPU, 0.5 TPU, and 2 TPU were 0.23, 0.67, 0.17, 0.16, and 0.05 mS/cm^2 respectively. The coated samples exhibited significantly larger ionic conductivity numbers and less resistance values in comparison to the commercial PP separator. In full cell configuration, where anode and cathode are used, the samples exhibited the same trend with neat TPU performing better than other samples. The ionic conductivities of the full cell samples were 1.53, 0.19, 0.05, and 0.03 mS/cm^2 respectively. The drop in the ionic conductivities of the samples can be referred to the effect of coating of the samples which lead to pore closure. This led to the domination of the diffusion phenomena in the samples which was demonstrated by the straight line in the Nyquist plot. In terms of thermal performance, significant enhancement was achieved. On the other hand, when these samples were examined for Li-ion separator tests, the ionic conductivities of Neat TPU, 0.5 TPU, 2 TPU, and PP separators were 0.10, 0.21, 0.09, and 0.07mS/cm^2 respectively. The 0.5 TPU sample showed the best performance and proved that calcium alginate can enhance the chemical performance of the separator. The coated samples showed 0% shrinkage in comparison to 63% and

100% shrinkage of the neat TPU and commercial samples. The samples also showed a significant fire retardation when exposed to flame source. A comparison between the condition of the samples after 1 and 10 seconds was recorded. Neat and pressed samples melted directly within the first seconds, while the treated 0.5 TPU and 2 TPU samples kept their integrity. 0.5 TPU sample showed marks of burning and its color started turning into brownish while the 2 TPU sample kept its initial state even after 10 seconds. The obtained results showed the high potential calcium alginate carries in battery applications. Studies to enhance the ionic conductivities of the calcium alginate can be conducted and better integrating methods can be proposed.

PİL SEPERATÖR UYGULAMALARI İÇİN YENİLİKÇİ MEMBRAN YAPILARIN ÜRETİMİ VE KARAKTERİZASYONUÖZET

Gelişen elektrikli mobilite endüstrisi ile birlikte, yüksek performanslı pillere ve enerji kaynaklarına olan ihtiyaçla birlikte verimli ve güvenli pillere olan talep her geçen gün katlanarak artmaktadır. Genel olarak piller üç ana kritik bileşenden oluşur; anot, katot ve ayırıcı (separatör). Anot ve katot şarj ve güç üretiminde aktif kısım iken, pil separatörleri aktif olmayan yalıtkan kısımdır. İyonların ileri geri geçişine izin veren gözenekli bir yapıda olan seperatör, doğası gereği elektriksel olarak yalıtkan malzemelerden yapılmaktadır. Ana görev olarak iki kutbun temasını engelleyerek herhangi bir kısa devre olasılığını önlemektedir. Pil separatörleri, çeşitli malzeme ve maddelerden üretilebilir ve birkaç temel özellik taşırlar. Amaçlanan uygulama için gözenek ve tanımlanmış gözenek boyutuna sahip olan herhangi bir yalıtkan malzemeden yapılabilir. Gözenekli yapıları boyunca yüksek kimyasal kararlılık, homojenite ve yüksek sıcaklığa maruz kaldığında büzüşmeye karşı direnç gösteren bir özellik taşımalıdır. Bir pilin içinde, hücre sıcaklığında artışa yol açabilecek çeşitli reaksiyonlar meydana gelmektedir, bu yüzden yüksek termal kararlılığa ve alev geciktiriciliğe sahip pil separatörleri üretmek için çeşitli yaklaşımlar kullanılır. Bu yaklaşımlar arasında separatörü doğal olarak alev geciktirici malzemelerle kaplamak yer almaktadır. Sodyum aljinat, kalsiyum ile çapraz bağlandığında önemli alev geciktirici performans gösteren doğal bir polisakkarittir. Çapraz bağlı kalsiyum aljinatın limiting oksijen indeksi (LOI) 34 olarak raporlanmıştır.

Pil separatörü üretmek için çeşitli polimerler kullanılır. Ultra yüksek moleküler ağırlıklı polietilen (UHMWPE), yüksek mekanik mukavemeti ve kimyasal kararlılığı nedeniyle pil separatör uygulamalarında yaygın olarak kullanılmaktadır. Film dökümü, pil separatörları üretimi için yaygın olarak kullanılan bir süreçtir. Islak işlem film dökümünde, UHMWPE, düşük moleküler ağırlıklı bir çözücü (parafin yağ, dekalin, p-ksilen vb.) ile süspanse edilerek, ısı ve kesme kuvveti altında karıştırılır. Daha sonra kalıpta film şeklini alan jel soğutulur. Çözücünün sistemden uzaklaştırılması ile gözenekli bir film elde edilir. Bu noktada çözücü hem proses ajanı hem de sistemden uzaklaşmasıyla gözenek oluşturucu bir eleman olarak çalışır. Çözücünün sistemden uzaklaşması için n-hekzan kullanılmaktadır. Kullanılan bir diğer seperatör tipi ise nanofiber bazlıdır. Bir rotorun, polimerik çözeltiyi çok yüksek hızlarda dönerken nanolif olarak püskürttüğü santrifüj eğirme sistemi de dahil olmak üzere çeşitli yöntemlerle üretilebilir. Bu tezin amacı, farklı imalat yöntemleriyle bir lityum ve sodyum iyon pil separatörleri üretmek ve bunları kalsiyum aljinat ile kaplayarak termal performanslarını arttırmaktır. İki farklı polimerden, iki farklı membran yapısı elde etmek için film dökümü ve santrifüj eğirme sistemleri kullanılmıştır. Film döküm işleminde UHMWPE ve paraffin yağı elle mekanik olarak karıştırılarak süspansiyon oluşturulmuş ve ardından çift vidalı bir ekstrüdere volumetrik beslenerek şerit şeklinde film yapısı elde edilmiştir. %30 UHMWPE, %69 parafin yağ ve %1 antioksidan karışımı hazırlandı. 6 ısıtma bölgesi ve kalıp sıcaklığı sırasıyla 130, 140, 150, 160, 170, 180 ve 180°C'de tutulmuştur. Vida dönüş hızı 35 rpm'de sabit çalışılmıştır. Üretilen film, 3 mm kalınlığında 5 cm genişliğindedir. Elde edilen filmler sıcak preste 180°C sıcaklıktai 8 ton yükte 8 dakika preslendikten sonra oda sıcaklığına soğutulmuştur. Sıcak pres sonrası elde edilen son filmlerin kalınlığı 200-400µm aralığındadır. Farklı çekme oranlarının etkisini, ekstraksiyon adım sırasının önemini, kısıtlı ve kısıtlamasız tek eksenli çekmenin etkisini ve sıcak çekme

yapılan numunelerdeki rezistans ile numune arasındaki mesafenin ürüne etkisini incelemek için optimizasyon deneyleri yapılmıştır. Çekim sonrası yağın ekstraksiyonunun, çekim öncesi yağ ekstraksiyonuyla, gözenek ilişkisi incelenmiştir. Çekim sonrası yağ ekstraskyionunun yapıldığı üretimde daha küçük gözeneklere, homojen bir gözenek boyutuna ve yapısına yol açtığı bulunmuştur. Numunelerin germe makinesinde ısıtılması rezistans kullanılarak açık sistem ile yapılmıştır. Numune ile rezistans arasındaki mesafeler sırasıyla 13,5, 16,5 ve 19,5 cm olarak konumlandırılmıştır. Rezistans ve numune arası mesafe 13,5 cm iken yüksek ısıdan dolayı filmin yüzeyinde erime meydana gelmiştir ve gözenek yapısını kaybetmiştir. Konumlandırma 19,5 cm'de yapıldığında gözeneklerin büyümesi ve gözenek oluşumu için yeterli miktarda ısı sağlanamamıştır. Numunelere İki farklı çekme oranı verilmiştir; 2×1.5 ve 4×1.5. Daha yüksek çekme oranları gözeneklerin kapandığını göstermiştir. Optimum parametreler, 16,5 cm rezistans mesafesi ve 110 ℃ rezistans sıcaklığı ile 1,5×2 kısıtlı çekme oranı olarak bulunmuştur. Optimizasyon çalışmaları yapıldıktan sonra üç numune (S1, S2 ve S3) üretilmiş olup, 280, 200 ve 280 µm'lik üç kalınlığa sahip numune sıcak prese tabi tutulmuştur. Bu kalınlık farkı, homojen olmayan preslemeden kaynaklıdır. Bu numuneler daha sonra çekmeye maruz bırakılmıştır ve üç farklı kalınlığa sahip (40, 60, 80µm) numune elde edilmiştir. Son olarak, bu numuneler, yağı ekstrakte etmek ve istenen gözenekli yapıyı ve nihai membranı elde etmek için n-hekzan içine yatırılmıştır. Bu membranlar daha sonra bir hücre konfigürasyonuna yerleştirilerek sodyum iyon (Na-iyon) pil separatörü performansı test edilmiştir. S1, S2 ve S3 numunelerinin iyonik iletkenlikleri sırasıyla 0.09, 0.48 ve 0.04mS/cm2 olarak ölçülmüştür. S2 numunesi, diğer numunelere kıyasla sayıca daha fazla gözenek ve homojen gözenek dağılımına sahip olduğu için daha iyi performans göstermiştir. Bütün bu koşullar ve özellikler baz alındığında daha efektif gözenek yapısına sahıp membran elde edebilmesi için, çekme işleminin kapalı sistemde gerçekleştirilmesi tavsiye edilmektedir.

Nanolifli membran ise santrifüj eğirme sistemi ile termoplastik poliüretandan (TPU) üretilmiştir. Nanolif üretimi için, TPU, dimetilformamid (DMF)/aseton karışımı içinde çözdürülmüştür. İşlemin optimizasyonu, polimer konsantrasyonu, çözücü oranları, iğne çapı ve santrifüj hızı değiştirilerek incelenmiştir. Optimum nanolifler, 30G iğne çapında ve 13.000 rpm dönme hızında, 2:1 DMF/aseton oranında çözünmüş %10 TPU'da elde edilmiştir. Elde edilen nanolifler, daha sonra 0.5%, ve 2% sodyum aljinat çözeltilerin içinde daldırılmıştır. Kuruduktan sonra numuneler, 10% lik kalsiyum klorür ($CaCl_2$) çözeltisi ile çapraz bağlanmıştır. Kalsiyum Aljinat (Ca-alg, CA) ile çapraz bağlanma işleminden sonra numuneler 120°C'de 8 ton yükte 2 dakika sıcak preslenmiştir. CA, Elde edilen kaplanmış nanolifli membranlar daha sonra 1M $LiPF_6$ ve 1M $NaClO_4$ elektrolitleri ile pil konfigürasyonuna getirildi ve separatör performansları ölçülmüştür. Nanolifli membranlar, ticari Celgard 2500 polipropilen (PP) separatör ile kıyaslandığında önemli ölçüde daha iyi performans göstermiştir. Neat TPU, preslenmiş TPU, 0.5 TPU ve 2 TPU'nun iyonik iletkenlikleri sırasıyla 0.23, 0.67, 0.17, 0.16 ve 0.05 mS/cm^2 idi. Kaplanmış numuneler, ticari PP separatörüyle kıyasla önemli ölçüde daha büyük iyonik iletkenlik ve daha az direnç değerleri sergilemiştir. Tam pil konfigürasyonundaki numunelerin iyonik iletkenlikleri sırasıyla 1.53, 0.19, 0.05 ve 0.03 mS/cm^2 idi. Numuneler ise, Neat TPU'nun diğer numunlerden en yüksek performans göstermiştir. Numunelerin iyonik iletkenliklerindeki gözlemlenen düşüş, gözeneklerin kaplama esnasındaki kapanmasından kaynaklıdırı. Bu, Nyquist grafiğinde düz çizgi ile gösterilen numunelerde difüzyon fenomeninin bariz bir şekilde yol açtığını gösterilmiştir.

Kalsiyum aljint membranların termal performansı bariz iyileştirme sağlamıştır. Kaplanmış numuneler, Neat TPU ve ticari numunelerin %63 ve %100'lük büzülmesine kıyasla %0'lık büzülme göstermiştir. Numuneler ayrıca alev kaynağına maruz kaldıklarında tutuşmada önemli bir gecikme gösterdi. 1 ve 10 saniye sonra numunelerin durumu arasında bir karşılaştırma kaydedildi. Neat ve preslenmiş numuneler doğrudan ilk saniyelerde erirken, 0.5 TPU ve 2 TPU numunelerin bütünlüğünü korumuştur. 0.5 TPU numunesinde yanma izleri ve başlangıç renginin kahverengimsi bir renge dönüştüğü görülürken, 2 TPU numunesinde 10 saniye sonra bile ilk durumunu korumıştur. Elde edilen sonuçlar, pil uygulamalarında kalsiyum aljinat pilin termal performansını geliştirecek özelliklere sahip olduğunu ispatlanmıştır. Kalsiyum aljinatın iyonik iletkenliklerini artırmaya yönelik çalışmalar yapılabilir ve daha iyi kaplama yöntemleri önerilebilir.

1. INTRODUCTION

Global demand for energy is increasing and the systems needed to supply and store energy is getting more critical and essential. Energy storage systems are mainly categorized into thermal, mechanical, and electrochemical systems. Thermal systems uses heating and cooling to store and transfer energy like in heat storage tanks, mechanical systems utilizes gravitaional energy as in hydraulic systems, and chemical storage systems like batteries employing the properties of chemical elements to reserve and supply energy [1]. The recent booming industry of electromobility (e-mobility) accelerated the demand on high performance electrical energy storage systems. The global sales of electric cars show an exponential increase in the global electric car stock hitting 16 million cars in 2021 while it was less than hundred thousand in 2010, spiking its global market share from 0.01% up to 8.57% [2]. To keep up with this high demand, high-performance electrical storage systems are needed. Lithium-ion batteries (LiBs) are the dominant storage energy system in various applications. Electric vehicles are mainly powered with Li-ion batteries which are known for their high performance, cycle-life, and relatively low cost as in our modern society it's being used in laptops and mobile devices [3]. This steady demand and the short supply caused during the covid-19 pandemic also pushed the research toward sodium ion batteries (NaBs) research as sodium is more abundant in nature (Na: more than 1% of the crust, Li: 10-100ppm) which can lead to a relatively lower cost [4]. The main obstacle for sodium ion batteries lies in their lower theoretical capacity along bigger atomic size (Na^+=1.02 Å, Li^+=0.76 Å) which make them behind LiBs in terms of energy density.

LiBs and batteries in general consist of three main components as shown in Figure 1.1; negative charge electrode (anode), positive charge electrode (cathode), and a separating layer soaked in electrolyte that separate the two poles (separator).

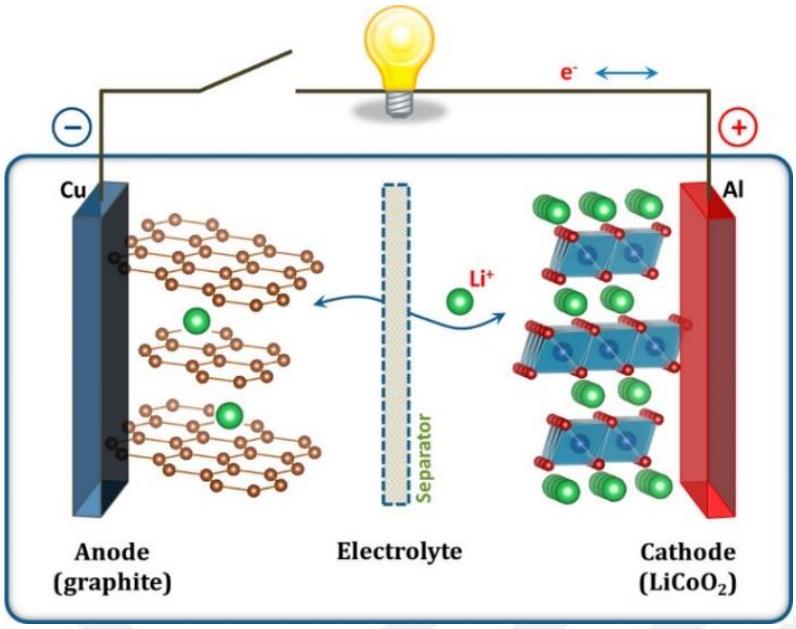

Figure 1.1 : Li-ion battery components [5].

Battery separators are a crucial part of Li and Na-ion batteries structure, as they allow the movement of ions while inhibiting short circuit formation employing their porous structure, working as a physical and electronical barrier between the electrodes. From a structural perspective, their porous structure should be designed in a way that they allow the tiny ions to pass while preventing any other non-desired materials from travelling through the separator. That makes the optimum pore size of the separator to be in the submicron range with commercial ones in the range of 400nm [6].

To obtain maximum functionality and performance inside the battery, separators have to carry several properties like being thin and light while exhibiting strong mechanical capabilities. Also, because of the continuous contact with the liquid electrolyte, it should manifest excellent chemical stability to achieve high safety level, since one of the main concerns of the usage of LiBs is their explosion possibility [7]. Separators have to withstand significant number of reactions that occur inside the battery. Defects on the separators could cause the failure of the separator and induce a series of unwanted incidents that could lead to devastating results. During the assembly process, particulate matter in the air or stretching caused on the production line could lead to these defects [8]. For that reason, standards recommend a high mechanical strength above 98.04 MPa [9]. Also, as the reaction occurs during high load applications, the heat increases, with some cases where the temperature of the surrounding environment is also high, separators should withstand these high temperature variations manifisting a high melt integrity with minimal shrinkage not more than 5% at 90℃ [9]. In terms

of chemical activity, battery separators also need to be chemically stable and does not react with other components as they should be electrochemically inactive to accomplish best performance and longest cell life [7].

Separators can be classified based on the electrolyte used into ionic liquid electrolyte separators, and polymer electrolyte separators. While they both accomplish the same purpose, there are some differences in their composition and behavior. Gel polymer electrolyte is a combination between a polymer matrix and an electrolyte forming a gel-like structure [10]. Ionic liquid separators use ionic liquid as an electrolyte without utilizing the polymer as a scaffold to hold the electrolyte together and prevent leakage. Ionic liquid separators are the most common in LiBs. Dissolved lithium salts are used to ease the movement of lithium ions back and forth between the electrodes and through the separator [7].

Separators based on ionic liquid electrolytes for LiBs are made of various polymers. They can be made of polyolefin separators which are the most common. These separators are mainly made of polyethylene and propylene and possess high mechanical strength with chemical stability [11]. Nanofiber separators are emerging as they have large surface to volume ratio and can provide high electrolyte uptake [12]. Also ceramic separators are used in high temperature applications and are made of materials such as aluminum oxide, silicon oxide, and lithium aluminum titanium phosphate [13]. Glass fiber separators can be used also, although they are mainly used in lead acid batteries as they are highly resistive to acid but they can function properly in LiBs as they may have extremely high heat and thermal resistance [14].

There are several materials and polymers used in battery separators. The most common and commercialized separators are made of polyolefins produced with film extrusion technique. Polyolefin separators are typically made from either polyethylene (PE) or polypropylene (PP) or a combination of the two. Porous polyolefin membrane can be generally fabricated by sintering of the polymer powder, extrusion of the melt and stretching (dry process), and extrusion of the melt followed by thermally induced phase separation (TIPS) [15]. Dry process and wet process are the common methods used to fabricate battery separators. Both processes have an extrusion and stretching step in common, they differ in the precursor mixture fed to the extruder. In the wet process a plasticizer/solvent is fed with the polymer and then extracted in the end of the process while the dry process no solvent is used. The two processes carry their advantages and disadvantages. In dry process, no solvent is used meaning less steps

and less material with no extraction is needed but in the same time slit-like pore shape is obtained. This porous structure makes the membrane better in dendritic growth resistance but lowerelectrolyte holding capability. In the wet process, a plasticizer is used to dissolve the polymer and is extracted by a non-solvent in the end. Pores formed by this technique are spherical and interconnected with fibrous structure [16]. For wet process, both semi-crystalline and amorphous polymer membranes can be fabricated [16].

PP is a thermoplastic polymer with high mechanical strength and chemical resistance and mainly produced through the dry process. Film casted PP is run through biaxial stretching process where thin PP sheets are stretched in both machine direction (MD) and transverse direction (TD) [17]. The microporous structure of PP separator is dependent on creating a precursor sheet that have β-crystals then growing these crystals by annealing the sample and finally stretching at high temperature below the melting point to initiate pore formation and enlarging them [17]. PE on the other hand is another polyolefin which have various applications and widely used in LiB separators and fabricated through the wet process. In this process, the polymer is firstly mixed with paraffin oil, antioxidants and other additives to prepare the resin. The resin is then fed into the extruder and extruded through a sheet die before entering extraction bath to extract the solvent. Polyolefins like PP and PE are known to be hydrophobic with a lower electrolyte uptake and limited ability to maintain good contact with the electrodes resulting in overall performance deterioration. But overall, polyolefin battery separators are widely used and well-established technology in the field of energy storage, and ongoing research is focused on developing new polyolefin formulations and processing methods to improve their performance and safety in emerging battery technologies.

Nanofiber mats are also used to fabricate battery separators. Several polymer-based nanofibers have been investigated such as Polyvinylidene fluoride (PVDF), Polyimide (PI), Polyamide (PA) and many others. These nanofibers can be fabricated with different spinning techniques. The most common method to obtain nanofibers is electrospinning where fibers are drawn by applying potential difference. Other techniques like solution blowing and centrifugal spinning are less common but they are getting more attention due to higher productivity and ease of operation. In solution blowing, the nanofibers are obtained utilizing the drag force of compressed air, where pressurized air is fed to a coaxial nozzle with polymer jet in the center. In centrifugal

spinning, the nanofibers are ejected by the centrifugal force from a high-speed rotating nozzle. There are several studies on battery separators fabricated using these techniques.

Therefore, designing and optimizing the separator is crucial to the performance and safety of lithium and sodium-ion batteries. A well-designed separator can improve the battery's energy density, cycle life, and safety, while a poorly designed separator can lead to reduced performance, shortened lifespan, and even catastrophic failure. For these reasons, the field of battery separators is always investigated, and the journey to reach effective and high-performance batteries is forever lasting.

In our work, we investigated the fabrication of both film-based and nanofiber-based polymeric battery separators. Surface and structural modifications were done to enhance the chemical, and thermal properties of the separators.

1.1 Purpose of Thesis

This work aims to fabricate film casted and nanofibrous membranes and analyze their performance for energy storage applications. In batteries, a separator is a membrane that is used to allow the ions passage between the cathode and anode without causing short circuit. This separator should carry several properties like high porosity, small pore size, and good thermal and electrochemical properties.

The fabricated membranes were tested as separators for sodium ion (Na-ion) and lithium ion (Li-ion) batteries. Full optimization of the process along altering the surface properties of the nanofibrous membrane was done to examine the enhancement of the surface properties of the separator. To accomplish better thermal properties, coating with natural flame-retardent polysaccaride (calcium alginate) is used. It is known for its inherent flame retardent properties.

1.2 Hypothesis

Paraffin oil works as a porogen and plasticiszer facilitating the pore initiation process and easing of the processability of ulta high molecular weight polyethylene (UHMWPE) which is known for its high viscosity. The cooling, heat stretching and then extraction of the film will give a porous structure in the range of 100 nm which is suitable for battery separator application while carrying the mechanical strength of

highly oriented films in comparison to other separators fabricated with different means.

For the nanofiber-based membrane, calcium alginate (CA, Ca-Alg) coating layer was applied to enhance the thermal properties of thermoplastic polyurethane (TPU). CA is known to have a limiting oxygen index (LOI) of 34 which is high comparable to 19 of TPU. Thermal performance of separators carries a huge importance in separator application owing to the enormous number of reactions occuring inside the battery which lead to heating of the battery and in some cases explosions.

Also, a comparison between the properties of conventinally common microporous stretched membrane with centrigally spun nanofibrous membrane is to be studied.

2. STRETCHED FILM CASTED MEMBRANE

2.1 Introduction

Membranes are porous structures that are made from different materials using distinct techniques and are used in various applications. Due to the unique structure of the membranes, they can be used as air filtration, distillation, and extraction. They can be used to filter particulate matters providing fresh air like in face masks which was intensively used during Covid-19 pandemic. Also, they can be used for water purification application as in UF [18], MF [19], NF and RO processes [20]. On the other hand, there is a huge role that membranes play in energy applications that doesn't cross people mind which is as separators between electrodes, prohibiting the electrons from causing a short-circuit in the system [7]. Polymer-based membranes are a key factor in the booming electro vehicle industry as it is used as a separator in Li-ion batteries. These membranes can be fabricated on different scales and geometries with different methods. They can be either flat sheeted or cylindrical. They can be fabricated using electrospinning [21], centrifugal spinning [22], melt-spinning [23], and film casting [24]. Membranes can be fabricated on different scales and geometries with different methods. They can be either flat sheet or cylindrical according to the production purpose. The main industrial process used for film production is by extrusion.

Extrusion process goes back to the eighteenth century and was established in the 1930s to become one of the most widely used processing technology in the plastics, rubber and food industries [25], [26]. It is versatile, where a various of materials can be produced in the same system. Melt extrusion is a process based on melting and shaping polymers. Melt extrusion is a process used to formulate raw plastic pellets into desired shape by melting the material by thermal and shear means and extruding it through a die to give it the desired shape. Extruders have a very high productivity and capabilities in comparison to other systems. The need for labor per unit is small which lowers their overall cost. Also, they are classified to have high product quality with no effluents and hazardous side products which make them extensively used in food and

pharmaceutical industries [27]. It is used in the pharmaceutical industry to achieve optimum mixing of active materials with thermoplastic carriers, and binders [25]. In the food industry, extrusion process carries a huge advantage over any other process. Extruders are used in food applications like snacks, cereals, pasta, protein supplements, and pet food [27]. A block flow diagram (BFD) of the extrusion process is shown in Figure 2.1.

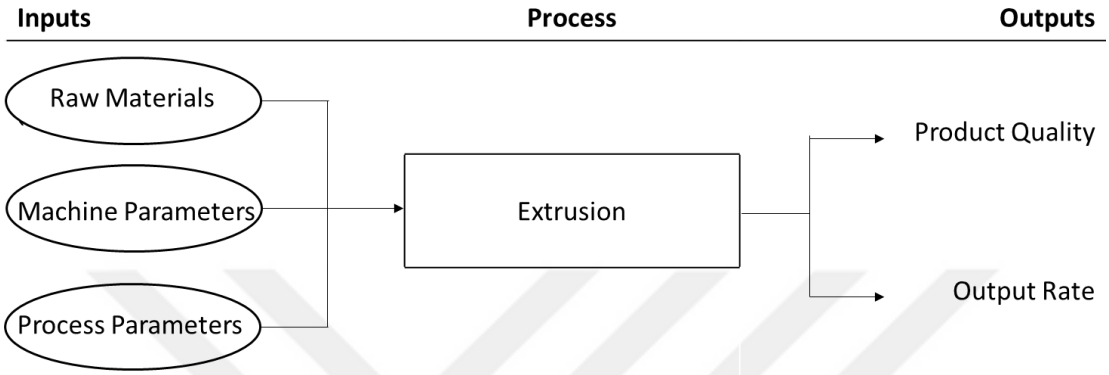

Figure 2.1 : BFD of the extrusion process.

Polymer extruders are machines consists of a hopper, a rotating screw inside a barrel, and a die. The polymer pellets are fed through the hopper, melted by the heat of the barrel, and the shear due to friction between pellets and the barrel [28]. Final melt is then shaped through the die. Extruders are classified into different types and designs. They can be classified by feeding type into filament fed, screw extruders (pellets fed), and syringe extruders. One of the basic types of extruders is the ram extruder (Figure 2.2). Ram extruders are made of piston that presses melted polymer through the die. It is used for polymers with very low flowability like UHMWPE and can cause degradation to polymers as it needs longer time to heat each batch uniformly [28].

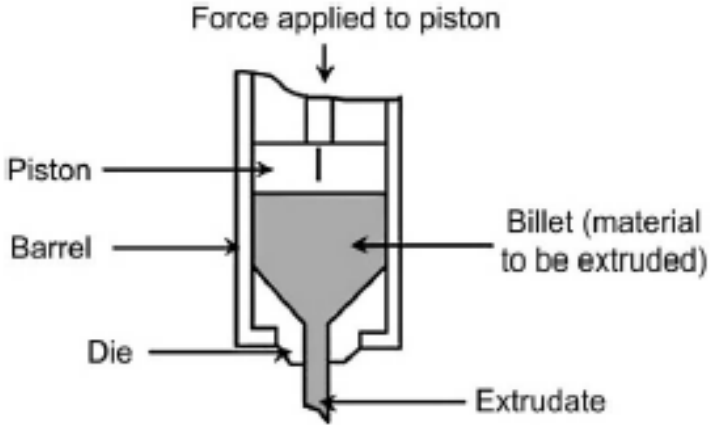

Figure 2.2 : Ram extruder [28].

Other than ram extruders, the most common extruder type is the single screw extruder. A schematic of the screw extruder is shown in Figure 2.3. Screw extruders can be classified into single and twin-screw extruders. Each have their definitive usages and applications.

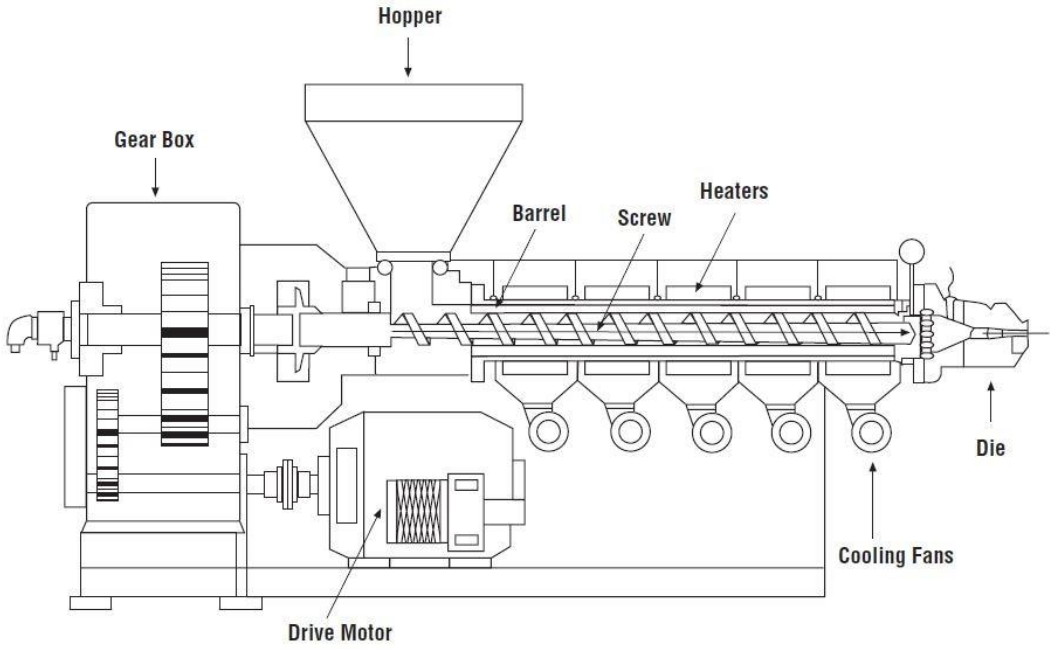

Figure 2.3 : Single screw extruder [29].

Single screw extruders (SSE) are extruders consisting of a single screw inside the barrel used for melting polymers and incorporating additives to obtain a homogenized melt. They are the most used types of extruders in processing polyethylene and many other polymers [30]. The screw design of SSE consists of 3 main zones (Figure 2.4); conveying zone where the feed (granular or powder) is conveyed before melting to reach the melting zone. In the melting zone, the polymer is gradually melted until it reaches the metering zone where only polymer melt is filling the gap between screw helical channels and the barrel. Finally, this melt is pumped through the die. SSEs are the oldest form of extruders and almost all polymers has been once passed through a SSE [31].

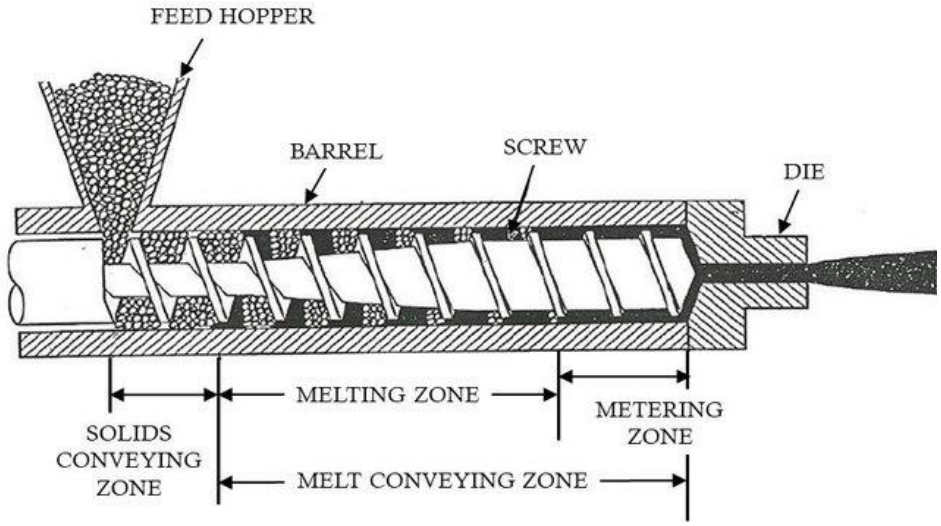

Figure 2.4 : Screw zones [31].

For processes that needs uniform mixing of polymers, twin screw extruders (TSE) are used. They are known to be versatile in terms of ability to mix and compound materials together. TSE originally used for kneading bread dough and conveying ceramics till the first usage of TSE for polymers in 1930 [31]. TSEs consist of a double screw inside the barrel. The screw can be co-rotating (rotating in the same direction), and counter-rotating (rotating in opposite direction). They can be intermeshing where screw flights go through the channel of the other screw, or they can be non-intermeshing where the screw flights don't engage with each other. The main difference between SSE and TSE, is that TSE have modular design where the screw and barrel sections are removable and can be changed according to the process which lead to fast modification ability [31]. They are used for reactive extrusion processes like grafting and saline functionality [30]. Visual illustration of the different screw geometries is shown in Figure 2.5.

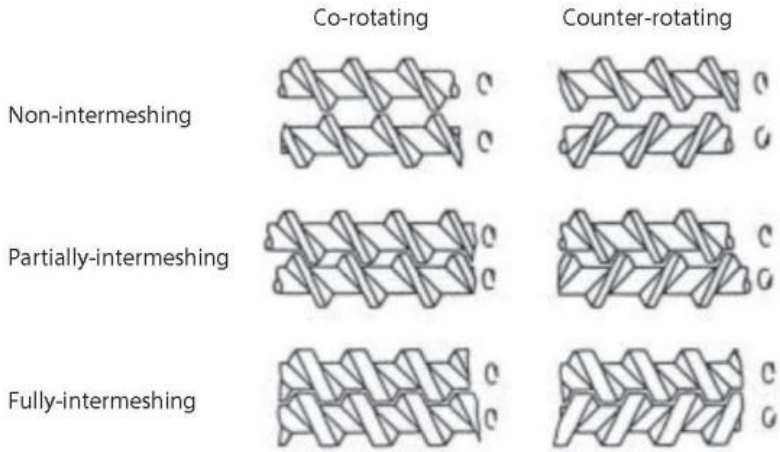

Figure 2.5 : Screw geometries in TSE [30].

2.2 Film Extrusion

Production of films using extruders can be done through either blown films, or cast films. Blown films extrusion is commonly used to produce biaxially oriented film for various applications. In this process, the polymer melt is pumped trough an annular film die where it is blown upward by thermally-controlled air. The film is then collapsed into sheet by the end of the bubble frame. An industrial film blown machinery is shown in Figure 2.6.

Figure 2.6 : Film blowing machinery [30].

In film extrusion, the polymer melt is extruded through a sheet/slit die to obtain a plastic film with various thicknesses and sizes making it more efficient in comparison to the blown films. Films are considered As The film is travelling through the process, it cools and solidifies. The film can be made from various types of plastic resins, such as polyethylene, polypropylene, PVC, and others, depending on the desired properties and application of the final product. Several polymer films are available with different applications. They can be used for industrial packaging, food packaging, plastic bags, constructional films, and many more. Figure 2.7 shows a simple scheme for a film extrusion process.

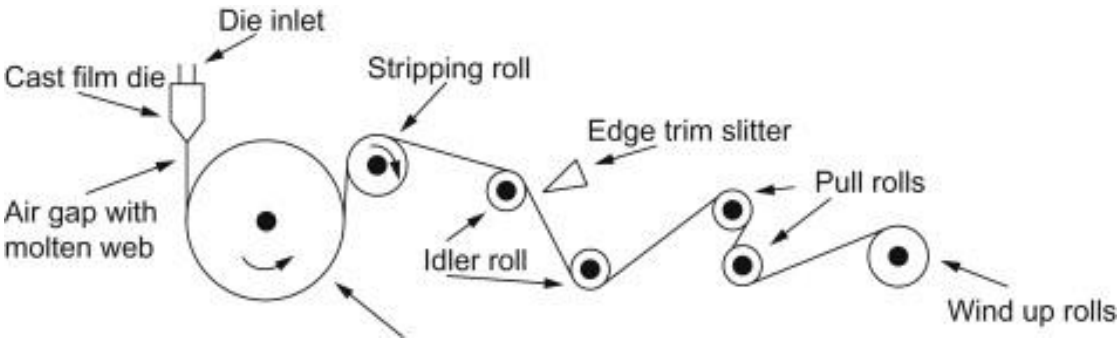

Figure 2.7 : Film casting Process scheme [32].

Casted films are also oriented in both machine and transverse direction. Rollers are used to convey the film, control the thickness, and give orientation for the polymer chains to achieve better optical, and mechanical properties. These casted films are more optically transparent due to the higher cooling rate achieved by quenching films between the rollers leading to a smaller crystalline structure. This results in better tensile and optical properties.

2.2.1 Film dies

The circular profile coming out of the extruder is shaped into sheets/films through the film die. Many factors affect the process flow. Nonhomogeneous velocity will vary the thickness. Die design have several key elements; a distribution manifold, a die land, and die lips as shown in Figure 2.8. T-slot and coat hanger dies are the most common ones in film extrusion dies.

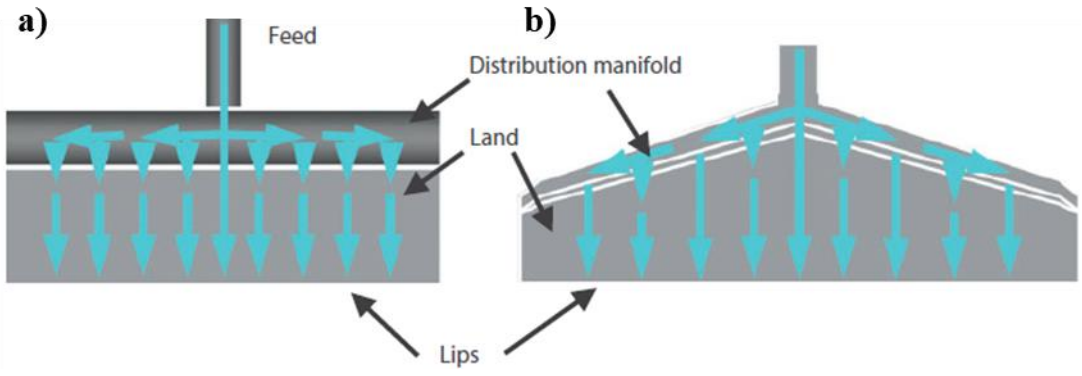

Figure 2.8 : Film die types a) T-slot and b) coat hanger dies used in film casting [30].

These two dies differ mainly in their distribution method. In the T-slot die, the manifold is straight so the polymer distribution is carried horizontally. T-slot dies are considered to be simple and suitable for different resins with different melt viscosities

which make them preferrable and have relatively lower costs. Coat hanger dies on the other hand provide more uniform distribution owing to their specific design. They perform better than T-slots when dealing with high viscosity polymers. Unlike T-slot dies, the cross-section and length of the manifold and the land of the die tapers gradually to provide uniform distribution and pressure drop. These dies are optimized according to the specific application and rheological properties of the polymer [30]. According to the desired film thickness and distribution, other pieces and fragments like restrictor bars, relaxation chambers and adjustable die lips are integrated into the design. Restrictor bars work as a controller to adjust polymer flow through the side of the die by restricting the polymer flow through the mid part of the die channel providing a fully uniform polymer flow throughout the die. Relaxation chambers are added to release the excessive shear stress before polymer discharge. Adjustable die lips are used to control the final thickness of the film coming out of the die. Figure 2.9 shows a detailed film extrusion die.

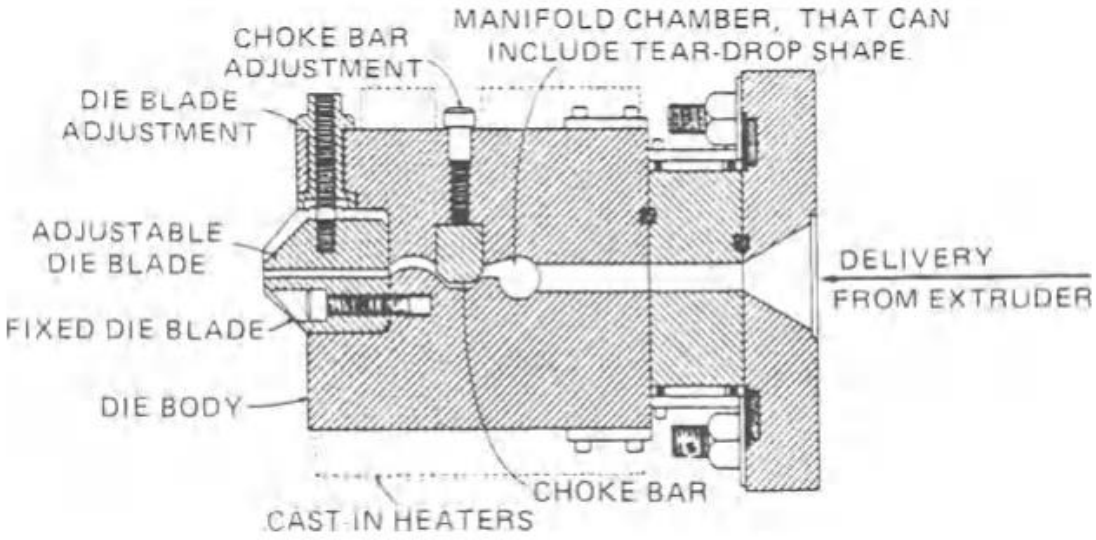

Figure 2.9 : Film extrusion die [33].

2.3 Membrane Fabrication Process

Membranes obtained from film extrusion can be fabricated through two main processes as mention before; dry process, and wet process.

2.3.1 Dry process

Dry process is a solid-state process where the polymer is melted and shaped into film structure though sheet die. The process depends on obtaining a row nucleated structure.

Then these row nucleated structures are then annealed and stretched to initiate micro-viods that after heat setting are stabilized to obtain a microporous structure. This row-nucleated structure is formed due to the strain crystallization occurring during the stretching between the die and the cast film. The control of the initial lamellar size is the main challenge.

2.3.2 Wet process

Wet process is a process where the polymer is mixed with a diluent or plasticizer where it helps in processing and pore formation of the extruded film and eventually being extracted leaving a membrane with definite porous formation. This process is known as thermally-induced phase separation (TIPS) method. In TIPS, the pore size can be controlled in a versatile and easy way. The polymer is melted and blended with the diluent until a homogeneous mixture is formed. The diluent normally is chemical with low molecular weight and high boiling point. The mixture is conveyed to the die to obtain the desired shape. After being casted, it's cooled down inducing the phase separation of the two phases due to thermal energy removal. Eventually, the diluent is extracted with a suitable solvent. In this process, wide range of polymers can be used despite their poor solubility.

2.3.2.1 Mechanism & thermodynamical consideration

To understand the thermodynamics that lie behind this phenomenon, phase-equilibrium diagrams are used. In semi-crystalline polymers, the mixture follows either a solid-liquid or a liquid-liquid phase separation according to the interaction parameter (χ) between the parts of the mixture in relation with melting temperature according to the following equation;

$$T_m = \frac{1}{\frac{RV_u}{\Delta \boldsymbol{H_u V_d}}(\emptyset_d - \chi \emptyset_d^2) + \frac{1}{T_m^\circ}}$$

When the equation is plotted in terms of polymer fraction $\emptyset_p$ ($\emptyset_p$=1-$\emptyset_d$) (Figure 2.10), a depression curve is formed, where we can determine whether a mixture will follow Solid-Liquid (S-L) phase separation or liquid-liquid (L-L) phase separation.

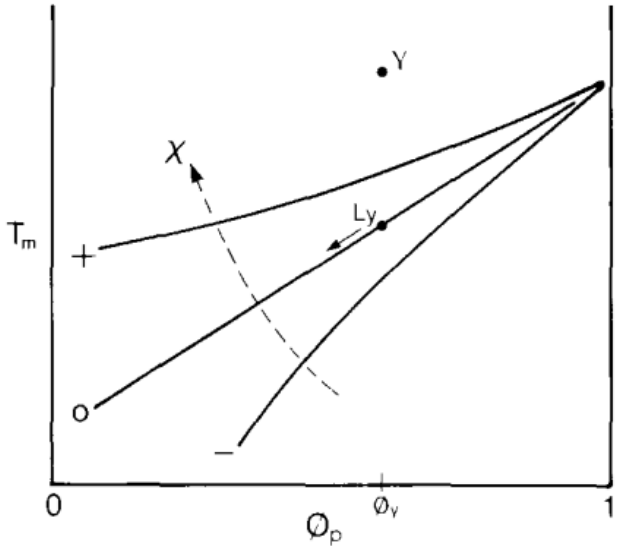

Figure 2.10 : Interaction parameter correlated with temperature and polymer **[34]**.

From Figure 2.10 we can understand that the higher the interaction parameter is, the weaker the polymer-diluent interaction is and vice versa. As the interaction parameter increases, the temperature where phase separation occurs increases. The determinant factors of the phase separation that the mixture undergoes, are the polymer concentration and the interaction parameter. S-L phase separation occurs when cooling a system of strong polymer-diluent interaction. In semi-crystalline polymers, polymer-diluent system undergoes L-L phase separation at low polymer concentration and S-L phase separation at high polymer concentrations [34].

2.3.2.2 Miscibility of the systems

The miscibility of any two-component system is determined by Gibbs free energy of mixing. ΔG_{mix} and its second derivatives with respect to polymer volume fraction, $\emptyset_p$ at a fixed temperature $\boldsymbol{T}$ and pressure $\boldsymbol{P}$ are the criterion for complete miscibility of polymers**.**

$$\boldsymbol{\Delta G_{mix} < 0}$$

$$\boldsymbol{\left(\frac{\partial^2 \Delta G_{mix}}{\partial \emptyset_p^2}\right)_{T,P} > 0}$$

Where $\Delta G_{mix} = \Delta H_{mix} - T\Delta S_{mix}$, with ΔH_{mix} and ΔS_{mix} representing the entropy of mixing. If one of the conditions is not met; phase separation would occur. The possibility of the path a mixture would follow is shown in Figure 2.11. It can follow

three main paths. It can follow a stable (miscible) path, or it could be partially miscible, and finally it can be unstable meaning completely immiscible. Depending on the polymer fraction and the solvent used, UHMWPE/mineral oil mixture could either follow the stable (miscible) path, or it can be partially miscible where critical temperatures are introduced and L-L phase separation occurs.

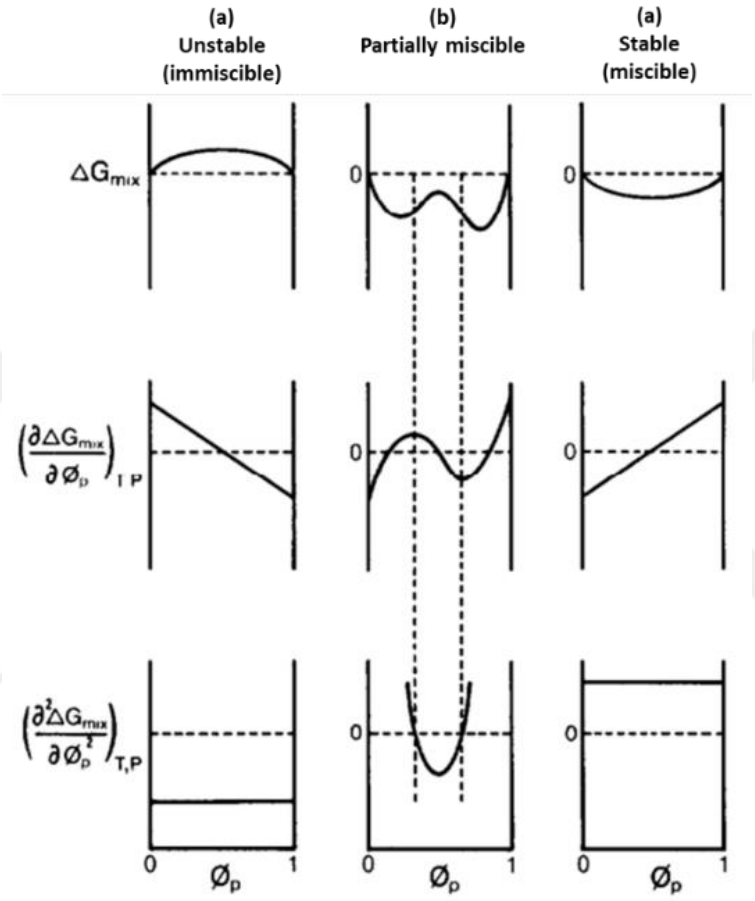

Figure 2.11 : Polymer/diluent thermodynamic miscibility curves [34].

2.4 Properties of UHMWPE

Ultra-high molecular weight polyethylene (UHMWPE) is a type of thermoplastic polymer with a very high molecular weight, typically ranging from 3 to 6 million g/mol. According to global standards it ranges above 3 million g/mol [ASTM D4020], while on other standards it ranges above 3 million g/mol [ISO11542]. UHMWPE exhibits a range of unique properties that make it suitable for a wide variety of applications. Some of the key properties of UHMWPE include:

- High strength: UHMWPE is extremely strong, with a tensile strength of up to 4 GPa, making it one of the strongest polymers available [35].

- High stiffness: UHMWPE has a very high modulus of elasticity up to 140 GPa [35], giving it excellent stiffness and rigidity.

- Low coefficient of friction: UHMWPE has a very low coefficient of friction, which makes it an ideal material for use in applications where low friction is important, such as bearings and gears [36], [37].

- High abrasion resistance: UHMWPE is highly resistant to abrasion, making it suitable for use in applications that involve sliding or rubbing contact, such as conveyor belts and bushings [37].

- Chemical resistance: UHMWPE is resistant to many chemicals, including acids, alkalis, and organic solvents, making it useful in chemical processing and other applications that involve exposure to harsh chemicals [38].

- Biocompatibility: UHMWPE is biocompatible, meaning that it does not elicit a significant immune response when implanted in the body. This property makes it useful in medical applications, such as orthopedic implants [37].

- Low water absorption: UHMWPE has a very low water absorption rate, which means that it is not affected by moisture or humidity to the same extent as other materials [39].

Overall, UHMWPE's combination of high strength, stiffness, low friction, and abrasion resistance, as well as its biocompatibility and chemical resistance, make it a versatile material that can be used in a wide variety of applications, including medical implants, ballistic armor, bearings, gears, and other industrial components.

2.4.1 Processability of UHMWPE

The processability of ultra-high molecular weight polyethylene (UHMWPE) can be challenging due to its high molecular weight and long chain structure, which can make it difficult to melt and process using traditional methods as most UHMWPE grades are known to have zero melt flow rate, which means that the polymer doesn’t flow. However, several processing techniques have been developed that enable the production of UHMWPE parts and products. Some of the common processing techniques used for UHMWPE include:

1. Compression molding: This process involves heating UHMWPE powder and pressing it into a mold under high pressure. This process can be carried in ram extruders where the powder is extruded through a die. The resulting part has excellent strength, stiffness and wear resistance [40].

2. Gel spinning: This process involves dissolving UHMWPE in a solvent, then spinning it into fibers or films using a spinneret. The fibers are then stretched and oriented to improve their strength and stiffness [41]. The main draw back of this process is the hazardous and extra extraction step needed which rise environmental considerations.

3. Melt processing: This process involves melting UHMWPE using high-temperature and high-pressure conditions. Due to the extremely high viscosity of UHMWPE, its powder is swelled and mixed with a low molecular weight and high boiling point plasticizer [42]. The mixture can be extruded with twin-screw extruder and the resulting material is molded into various shapes and forms according to the used die.

While UHMWPE can be processed using these techniques, it's important to note that the high molecular weight and long chain structure of UHMWPE can make it difficult to process using traditional techniques. Careful consideration of processing conditions, such as temperature, pressure, and processing speed, is needed to achieve the desired properties in the final product.

2.4.2 UHMWPE miscible solvents and polymers

To evaluate the solubility of various polymers in various solvents, a solid-liquid equilibrium (SLE) curve is necessary. When calculating the Solid-Liquid Equilibrium, distinct thermodynamic models are employed for the different phases participating in the process. While a state equation is utilized for the liquid and vapor phases, a distinct model is employed for the solid phase, which can only be applied to solid phase materials. A typical SLE curve is shown in Figure 2.12.

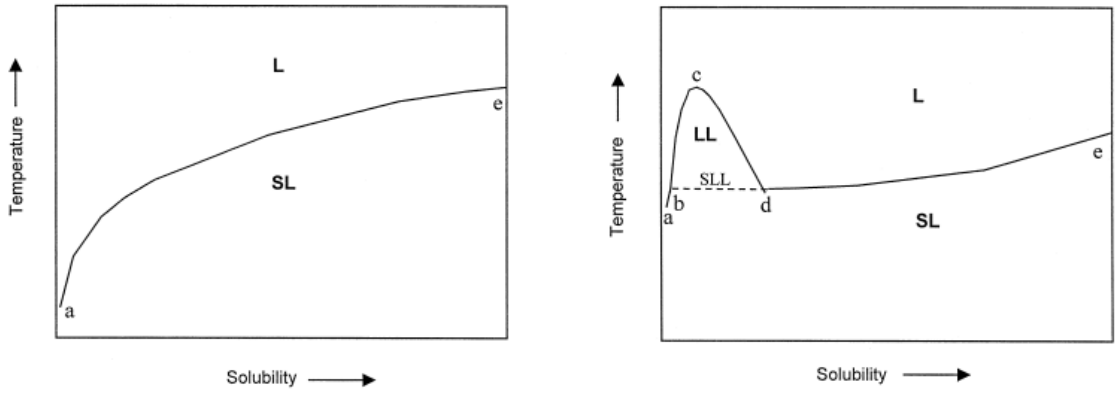

Figure 2.12 : Typical SLE curve [43].

There are several diluents or solvents studied for UHMWPE. Liquid paraffin (LP) constitutes of 60% of diluents investigated along DOP, toluene, xylene, and other aliphatic and aromatic hydrocarbons [44]. In mineral oil/UHMWPE mixtures, it has been shown that S-L phase separation occurs at all polymer concentration ranges but it started following L-L phase separation transition at low concentration when PEO was used as a second diluent along SiO_2 as an additive [45]. Several patents examined the usage of mineral oils and paraffin oil to fabricate UHMWPE membranes [46]–[48]. The miscibility of the polymer with the solvent can be enhanced by reducing UHMWPE polymer size, chain entanglement degree of the UHMWPE grade, and processing means [49].

2.4.3 UHMWPE pore formation mechanisms

UHMWPE derived membrane formation methods can be classified into two main divisions. It can be either Solvent-free or it can be solvent-based. Figure 2.13 shows theses formation methods.

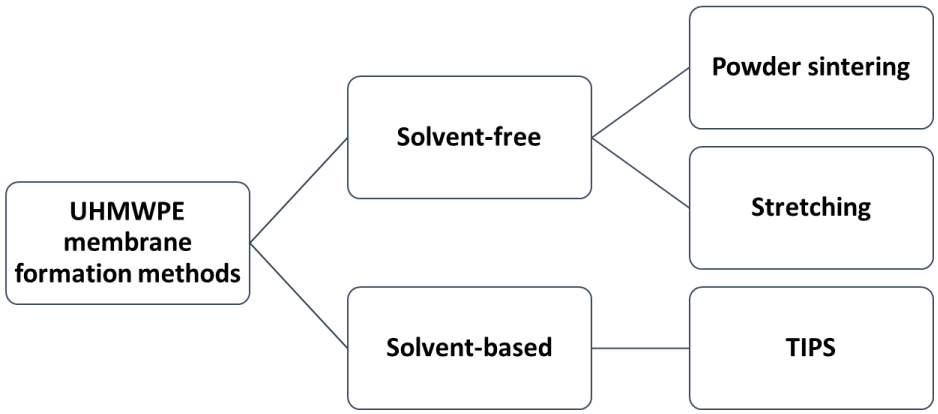

Figure 2.13 : UHMWPE membrane formation methods.

Powder sintering is a solvent-free method where polymer powder is placed into a mold with the desired shape and then partially or completely melt the powder. This methods lacks pore formation control, as it hugely depends on the particle size used and the uniformity of the diameter distribution of these particles [44]. Also, this method is considered to have less porosity than membranes formed by other means like TIPS and precipitation.

Despite this limitation, powder sintering is a popular method for ultrahigh molecular weight polyethylene (UHMWPE) membrane formation, as it does not require complex equipment or organic solvents. The structure and transport properties of these membranes can be controlled by changing the sintering time, polymer molecular weight, and sintering external pressure and temperature. UHMWPE powder sintering methods have been proposed and typically involve mixing the powder with a liquid or salt crystals before sintering. The resulting membranes have high mechanical strength and water flux, but relatively low overall porosity compared to microfiltration membranes obtained from other polymers. Additionally, UHMWPE membranes prepared by powder sintering are several millimeters thick and have a wide pore size distribution, which limits their separation performance in microfiltration processes. Figure 2.14 shows powder sintering method.

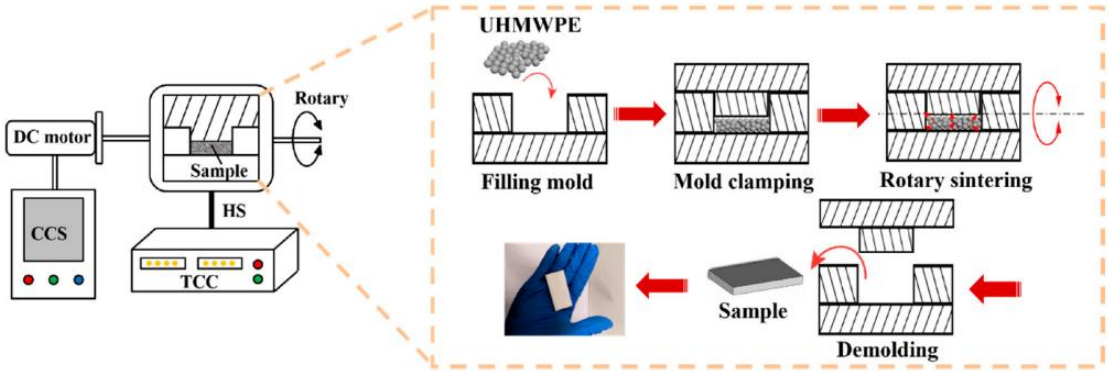

Figure 2.14 : Powder sintering mechanism [50].

Another solvent-free method is stretching. This method is widely used to fabricate membranes of semi-crystalline polymers. Figure 2.15 show β-PP membrane prepared by stretching with different ratios.

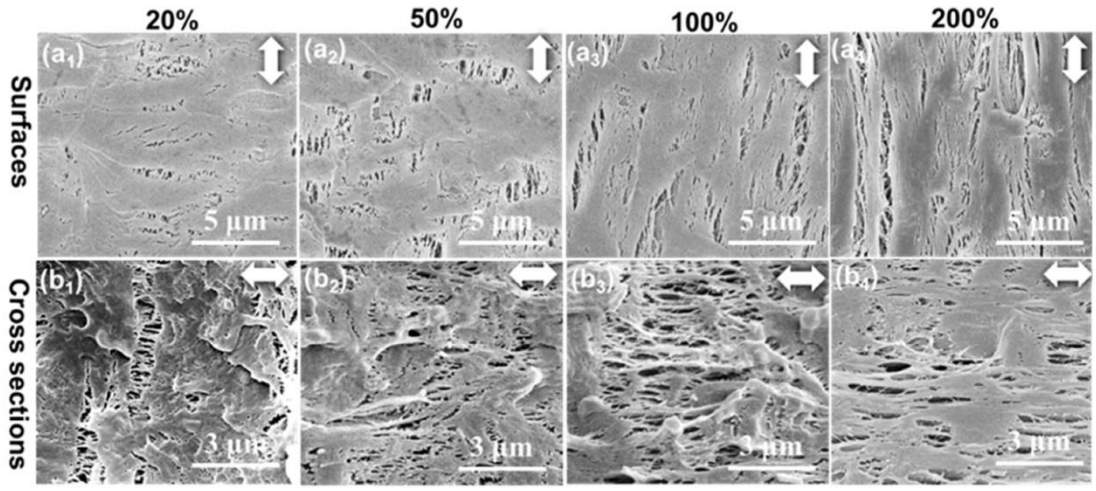

Figure 2.15 : β-PP membrane prepared by stretching method [51].

Stretching method depends on the craze forming mechanism to initiate pore formation. UHMWPE films that is used in this method are fabricated by hot pressing polymer particles, skiving off the block [52], and calendaring [53]. Very few studies have been investigated on solvent-free stretched membrane. Uehara et al prepared made a comparison of membranes formed by stretching powder sintered and roll pressed UHMWPE [54]. They obtained membranes of thickness as low as 8µm after up to 8x8 draw ratio. They found that roll pressed samples showed better overall tensile strength. In another study [55], they prepared UHMWPE membranes by a method called environmental crazing where they stretched precursors films inside a water/oil emulsion applying a tensile strain up to 250% achieving a porosity of 45%.

On the other hand, solvent-based membrane formation is mainly done by TIPS and its alternatives. This method which was previously explained in detail is the main method used to obtain UHMWPE membrane due to the uniformity and ability to control the porous structure of the membrane. This process is dependent on several factors. Molecular weight, solvent and polymer interaction, cooling rate, and the presence of nucleating agents, etc. The main solvent used is liquid paraffin or paraffin oil along some other less used solvents like soybean oil and Dioctyl Phthalate (DOP). The main problem of using a solvent to produce these membranes, that even with a good thermodynamic affinity toward PE, homogeneous mixture can't be obtained easily because of the high viscosity caused by the high MW of the polymer [44]. Significant studies worked on combining TIPS process with stretching to obtain best porous structure of UHMWPE membranes. Table 2.1 Summarizes the advantages and disadvantages of each method.

Table 2.1 : Comparison between UHMWPE preparation methods.

Method of preparation	Advantages	Disadvantages
Powder sintering	• A homogeneous solution is not necessary • Simple machinery design • No shrinkage • High mechanical strength (tensile)	• Low porosity • Wide pore size distribution • Difficulty to control the porous structure
Stretching	• A homogeneous solution is not necessary • High mechanical strength (tensile)	• high thermal shrinkage • Difficulty to control the porous structure
TIPS	• High porosity • Controllable porous structure • Ability to modify the structure	• Low tensile strength • High shrinkage • Low surface porosity
TIPS and stretching	• High porosity • Controllable pore structure • Ability to modify the structure	• High shrinkage • Homogeneity

2.4.4 UHMWPE membranes in literature

Since UHMWPE is known to be of the strongest commercial plastics. It has high tensile strength, high chemical abrasion resistance with high puncture strength. Several studies were conducted on obtaining microporous UHMWPE membranes with different methods and mixtures. Binary or trinary polymer/diluent mixtures can be used to control and obtain desired porous structure.

Jeon et. al. [56] fabricated a PE membrane using a ternary mixture of HDPE, soybean oil (SBO), and DOP and examined the effect of droplet size on the pore formation. They found that droplet size increased then decreased along increasing the oil content and the phase transition temperature allowing them to control the pore size accordingly. They were able to obtain pore sizes of 0.2, 0.6, and 1.2 μm by altering the polymer/diluent ratio and phase transition temperatures.

Zhao et. al. [57] prepared a membrane using UHMWPE/paraffin oil mixture and studied their performance for li-ion battery separators. Their trials were done on 10, 20, 30, 40, and 50% UHMWPE mixtures. Low polymer concentrations membrane showed weaker mechanical strength while high polymer concentrations mitigated the porous structure and formed a rigid film. As with several other studies [3], [57], [58], 25-30% is found to be the optimum weight ratio for proper membrane with ideal

porosity and mechanical strength. Their membrane also showed a good ionic conductivity performance with 38% porosity.

The process to develop the properties of the membrane is continuous. UHMWPE are known to be hydrophobic and of low thermal dimensional stability. Several studies were conducted to enhance the surface properties of these membranes. Integrating some chemical into the compound such as inorganic particles is one method. Hybrid UHMWPE/SiO2 nanocmposites were used to increase the electrolyte uptake and the thermal performance of the membrane [59]. 10% wt SiO2 nanoparticles increased the overall porosity, double the electolyte uptake and the ionic conductivity, while keeping almost the same mechanical performance of the membranes. Thermal shrinkage went from the 30% level down to lower than 2%. In another work [60], Al2O3 nanoparticles were used to overcome the low surface energy of UHMWPE membranes. They found that membranes with alumina nanoparticles showed more homogenous pore structure along better thermal shrinkage on elevating temperature while showing less ionic resistivity.

Some polymer mixtures can also be used to modify the properties of the UHMWPE membrane. A mixture of dfferent polyethylene (PE) grades or from another polymer family can be used. Poly(4-methyl-1-pentene) (PMP) has a high thermal stability and excellent permeability with a melting point around 230°C. UHMWPE/PMP blend was prepared to fabricate a membrane for Li-ion battery separators [61]. Higher PMP ratios increased the air permeability results significantly as the pore size and porosity also went higher.

2.5 Experimental & Methods

2.5.1 Materials

In this study, Ultra High Molecular Weight Polyethylene (UHMWPE) with a molecular weight of 5.5 million g/mol was used. AROMEL pharma grade paraffin oil was used as a plasticizer. Antioxidant Irganox 1010 was used to stabilize extruding the polymer.

2.5.2 Production of UHMWPE sheets

The polymer/oil mixture was melt-mixed by Areka counter-rotating twin screw extruder. The extruder (Figure 2.16) consists of 6 heating zones and a stripe die.

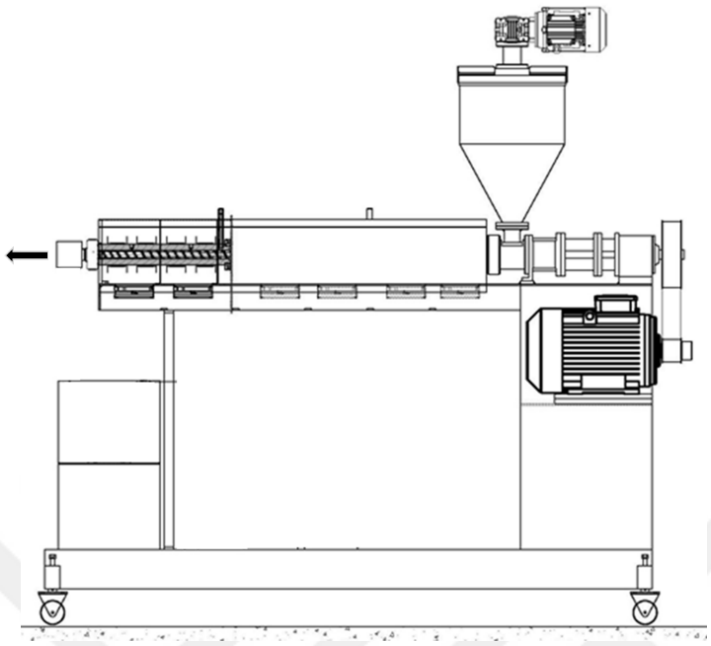

Figure 2.16 : schematic of TSE used.

UHMWPE powder was firstly mechanically mixed with paraffin oil then fed to the TSE gradually. Processing parameters are shown in Table 2.2.

Table 2.2 : Processing parameters.

Feed composition	30% UHMWPE, 69% Paraffin oil, and 1% antioxidant						
Heating zones	1	2	3	4	5	6	Die
Zone temperature (°C)	130	140	150	160	170	180	180
Screw speed (rpm)	35 rpm						

The sheet was extruded through stripe die with a thickness of 3mm. Obtained samples was hot pressed at 200C for 8 mins with 8tonn of force to reach sheet thickness of 300-400um. These samples are then stretched below melting point then cooled down before being washed in extraction bath. Three final samples were fabricated after the optimization of the system. They all were prepared ın the same means but with different stretching ratios. The samples differ in the initial thickness before stretching which is caused by non-uniform pressing of the hot press machine. The samples were named as S1, S2, and S3. Weights of the samples before and after n-hexane extraction was recorded to assure proper oil removal from the membranes.

2.5.2.1 Uniaxial stretching of the sheets

The stretching of the film was done using home-made uniaxial stretching machine shown in Figure 2.17. The machine consists of a sample holder, a stretching rail, a heating source set at a known distance above the sample, and a thermocuple to measure the temperature.

The hot-pressed samples are cut into 7cm×16cm rectangular samples and then stretched. Since the heating source temperature isn't controllable, a heating gradient of 50-90 ℃ was used. Distances of 13.5, 16.5, and 19.5 cm are investigated between the radiation source and the film.

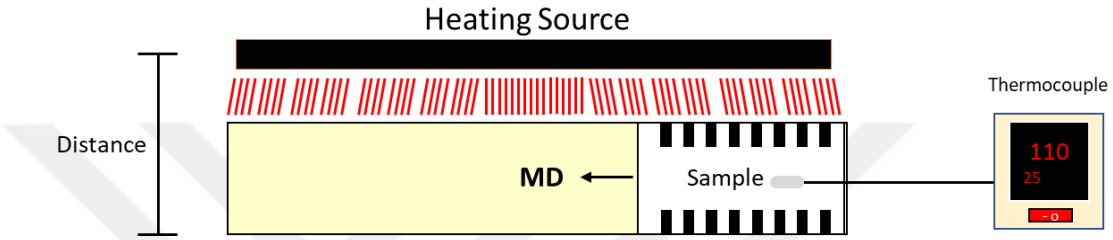

Figure 2.17 : Custom-made uniaxial stretching machine.

2.5.2.2 Extraction of the oil

Final stretched film samples are washed with n-hexane bath for 24h then for another 3h using ultrasonic to fully extract paraffin oil. Finally, the samples are taken out and left to fully dry. Weight of the samples before and after extraction is recorded and the weight loss is calculated to determine the efficiency of the extraction process

2.5.3 Characterization and analysis

2.5.3.1 Morphological analysis

The sample's morphological Analysis was done using Scanning Electro Microscopy (SEM). SEM is used to scan the surface of the sample and produce an image of its topography and composition. An energized highly-accelerated electron beam is produced from a heated filament and ejected toward the sample in a vacuumed chamber. When the beam hits the sample, electrons are emitted while others are scattered and deflected of the samples. These electrons are collected by image detector where an image is formed based on the intensity of these electrons to produce a contrast image revealing the topography of the sample.

TESCAN VEGA 3 SEM was used with Au/Pd sputter coating, 2-5nm for 180s. Images with magnifications in the range of 500x to 60,000x was taken with a voltage of 5-10kV and 3.0 beam intensity.

2.5.3.2 Thermal analysis

Melting temperature and crystalllinity of UHMWPE gel and UHMWPE membrane was analyzed using differential scanning calorimetry (DSC). The spanning range was done between room temperature and 160℃ with 10℃/min heating and cooling pace.

2.5.3.3 Electrochemical impedance spectroscopy (EIS)

EIS is a powerful, non-destructive in-situ and ex-situ technique used to characterize electrochemical systems and their interfacial properties by sending an amplitude and detecting the response. Reactions, electroactive species, mass transfer, charge transfer, diffusion and the resistance are all measured [62]. These features responses are mimicked and interpreted by electrical circuits and their elements like resistors, capacitors and constant phase elements and whether they are in series or parallel. While resistance is observed in DC circuits, impedance is its counterpart in AC circuits that doesn't follow Ohm's law.

Tests were carried on SP-150 workstation in a frequency range of 10mHz-10kHz with 10mV amplitude. Three UHMWPE samples were prepared and tested in full cell configuration using stainless steel spacer electrodes and 1.0 M sodium perchlorate (NaCI04) in EC/DEC/PC (1:1:0.05 by volume) . The samples names are S1, S2 and S3 according to their stretching ratios. Carbon cloth/separator/Sodium metal configuration is shown in Figure 2.18.

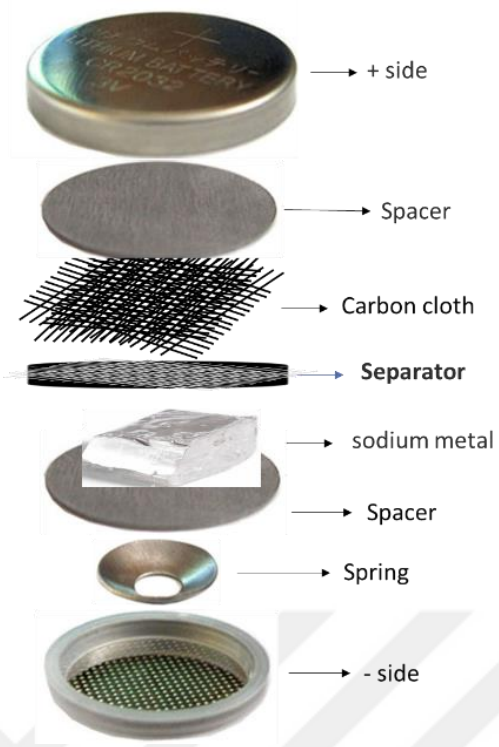

Figure 2.18 : Full cell configuration.

2.6 Results and Discussion

Samples obtained from the strip die tend to be thick white in color when cooled down as shown in left side of Figure 2.19. The thickness of these sheets is in the range of 3-5mm. These slabs are taken into hot press with consideration for the machine and transverse direction for stretching and extraction process. On the right of Figure 2.19, the pressed sample is shown.

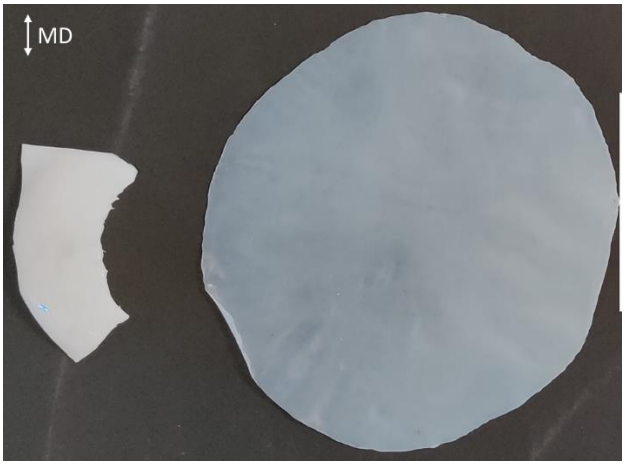

Figure 2.19 : Stripe die slaps before (left) and after (right) hot press.

Rectangular thin sheets are turned into final circular shape after hot press. Lack of proper thin molds and imbalances in the hot press machine plates caused the loss of the rectangular film shape and non-uniform thickness of the hot-pressed samples. Overall hot-pressed samples had a thickness in the range of 200-400 μm. First trials were done to examine the film structure without applying any stretch. Figure 2.20a shows extracted film with no treatments applied. The film didn't show any porous structure. While in some areas, surface deformation can be observed due to the extraction of oil. Figure 2.20b shows that oil extraction without applying any form of extraction causes some cracks on the film surface. For that reason, stretching is applied before extracting the oil to obtain proper porous structure.

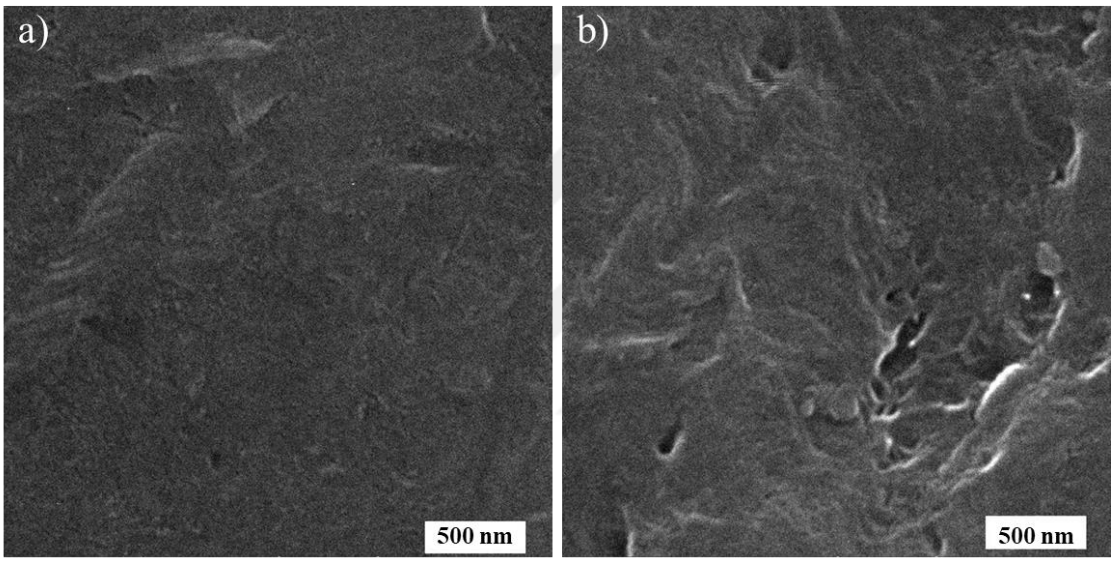

Figure 2.20 : UHMWPE film; a) full film structure, b) aperture areas.

In order to determine proper stretching temperature range, DSC analysis was done on the gel samples. It was found that stretching above melting point of PE (T_m=135℃) lead to sample break and melting of the film which is known to be neck stretching. This made the stretching window of the film lies below 135℃. The range that was found according to the preliminery studies and literature [63] lies in the range of 90-115℃ as shwon in Figure 2.21**.**

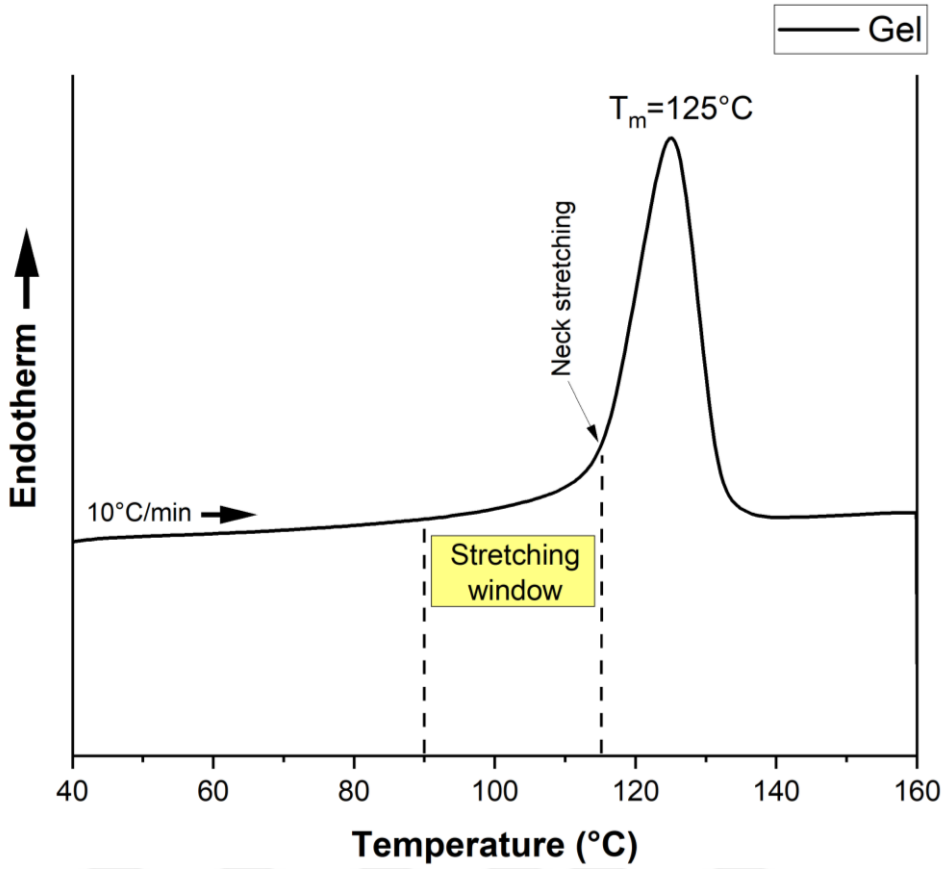

Figure 2.21 : DSC graph of the gel film.

After that, experiments were conducted to compare whether n-hexane extraction stage should be carried before or after stretching of the samples. shows SEM images of the samples. Figure 2.22 shows SEM images of the samples. Both samples were stretched at 110℃ with a stretching ratio of 700%. It can be seen in Figure 2.22a that slit-like pores are formed with big diameter in the longitudinal direction up to 5 μm. While in Figure 2.22b and Figure 2.22c, it shows smaller pores in the range of 50-200nm with higher overall porosity. Overall, extraction of the oil after the stretching process resulted in smaller pore size, and more uniform distribution which corresponds to what was found in another study [64]. Where 100-130nm pore size was obtained by stretching before extraction process and 240-340nm from the extraction then stretching process.

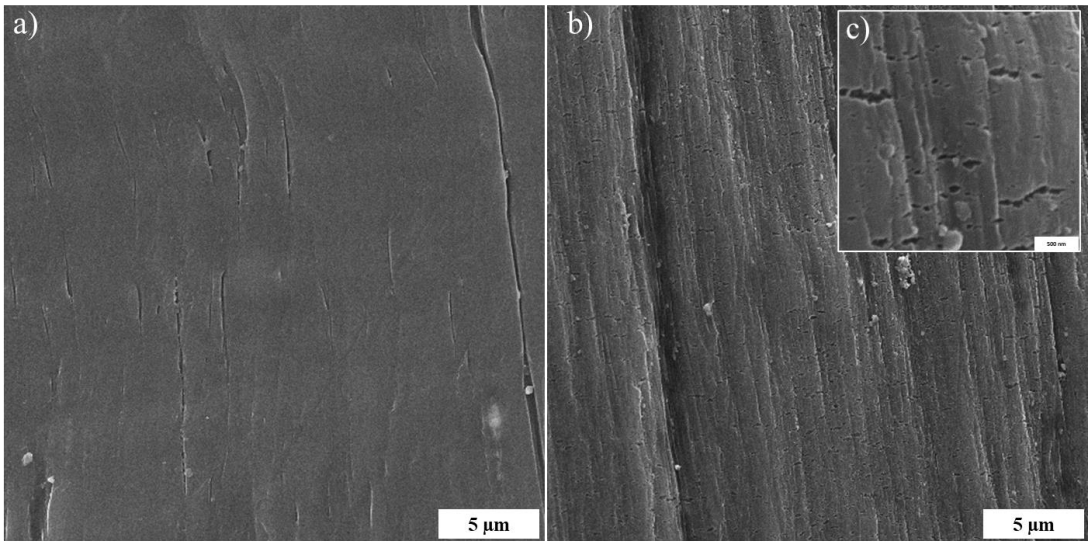

Figure 2.22 : Effect of extraction step, a) extraction → stretching, b) stretching → extraction, c) magnified image of b (500nm scale).

At higher stretching ratio up to 800%, the pores are closed and all chains are fully extended as can be seen I n Figure 2.23a. While in Figure 2.23b and Figure 2.23c, the pore structure is still intact and semi-porous membrane is achieved.

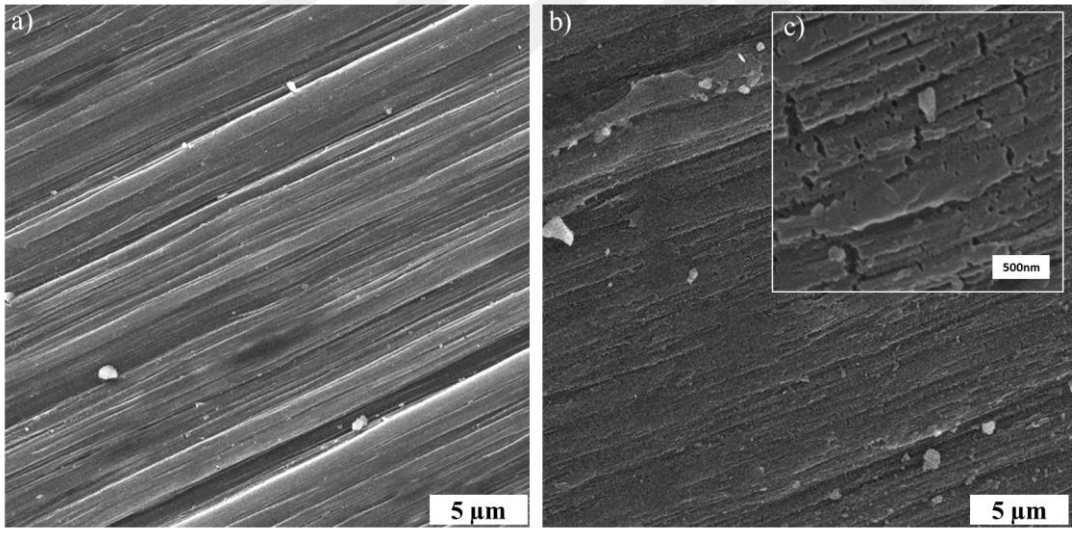

Figure 2.23 : Effect of stretching ratio (800% stretching ratio), a) extraction → stretching sample, b) stretching → extraction sample, c) magnified image of b (500nm scale).

It can be concluded from the previous figures that stretching the samples before extraction of oil achieved better pore formation. Also the higher stretching ratios (Figure 2.23) could achieve better chain orientation which in consequence are preferrable to achieve higher mechanical strength [63]. For these reasons, all

experiments were conducted by stretching the samples before dispatching them into n-hexane extraction bath.

2.6.1 Constrained uniaxial stretching optimization

After the preliminary experiments, stretching of the samples was done using the home-made uniaxial stretching machine. Since the home-made uniaxial stretching system is based on open system design and thermal radiation heating is used, optimization of the system was needed to determine optimum distance for thermal radiation heat to be applied from. Also, determination of the stretch ratio limits in MD and TD is needed. Firstly, proper stretching ratio was determined. It was found that with almost 100% stretch ratio in MD and 50% in TD (Figure 2.25a), acceptable pore structure was obtained. Upon further stretch of the sample, the pores started to take more of a linear shape and the chains showed observable chain orientation toward highly oriented shish-kebab formation (Figure 2.25b). All fabricated samples were stretched without exceeding the 2×1 (MD×TD) stretch ratio. Later on, the distance between the thermal irradiator and the samples was tested. Distances of 13.5, 16.5, and 19.5 cm was tested. As can be seen from Figure 2.24, when distance was 16.5 cm (Figure 2.24b) optimum mebrane was obtained. Shish kepap-formation with acceptable homogeneous pores were acquired. The SEM image gained in Figure 2.24b looks typical to other membranes fabricated by Wang et al and his group [65]. While for Figure 2.24a, the pores almost vanished due to the excessive heat applied and melting of the film. In Figure 2.24c, no pores can be observed at all. That was referred to the fact not enough heat reached the membrane, so the chains crystals didn’t align properly and fibrils in the amorphous region didn’t form.

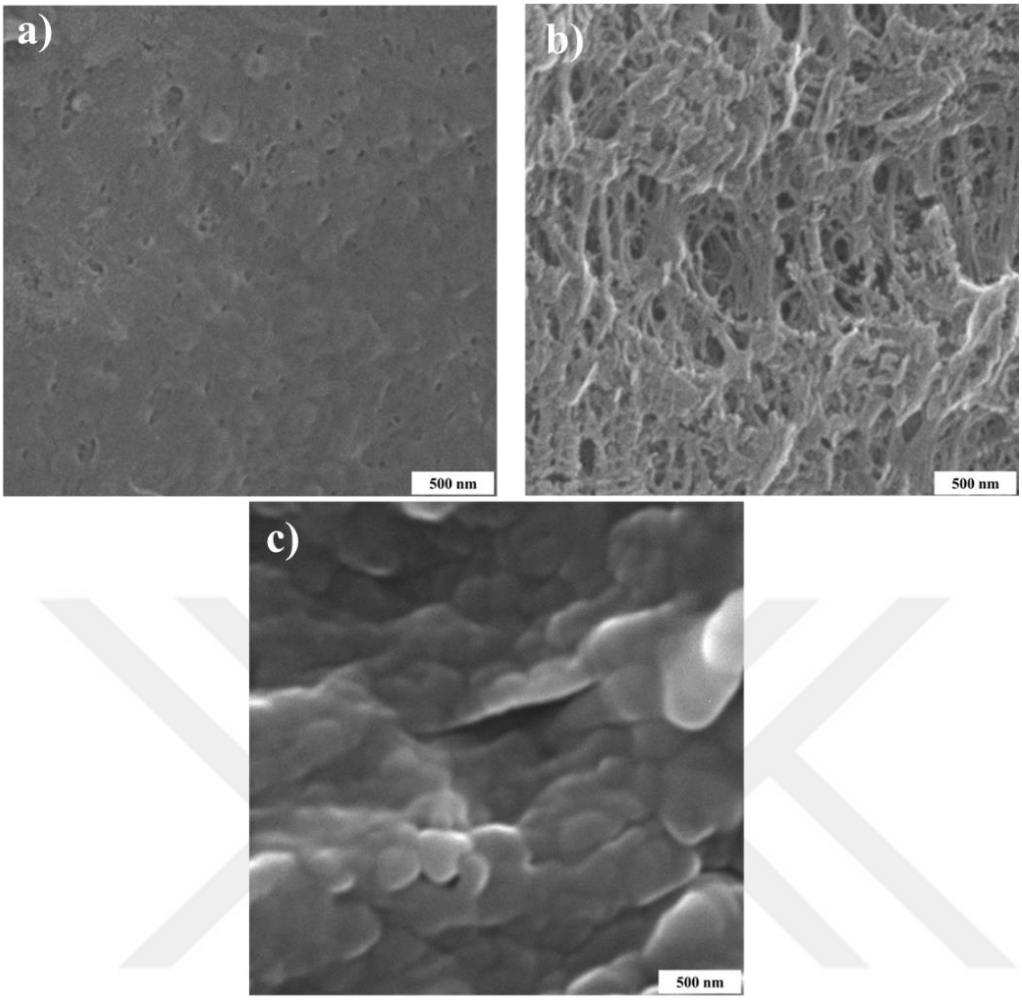

Figure 2.24 : Effect of heating distance on membranes with a) 13.5cm, b) 16.5 cm, and c) 19.5cm distance between sample and the heat source.

After optimizing the proper distance and temperature needed to achieve best pore structure, optimization of the stretch ratio to be applied is carried. Samples were stretched in both MD and TD. The stretch ratio is denoted in MD×TD structure. Two stretching ratios applied in which they are 2×1.5 and 4×1.5. The TD stretching was held constant due to the machine limitations. The SEM images show that the 2×1.5 stretching ratio (Figure 2.25a) achieved acceptable pore structure with good porosity. Upon further stretching in both MD and TD, formation of highly oriented shish kebab is achieved and pores started to take more of a slit-like shapes (Figure 2.25b).

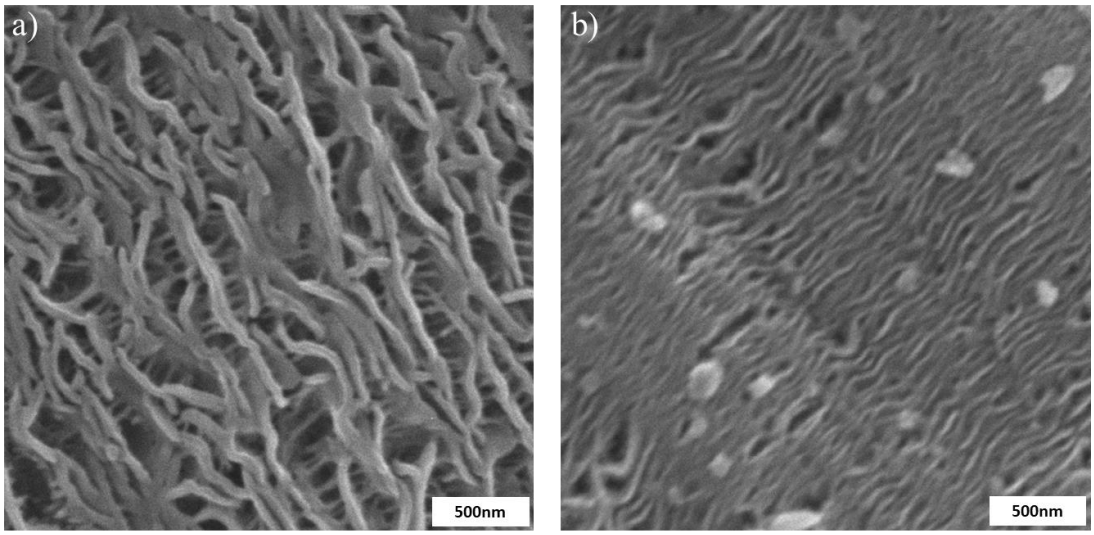

Figure 2.25 : Biaxial stretching, a) 2×1.5 stretch ratio, b) 4×1.5 stretch ratio.

These results lead to optimum of 2×1.5 stretching ratio, and a distance of 16.5 cm between the heat source and the sample.

2.6.2 Membrane formation

After the preliminary studies, three samples (S1, S2, and S3) were fabricated and studied under the same conditions excepet for the stretching ratio. The SEM images of these membranes are shown in Figure 2.26. These sample were stretched under the same conditions with same stretching ratio and heating distance. The difference is in the precursor sample which lead to different porous structures and diffirent final thicknesses. It can be seen that the sample with antixoidant (S1) in Figure 2.26a showed more heterogeneuos structure and lead to breakage of some samples while stretching. That could be referred to nonsufficient mixing in the extruder which lead to film breakage yet a proper sample was obtained and characterized. S2 sample (Figure 2.26b) shows a perfect porous structure with oriented lamellae structure. This ordered structured is gained due to the high plasticization ratio (70% PO) where the slip of lamella is dominant [66]. Figure 2.26c shows S3 sample which carries the highest thickness which is similar to other UHMWPE membranes in literature [65].

Table 2.3 summarizes the process conditins and obtained properties of the samples. The weight drop after extraction with n-hexane shows variation in extraction efficiency. This could be casued by various reasongs. Eventhough the inital or expected concentration of the oil in the samples is aimed to be around 70%, the oil loss

starts from the moment the sheet comes out of the dies and starts to coold down. Because phase separation occur at lower temperatures in the wet process.

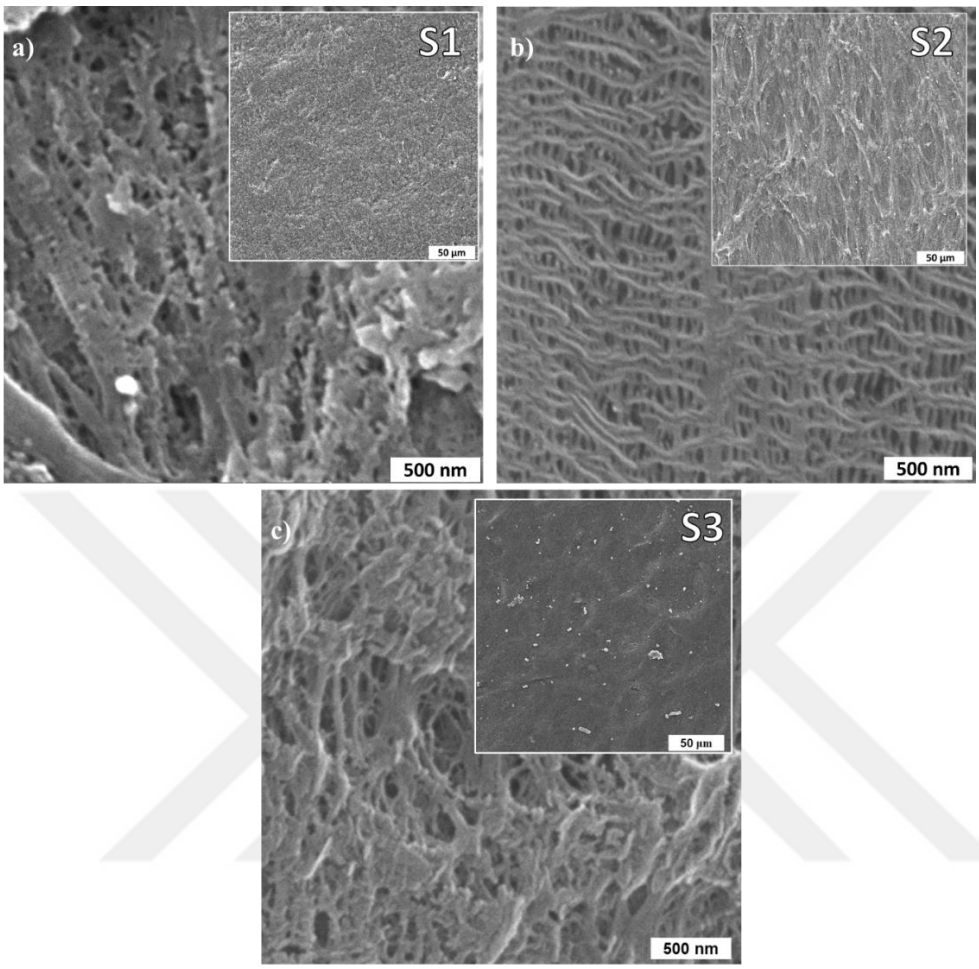

Figure 2.26 : Fabricated membranes, (a) S1, (b) S2, and (c) S3 membrane samples.

Table 2.3 : Fabricated membranes properties.

Sample name	Pre-stretching thickness	Post-stretching thickness	Stretching ratio MD/TD	% weight drop (after extraction)
S1	280	40	3.75	53
S2	200	60	1.25	44
S3	280	80	1.85	42

S1 sample showed a degree of deformation and nonhomogeneous structure that could be interpreted by the fact that it bared the higher MD/TD stretching ratio. even though it has the least final thickness. This shows that the precursor condition is detrimental for the final membrane structure. On the other hand, when smaller stretching ratios were applied (S3) for the same initial thickness, the final thickness was relatively higher and the pore structure and porosity of the samples are less in comparison to S2 samples.

2.6.3 EIS

In terms of the chemical performance, the three seprators were characterized with full cell configuration. Figure 2.27a shows the nyquist plot of the samples the x-intercept of the curves denots the bulk (separator) resistance. Figure 2.27b shows the equivalent circuit for the full cell system. In this circuit, anode region, electrolyte region, and cathode region is considered. In the anode region, the movement of lithium ions is impeded by resistance that occurs at the solid electrolyte interphase (SEI) and solid-liquid (S-L) interface. This resistance can be characterized using a circuit model that includes a constant phase angle element (Q2) in parallel with a mass transfer resistance (R2), as well as a double electric layer capacitor (C1) in parallel with a charge transfer resistance (R1) [67]. The ohmic resistance of the electrolyte with the porous structure of the film is denoted by R3. Cathode region consists of a two parallel CPE and resistance circuits. Which also refers to the S-L interface and lithium transmission through passivation film [68]. The calculated ionic conductivities of the samples are shown in Table 2.4. It can be seen that S2 has the higher ionic condutivity and least resistance which is expected as Figure 2.26b shows that the sample had high porosity with homogeneous structure, which led for better electrolyte uptake and ease of ion transfer. S3 had the least ionic condutivity and highest resistance. This significant increase is correlated to the significant larger thickness of the sample.

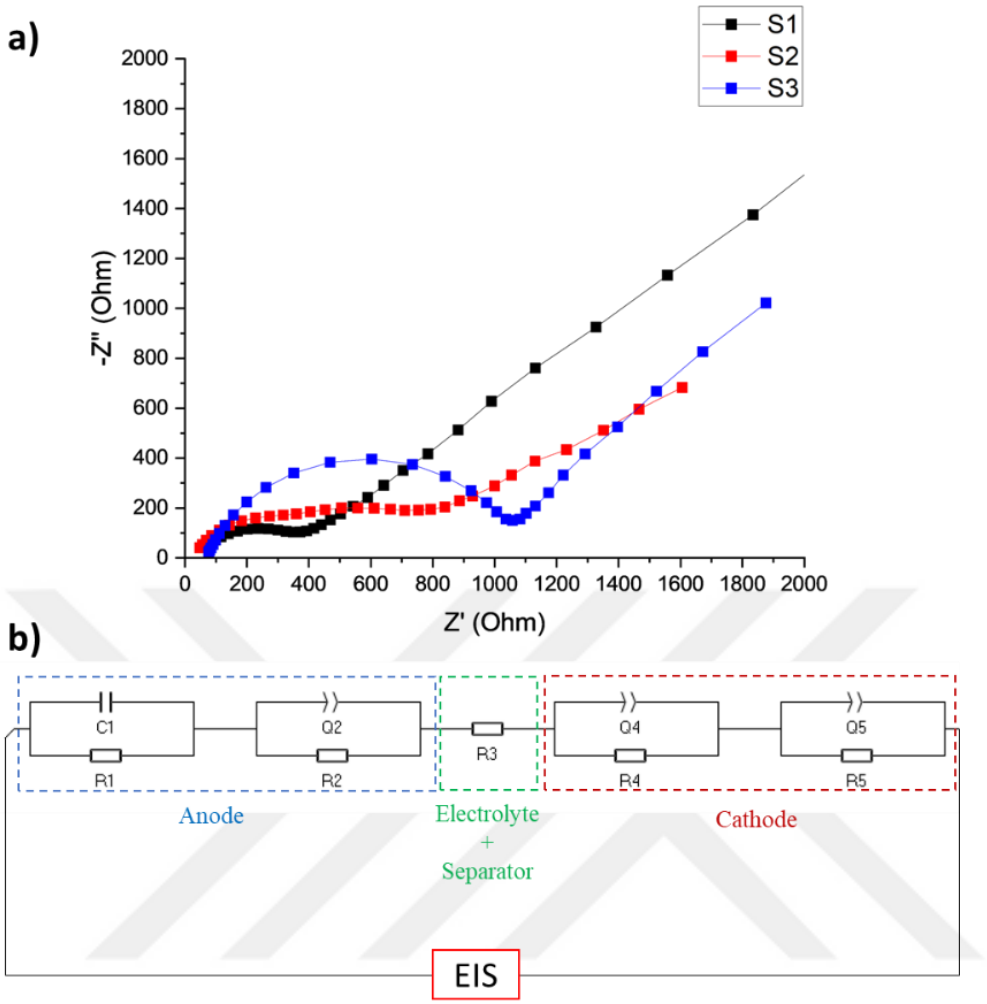

Figure 2.27 : EIS analysis, a) Nyquist plot, b) proposed quivalent circuit.

Table 2.4 : Ionic conductivities of the samples.

Sample	Thickness (µm)	Bulk resistance (ohm)	Ionic Conductivity (mS/cm^2)
S1	40	16.15	0.09
S2	60	4.413	0.48
S3	80	69.38	0.04

3. NANOFIBROUS MEMBRANE

3.1 Introduction

In the last decade with booming innovation technology, nanomaterials come among the top research topics that hold a lot of potential to revolutionize our world. Nanostructures like nanofibers, nanorods, and nanotubes has even found its road out of research centers into real-life applications [69]. Nanofibers are one-dimension (1D) nanostructures with one of its dimensions within the nanometer range. Nanofibers can be synthesized using different techniques like phase separation, drawing, self-assembly, and electrospinning with the latter being among the most popular ones. Electrospun nanofibers exhibit a high porosity, high surface area to volume ratio and high versatility while the main drawback of the technique is its low draw ratio [70]. Current research on nanofibers is concentrated on more complex architectures like hollow, and porous nanofibers where they carry better porous connectivity, higher volume to surface area ratio, and high versatility [71]. Hollow nanofibers can be obtained by several methods as self-assembly [72], template synthesis [73], electrospinning [74], and recently arising solution blowing [75]. Solution blowing utilizes pressurized air as the driving force to eject nanofibers. This technique is cost-effective and carries the advantage of reaching high throughputs suitable for industrial mass production. For hollow nanofiber production, a coaxial spinneret is used where a path for two solutions to be spun is provided.

3.2 Nanofiber Production Techniques

3.2.1 Electrospinning

Electrospinning is the most common and widely used method in research and production of nanofibers. It is a simple electrostatic technique. As shown in Figure 3.1, the system consists of a syringe holding the polymer solution, a syringe pump to supply continuous feed, a power supply to create voltage difference, and a collector to collect synthesized nanofibers. The polymer solution under the force of voltage is elongated and thrust toward the collector in

conical shape. The solvent is evaporated while the fiber jet is travelling from the nozzle toward the collector. The fiber formation and diameter depend on several factors. The polymer viscosity and spinnability, the feed rate, nozzle to collector distance, and the voltage supplied [76].

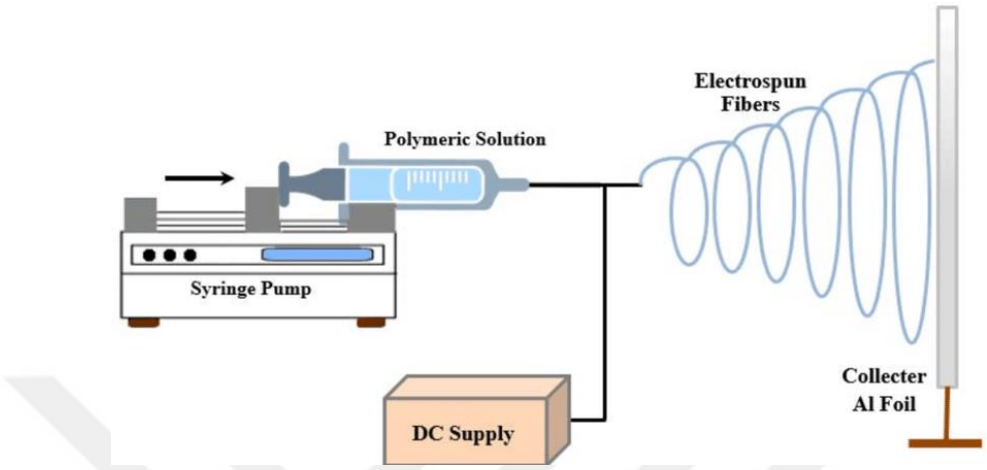

Figure 3.1 : Electrospinning system **[77]**.

While in common electrospinning technique, the solution is dissolved in a solvent and then evaporated, in melt electrospinning (Figure 3.2) the polymer is melted by heating resistance around a metal syringe and without the use of any solvent under the force of electricity the nanofibers are ejected. Melt electrospinning is known to be more environmental friendly approach as it doesnt utilize additional solvents that could be released to the surrounding environment.

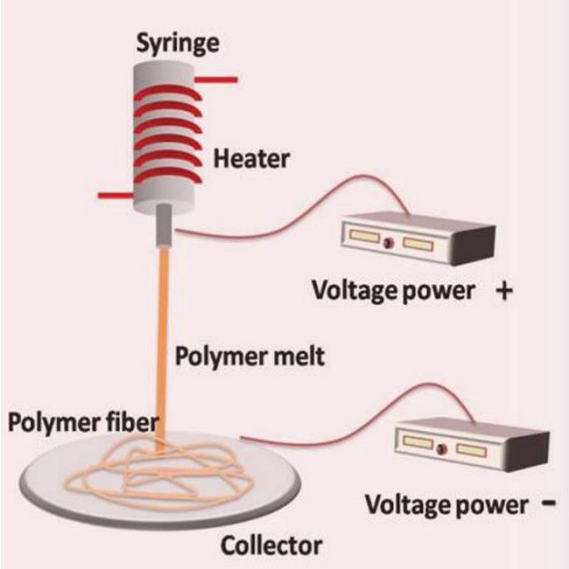

Figure 3.2 : Melt electrospinning scheme [70].

3.2.2 Melt blowing

The other method used to fabricate fibers and nanofibers is melt blowing. This method goes back to the 1950s to the naval laboratories in the united states where the research was going to collect radioactive particles un the upper atmosphere, then thermoplastic microfibers started to be produced with this technique [78]. Through the years, the method was developed and nanofibers with diameters below 100 nm range is fabricated through this technique [79]. A schematic of the melt blown system is shown in Figure 3.3. In this system, a heated air is pressurized through the die ejected the melt extruded thermoplastic fibers into the collector.

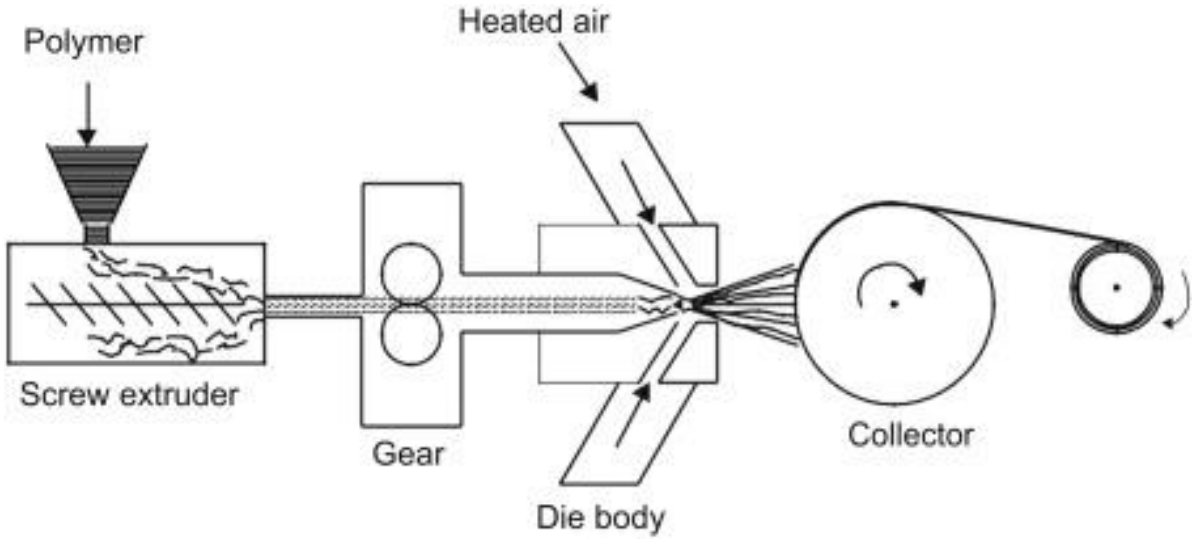

Figure 3.3 : Melt blowing system [80].

3.2.3 Solution blowing

Solution blowing is similar to melt blowing where the driving force used to eject the fibers is the pressurized air. But it differs in the polymer feeding state. In solution blowing, the polymer is dissolved in a solvent and fed with a syringe pump to the nozzle, then pressurized air discharge the polymer elongating the fibers and evaporating the solvent in the way toward the collector. This method can be classified as a combination between melt blowing and electrospinning techniques. In solution blowing, electricity can be introduced as a secondary driving force along side the drag force. Air pressure is a key factor in this process [75]. Solution blowing process scheme is shown in Figure 3.4

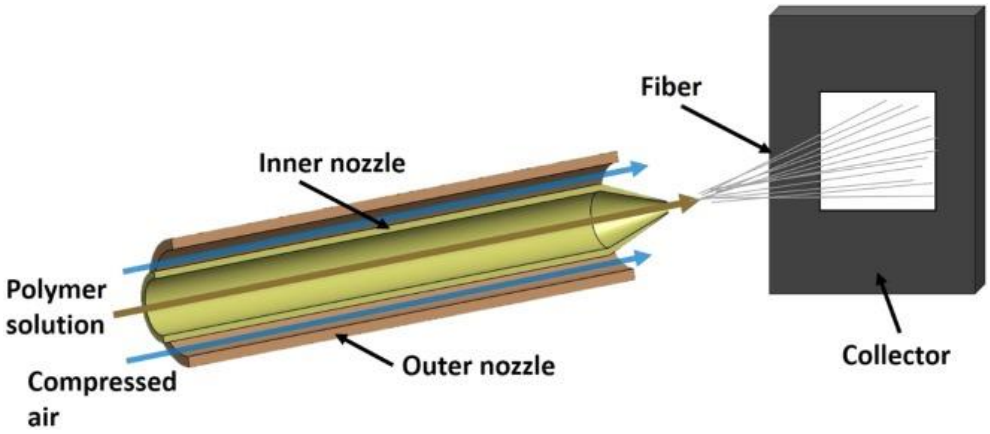

Figure 3.4: Solution blowing system [81].

3.2.4 Centrifuge spinning

This technique depends on the centrifugal forces to obtain nanofibers insted of using voltage or pressurized air. It consistes mainly of a motor-driven rotating spinneret about its axis. Which when spinned with enough angular speed, the polymer will be ejected to the collector [82]. Scheme of the process is shown in Figure 3.5.

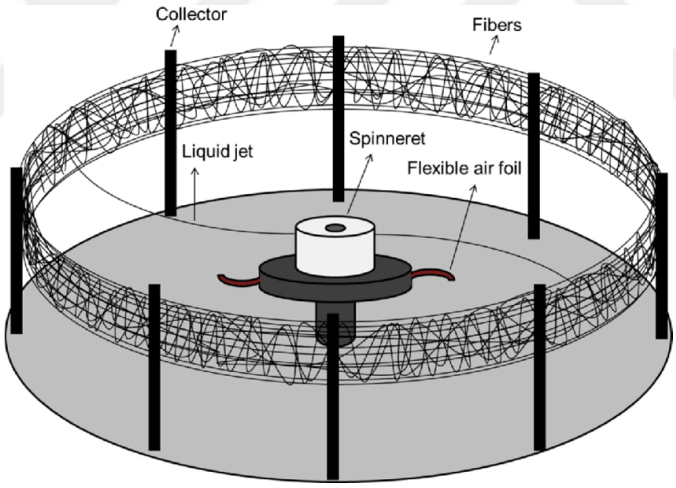

Figure 3.5 : Centrifugal spinning [83].

3.2.5 Template synthesis

In this method (Figure 3.6), the nanofibers are synthesized using a specially designed template or mold. The desired structure are obtained then using this template. Normally, the polymeric solution is deposited on the template which is normally a porous metal oxide membrane. The polymeric solution is pressurized through the metal membrane where solydifying solution is set underneath. Nanofibers are then extruded from the nanopores of the template [84].

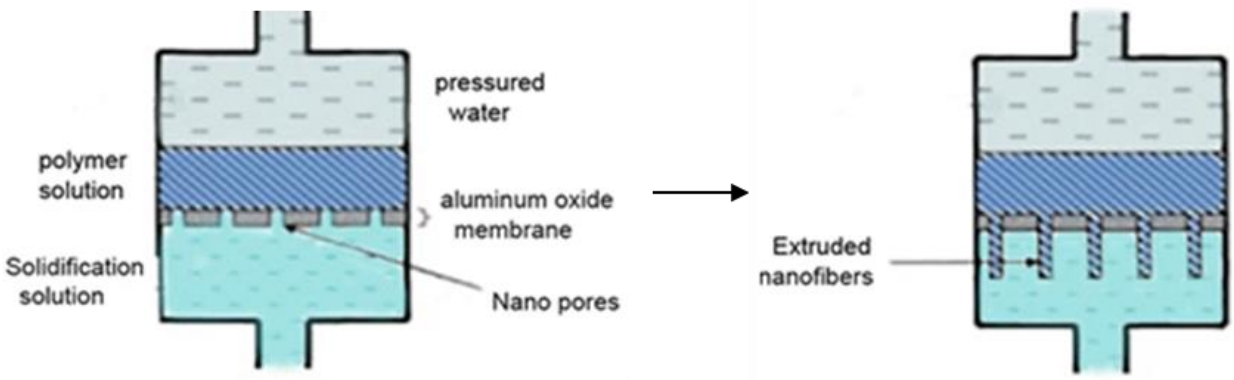

Figure 3.6 : Template synthesis method [84].

3.2.6 Self-assembly

This method is classified as one of the bottom-up methods used to fabricate nanofibers. In this method, polymer molecules arrange themselves in patterns and structures without forming covalent bonds. Instead, these formations are hold by other forces like electrostatic forces and hydrophobic forces [85]. Small nanofibers are fabricated with this technique. Nanofibers with lengths of 100nm up few micrometers. The main drawback of this method is its low productivity, complexicity and extremely time consuming [84].

3.2.7 Coaxial spinning

In the coaxial spinning of nanofibers, the polymeric solution is fed into a nozzle with two outputs. In this process multiple materials can be released even in the precense of immiscible solvents. The most common form nanofiber produced using this technique is known as core-shell nanofibers where one polymer forme the core of the nanofiber and the other forms the shell. Hollow nanofibers are another formed obtained by coaxial spinning process (Figure 3.7). Where in hollow nanofibers, the inner fluid works as an immiscible template [86].

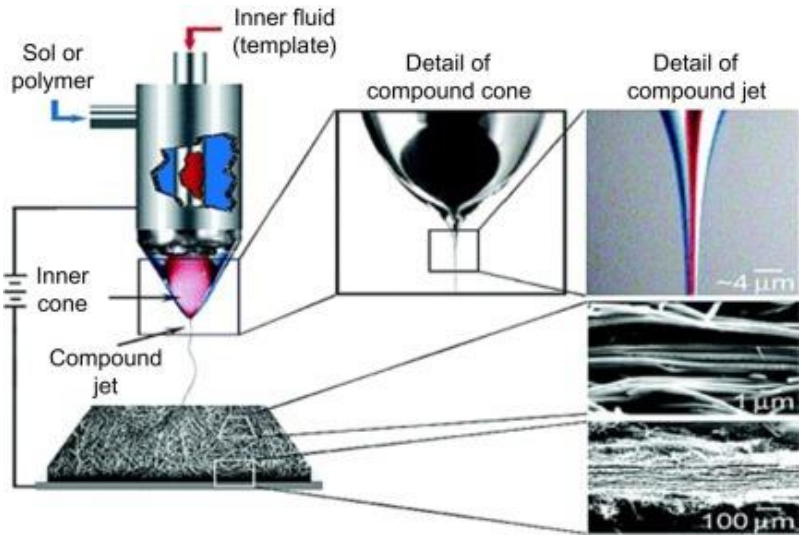

Figure 3.7 : Coaxial spinning scheme [86].

3.2.8 Centrifuge Spinning Process

Centrifuge spinning is an old technique was used in fiber glass production. Where the melted glass was coming to a hot rotor releases fiber glasses with diameters aroun 1 µm. This happens due to the centrifugal force casued by high speed rotation of the rotor where melt is elongated and discharged outward forming fibers [87]. In terms of nanofibers, in centrifugal spinning, the polymeric solution is pushed out of the rotating nozzle by the centrifugal force, where the solvent evaporates and fibers are formed and collected around the collector [88]. Revolutions up to 30000rpm is acieved and nanofibers of diameters below the 100nm range [89].

3.2.9 Working principle

Figure 3.8 shows a schematic view of the centrifuge spinning process used in this study.

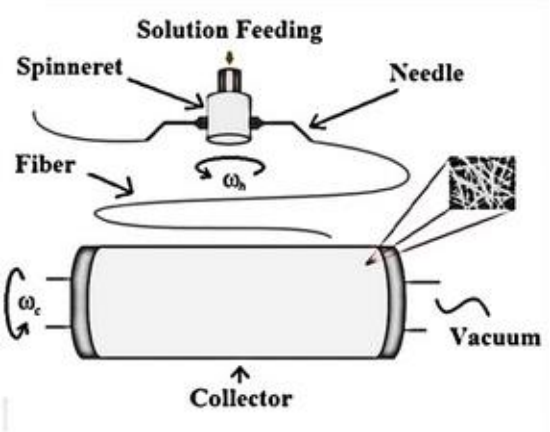

Figure 3.8 : Centrifuge spinning system [90].

The polymer solution is fed into a motor-rotated spinneret that rotates around its axis, when the limitation for fiber formation is overcome, fibers are ejected and formed. The limit is considered to be the balance between the surface tension of the solution and the centrifuge force. When the centrifugal forces are increased significantly, the fibers are broken and bead spraying started to take place [90]. The fibers follows a twisted path lead by the centrifuge force before it faces the air resistance along their way toward the vaccum-equipped collector. In some other systems, air flow is used to directorate the path of fibers [91].

The stages a polymer solution follows in the centrifuge spinning can be summarized into three stages. The first stage is where polymer solution is fed to the nozzle. As the material rotates along with the spinneret, various forces such as friction, gravity, surface tension, and centrifugal force come into play. However, it is primarily the surface tension and centrifugal force that dominate the process, while the other forces can be considered negligible [87]. In the second stage the polymer is expelled off the nozzle because of the centrifugal force. In the third and finals stage fibers foolow a curved way reaching the collector while vaporating the solvent. The movement of fibers in this stage is accounted to the force of inertia. The solidified fiber diameter become less and less while travelling along the way as shown in Figure 3.9 I and II.

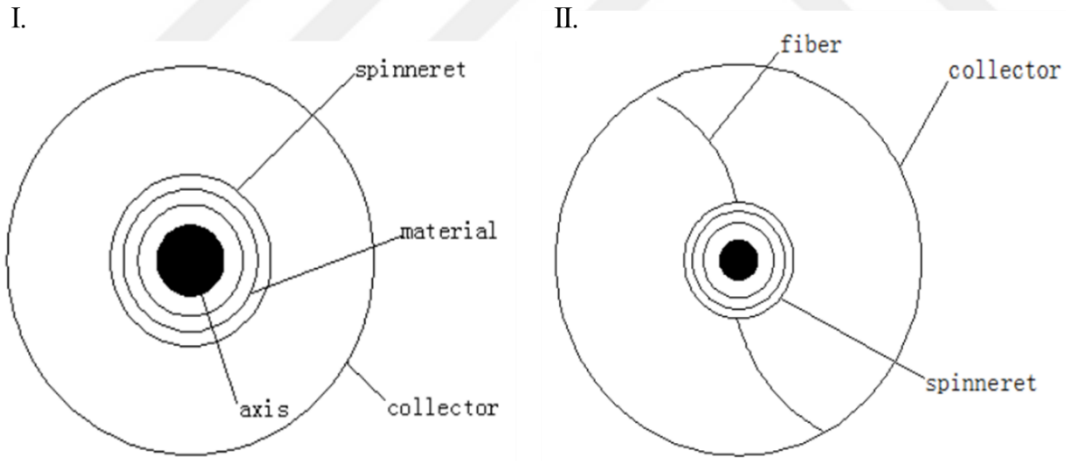

Figure 3.9 : Solution path during spinning I) material rotating with the spinneret, II) fibers are expelled toward the collector [87].

3.2.10 Process parameters

There are several factors comes into play when a solution is being spun and the fibers are formed. They can be divided into material-related parameters, and process-related parameters.

Material properties like surface tension, viscosity or concentration, and solvent ratio plays a key role in the fiber formation. Process parameters includes; spinning speed, feeding rate, needle gauge, and distance to collector.

The surface tension of the soluion increases the surface energy casuing droplet formation. Increasing the centrifugal force will help connecting the beads and obtaining fiber structure. In terms of viscosity, the higher the viscosity, the higher the force needed to eject fibers. The force needed to prohibit tangling of molecules together sometimes can't be achieved due to the high viscosity of the material Several factors could affect the viscosity as temperature, and molecular weigth of the polymer. Solvent ratio and type is also of great importance as it evaporates leaving a solidifyied polymer fiber structure. The solvent type and ratio affects the evaporation rate which in turn affect the final fiber diameter.

In terms of process parameters, spinning speed is the biggest player in fiber formation It's the driving force of the whole process. Low spinning speeds could lead to inadequate force to eject fibers or connect the formed beads. Excessive speed could lead to breaking the fibers as they overwhelm the surface tension of the solution. Feeding rate is directly related to the spinning speed. Needle gauge is a detrimental factor in obtaining a beadless small diameter fibers. Large guages results in drop formation while small gauges results in smaller final fiber diameters [87]

All these factors should be optimized and taken into precise consideration to gain optimum nanofibers.

3.2.11 Literature Review

Nanofibers has been used in different fields for distinct purposes. They can be used in electronics, biological and health care, energy, and environmental sectors [92]. PVP and gallium oxide nanofibers were obtained by sol-gel method and were used in optoelectronic devices exhibited excellent charge carrier mobility, significant fluorescence quantum yields, and high thermal-chemical stability [93]. Electrospun PVC nanofibers loaded with some chemicals showed powerful performance in detoxifying paraoxon (pesticide) [94]. Half of currently used membranes are used in water and wastewater treatment applications as water and air purifications are of the greatest demand. Membranes are defined as a polymer-based barrier with a porous structure. Figure 3.10 shows a membrane in action separating some contaminants.

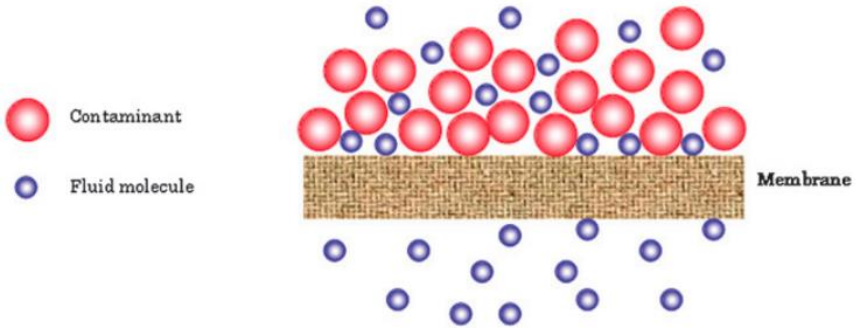

Figure 3.10 : Nanofiber membrane separating some contaminants [95].

Nanofiber mats compared to conventional fibers has much smaller pore size and distribution. Also, dust capturing membranes are used to capture the particulates coming from natural sources like soil or from coals. These particulates could lead to serious health issues. Due to the small pore size of nanofibers, clogging of the filtration media and the drop in the air flow rate is slowed down. These particles could then remove and the performance is recovered by back flushing. This results in a high shelf life of nanofiber membranes [95]. With the high demand on water, nanofibers flourish in the field of water filtration. PVDF nanofiber membranes were exposed to plasma inducing copolymerization of poly(methacrylic acid) and compared to MF membranes in terms of water flux. Electrospun nanofiber membranes exhibited flux up to 50,000 kg/hr*m^2 in comparison to less than 10,000 for the commercial PVDF MF membranes [96]. Nanofibers perform better in air filtration applications and small fibers accomplish higher efficiencies due to the interception and inertial impaction, which make them have lower pressure drops in comparison to big fibers [97].

In environmental management strategies, sensors play a critical role in detection threats and contaminations. Nanofiber-based sensors are gaining more popularity by the day. Many pollutants that carry severe threats on livings exist in water. Nanofibers based sensors with their molecularly imprinted nanoparticles is able to detect propranolol in tap water. Which is a medicine that used for heart rate and blood pressure control [95]. Air pollution is another serious issue of industrial cities and areas. The detection and filtration of particulate matter in theses places is extremely important for the well-being of living and non-living matters. Greenhouse gases, nitrogen oxides, and sulfur oxides cause severe environmental consequences. Detection of NH_3 and NO_2 in air was achieved by MoO_3 electrospun nanofibers [98]. These nanofibers were found to have critical and superior characteristics in comparison to normal film-structured

membranes. The future sensors have to be more sensitive and able to detect broad range of materials. For that reason, Nanofibers would enhance the performance of them.

He Lian and Zhaoxu Meng (2016) made a comparative study between melt and solution electrospun fibers for drug loading applications [70]. They've made Curcumin-loaded poly (ε-caprolactone) (PCL) fibers using the two electrospinning techniques. PCL fibers are biodegradable, biocompatible and has low melting points. This feature makes it among the best polymers for encapsulating many drugs within wide range of temperatures. Curcumin, with its excellent fluorescent ability is an anti-cancer drug. It also not affected by melt spinning temperature and exhibits stable performance and easy to detect and follow. The melt spun fibers showed a smooth surface and high crystallinity in comparison to the more porous and more amorphous solution electrospun fibers. These differences showed a different in drug release rate. The melt electrospun showed a more stable releast rate while the melt electrospun had a high release rate with a burst behavior. They showed that along the no toxic solvent usage in melt electrospinning, it also showed better properties that is more suitable for drug delivery [70]. Zupancic et. al. studied the preparation of drug-loaded PCL nanofibers and their antibacterial and drug-release abilities [99]. In this study, three types of drugs were used with different activities in periodontal pathogens. PCL fibers were loaded with metronidazole (MTZ), which is used in treatment of periodontal disease (bacteria in teeth root), and ciprofloxacin (CIP), which has antibacterial activity. Electrospinning reduced the drug crystallinity compared to the pure substances [99]. Nanofibers holds the potential for controllable, efficient drug release applications.

Nanofibers can be used also in different parts of the batteries as they can be used in anodes, cathodes, and separators. As carbon is the dominant component of the anode in lithium-ion batteries, carbon-based nanofibers (CNFs) were investigated with various polymers. PAN-derived CNF anodes [100], and PVP-based CNF anodes were investigated [101]. Nanofibers with their unique structure have been intensively studied for Li-ion battery separator purposes. Battery separators need to have good chemical stability, good thermal stability, and adequate mechanical performance. Several polymer-based nanofibers were investigated. PVDF nanofibers were studied a lot for battery separators, whether only PVDF separators [12], or with some addition of other inorganic nanoparticles like SiO_2 [102]. Several other nanofibers like PI and PAN were also studied [103].

3.2.12 Thermoplastic polyurethane (TPU) nanofibers

Thermoplastic polyurethane (TPU) is a high toughness, high strength, with high durability and wear resistance polymer. It attracts the scientific research as it's also biodegradable and biocompatible, several studies were conducted on TPU nanofibers for various applications including medical [104], food [105], textile [106], and other industries [107]. 200-250nm TPU fiber diameters were obtained using electrospinning for wound healing applications [108]. The implementation of TPU nanofibers in energy applications is increasing. Several research papers covered the usage of these nanofibers. Shehata et al prepared stretchable TPU/PVDF nanocpomposite for piezoelectric energy harvesting applications [109]. The elastic nature of TPU improves the mechanical strength of the composite which increases the the piezoelectric response of the nanocomposite. TPU is also used in battery separators, particularly in flexible batteries for wearable devices and other applications where flexibility and stretchability are required. TPU is a versatile polymer that has good mechanical properties, chemical resistance, and low permeability, which make it suitable for use in battery separators. Additionally, TPU can be easily processed into nanofibers, which can further enhance the performance of the battery separator. Tang et al used PAN nanofibers lack of elasticity by integrating TPU in the structure, gaining a flexible structure even on high temperatures [110]. This combination made the performance of the separator in LiB higher than the performance of the commercially available Celgard 2400 separator. In another work [111], non-flammable TPU gel polymer electrolyte (GPE) was fabricated without the usage of any flame retardent additives. PVDF-HFP sandwiched TPU achieved significant flame retardency. It was found that $LiPF_6$, the common electrolyte used in LiBs, enhanced the TPU flame retardency ability due to the protective layer formed on the TPU due to the side reactions occuring upon burning. Cone tests has indicated that $LiPF_6$ encourages the creation of char in TPU, leading to a noteworthy decrease in the Heat Release Rate (HRR) and Total Heat Release (THR) of TPU GPE. This thermal insulation protective layer prevents TPU GPE from decomposing and catching fire. In term of electrochemical performance, it was found that TPU based films manifest sufficient ionic conductivity of 0.48 mS cm^{-1}, a capacity retention of 91% after 200 cycles, and high lithium ion transport number ($t_+ = 0.68$) [112]. ion transport number, also called the transference number, is the fraction of the total electric current carried in an electrolyte by a given ionic species *i* and is calculated by the following equation; $t_i = \frac{I_i}{I_{tot}}$. TPU nanofiber

combination with other polymers like PVDF as a battery separator has been investigated in several studies [113]–[115].

3.2.13 TPU surface modification

As TPU is considered to be a hydrophobic biodegradable polymer, with some commercial grades are classified to be hydrophilic, it was mixed with starch to increase its hydrophilicity aiming to enhance its cellular affinity [108]. In another work, hydrophobic TPU was coated with collagen to enhance its cellular adhesion, where the water contact angle was dropped from 99.5º to 21-30º by crosslinking collagen using glutaraldehyde, CMC, and thermal crosslinking [116].

Sodium alginate (Na-Alg, SA) is a natural bio-based polymer mainly used as a thickening agent and stabilizer in the food industry [117], gel in the pharmaceutical industry[118], [119], and thickening liquid dyes in the textile industry [120]. As it is a naturally occurring polymer, it is biocompatible, non-toxic with a relatively low cost [118]. SA can be gelated by addition of divalent ions like Ca^{2+}, Ba^{2+}, and Mg^{2+}. SA is considered as a hydrophilic polymer which after crosslinking with $CaCl_2$, it can provide significant thermal stability as the limiting oxygen index (LOI) value of Calcium Alginate (Ca-Alg, CA) fiber is 34 [121]. Alginate worth investigating its ability to modify surfaces and approach a hydrophilic, thermally stable structure.

Free standing TPU nanofiber as a battery separator and the analysis of its performance hasn't been thoroughly investigated. In our work, we investigated the performance of TPU nanofibers in battery separators and applied crosslinked CA coating to enhance the performance of the composite membrane. In this work, SA with different concentrations was used to enrich the surface properties of centrifuge spun TPU nanofibers and obtain a better hydrophilic surface.

3.2.14 Flame retardancy mechanism

Flame retardancy of polymers can be divided into three main mechanisms;

1- Gas-phase mechanism where active radicals are captured to inhibit the chain branching reactions during burning.

2- Condensed-phase mechanism where char formation is promoted on the surface of the material working as a heat barrier.

3- Diluting the fuel with non-flammable gases and cooling the system by endothermic decomposition.

In opposite to most polysaccharides, calcium alginate is an inherently flame-retardant material when corporated with divalent ions due to the production of inorganic particles and volatile compounds dur ing combustion. The results obtained are referred to the formation of what is known as char layer from the divalent ions which provide high thermal stability ofchar residues [122]. Figure 3.11 illustrates the layers formed above the membrane. The char layer first covers the membrane suppressing the flames and forming a barrier layer.

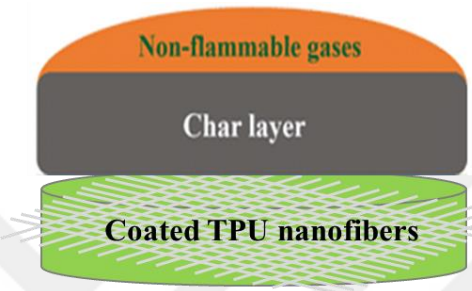

Figure 3.11 : Layers formed above nanofibers during pyrolysis.

The other mechanism that enhances the flame retardancy can be understood by the pathways that alginates pyrolysis follows. Two main chemical pathways, where volatile compounds are produced, is noted in Figure 3.12. The side reaction results in the production of furfural and butanedione as volatile compounds.

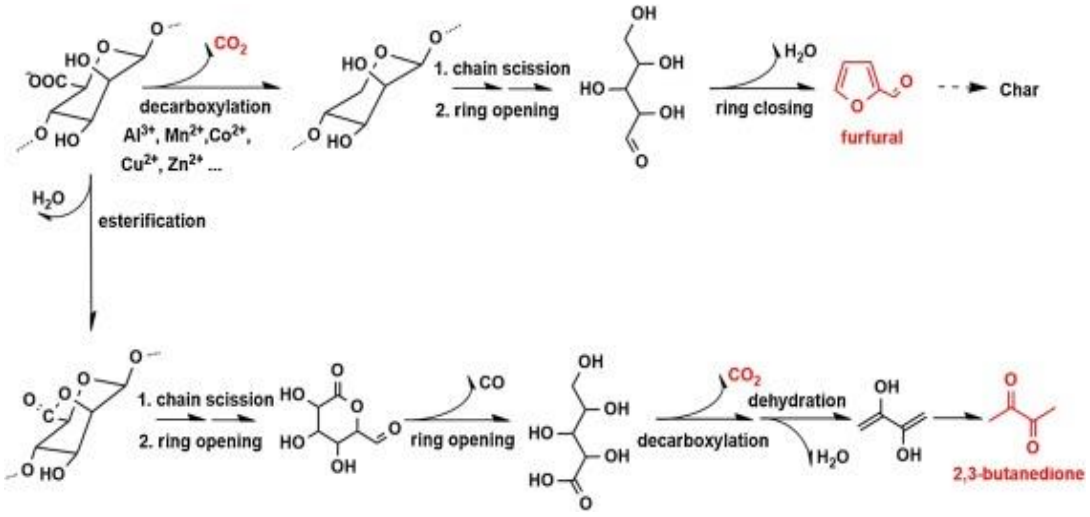

Figure 3.12 : Proposed pathways for alginate pyrolysis [122].

Those compounds result in less production of flammable gases by the alginates, and diluting the existing flammable gases. Thus, there was a significant delay in the ignition and propagation of flames through the membrane.

3.3 Experimental & Methods

3.3.1 Materials

Desmopan 385e thermoplastic polyurethane (TPU) was used as the polymer precursor. Dimethyl formamide (DMF, 99.9% purity, Merck) and Acetone (99.9% purity, Merck) were the co-solvents for TPU with different ratios. The fibers produced were collected onto 13 gsm Polypropylene (PP) spunbond support fabrics (Mogul Company). Sodium alginate (Isolab), calcium chloride ($CaCl_2$, food quality, Tekkim) and distilled water (DI) were used to achieve calcium alginate crosslinking.

3.3.2 Methods

Solvent Preparation

TPU solution was prepared by dissolving TPU pellets in DMF/acetone at 70 ºC by magnetic stirrer. The solution was fed to the centrufuge nozlle using syringe pump with a feeding rate of 30ml/h. A total volume of 60ml was produced for each TPU sample. Both Sodium alginate powder and cacium chloride was dissolved in DI by magnetic stirrer at room temperature.

Fabrication of nanofibers

TPU nanofibers were obtained by centrifuge spinning method. The system consists of motor-rotated nozzle spinning fibers from the top of the machine. Ejected fibers are collected on a PP substrate wrapped over a rotating vacuumed drum. Fibers are oriented toward the collector by pressurized air of 2 bar. Collector speed of 200 rpm was hold constant throughout all sample production.

Preparation of coated nanofibers

TPU nanofibers were coated with sodium alginate solution and then dried for 24 h. The coated sample is then dipped into $CaCl_2$ coagulation bath for 10 minutes to accomplish full crosslinking. The sample is then washed with DI and left to dry for another 24 h before being sent to hot pressing machine.

Working parameters & scheme

The scheme of the whole process is summarized in Figure 3.13. Firstly, the solution with diesired concentration is prepared then spun in centrifuge spinning with desired rotation speeds. After that, the nanofibers are dipped into SA solution and dried befor dipping again into $CaCl_2$ solution. Dried samples are then hot pressed befor being sent into analysis and characterization for its intended purpose. The working flow of the experiments is illustrated in Figure 3.13.

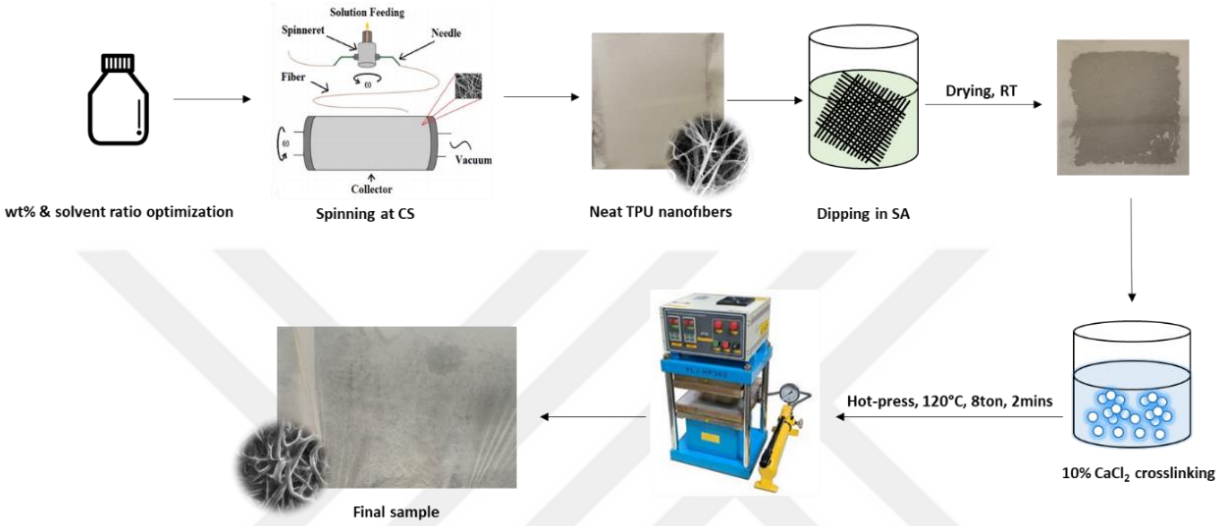

Figure 3.13 : Working scheme.

All experimental parameters are summarized in Table 3.1.

Table 3.1 : Working parameters.

Parameter	Working range
Concentration (wt%)	5%, 10%, 15%
Solvent ratio DMF:acetone	1:0, 1:1, 2:1, 3:1
Needle gauge (G)	23G, 25G, 30G
Rotating speed (rpm)	8000, 10000
Sodium alginate concentration (wt%)	0, 0.5, 2
Hot press duration (minutes)	2, 5

3.3.3 Characterization

Contact angle

The measurements were taken with Theta Lite optical tensiometer on Young-Laplace analysis mode with distlled water as the liquid.

Porosity

Custom-made lab-scale porosity device build on bubble point method was used with a very low surface tension liquid to measur the pore size of the samples.

Dimensional stability

Coin cell size samples were cut and treated in an oven at 200°C for 2h. A reference commercial PP separator sample was also used.

Flammability test

Flame tests were conducted by the following setup. Similar squared samples were cut and exposed to fire source. The behavior of the samples was recorded in respect to time (1 second and 10 seconds).

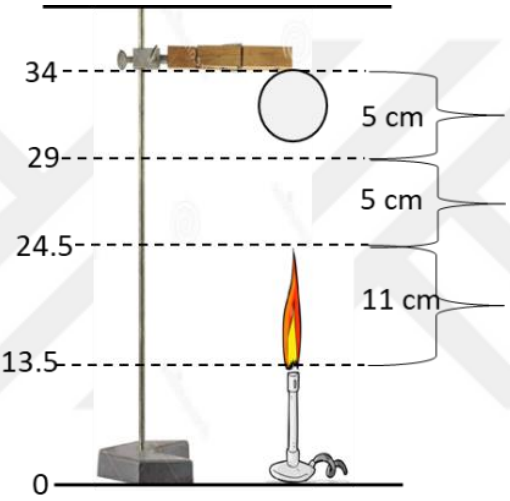

Figure 3.14 : Flammability test setup.

EIS

Electrochemical impedance spectroscopy (EIS) is a powerful, non-destructive in-situ and ex-situ technique used to characterize electrochemical systems and their interfacial properties by sending an amplitude and detecting the response. Reactions, electroactive species, mass transfer, charge transfer, diffusion and the resistance are all measured [62]. These features responses are mimicked and interpreted by electrical circuits and their elements like resistors, capacitors and constant phase elements and whether they are in series or parallel. While resistance is observed in DC circuits, impedance is its counterpart in AC circuits that doesn't follow Ohm's law.

Tests were carried on SP-150 workstation in a frequency range of 10mHz-10kHz for full cell tests and 100mHz-10kHz for the symmetric separator cell. Both tests were conducted with 10mV amplitude. Five TPU samples were prepared and tested in configuration shown in Figure 3.15 using stainless steel (SS) spacer electrodes and 1.0 M sodium perchlorate ($NaClO_4$) in EC/DEC/PEC (1:1:0.5) by volume). Full cell samples consists of carbon cloth/separator/Sodium metal. Figure 3.15 shows the configuration of both symmetric and full cell samples.

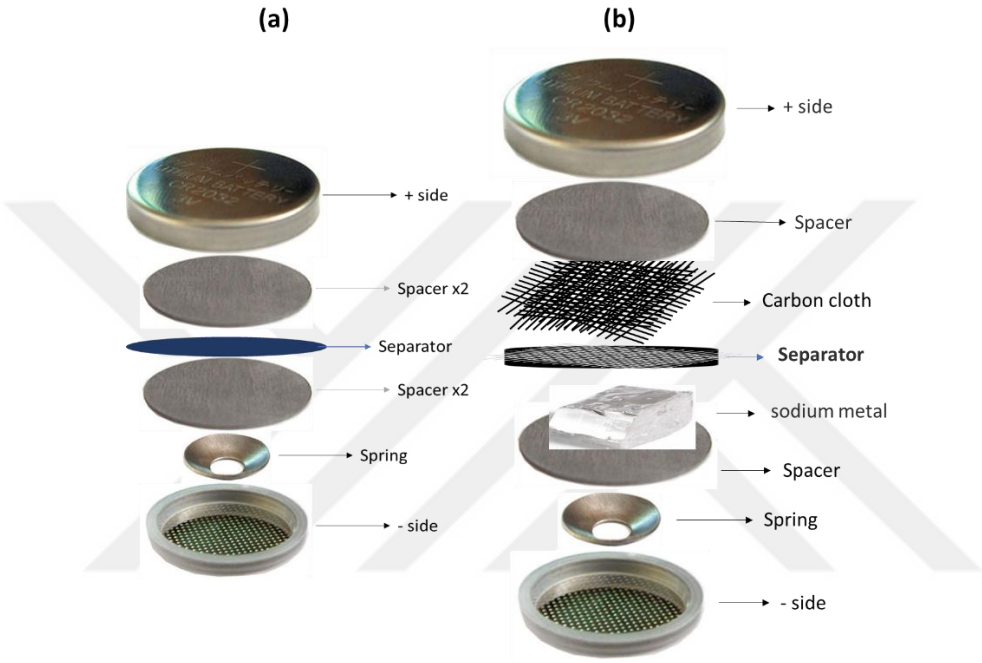

Figure 3.15 : Coin cell configuration, (a) symmetric cell, (b) full cell.

3.4 Results & Discussion

To achieve the best performance out of the nanofibrous mmebranes, optimum morphological structure should be accomplished. Minimum attainable bead-less fiber diameter is the main goal. For that reason, concentration of the polymer, solvent ratio, needle gauge, and rotating speed optimization must be done. After that, hot press temperature and duration along SA concentration optimization was conducted

3.4.1 Concentration optimization

In the concentration trials, the DMF:Acetone ratio was chosen as 3:1. Beads and droplets in the structure decreased with the increasing concentration in the productions. However, the fiber

diameters increased considerably. Fibers with a diameter of approximately 200 nm were obtained with 5wt.% concentrated TPU solution, while fibers with a diameter of approximately 800 nm were obtained with 15wt.% TPU solution. At the same time, the standard deviation between fiber diameters was too high. For this reason, the solution of 10wt% concentration had a negligible amount of bead with the thinnest fiber diameters (342 nm) was chosen.

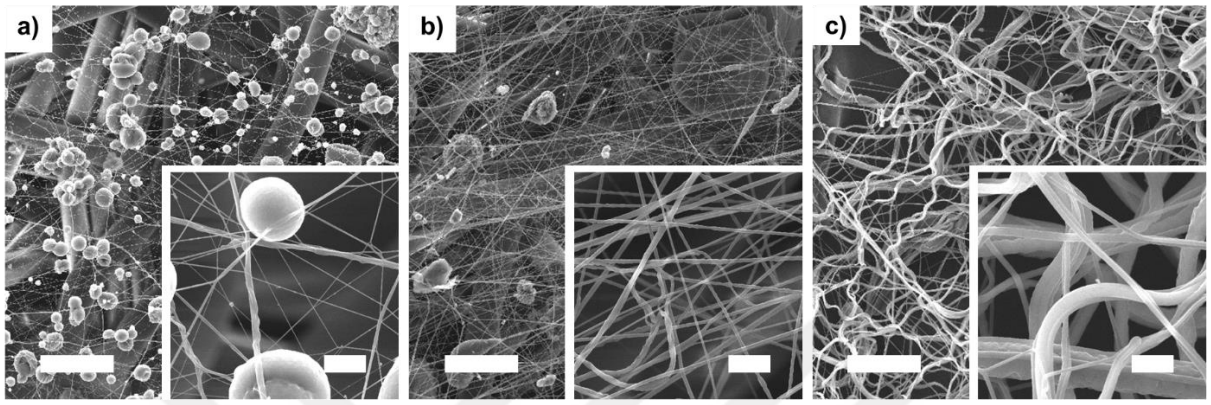

Figure 3.16 : SEM images of the TPU nanofibrous mats according to effect of solution concentration a) 5wt.%, b) 10wt.%, c) 15wt.%, and d) fiber diameter distribution.

3.4.2 Solvent optimization

On the next phase, the DMF:Acetone ratio was changed to further reduce the beads in the fibers. Firstly, only DMF as a solvent was used. Significant bead formation occurred and minimal fiber density gained as show in Figure 3.17. For that reason, acetone was used as a co-solvent to accomplish better fiber formation.

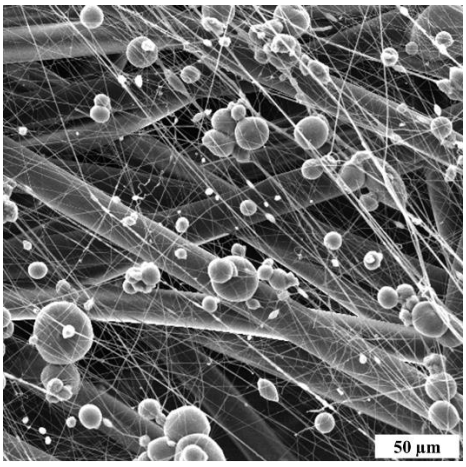

Figure 3.17 : TPU dissolved in 100% DMF solvent.

The acetone ratio in the solvent was changed to examine the morphological changes of the fibers. It is obviously seen that as acetone ratio increased, the beads in the structure decreased. However, due to the increase in viscosity, the fiber diameters also increased. For this reason, the DMF:Acetone ratio (2:1) was chosen, where the minimum bead and the thinnest fiber diameters (484 nm) were obtained. Figure 3.18 shows the change in bead formation with solvent ratio change and fiber diameter drop with the increment of acetone ratio.

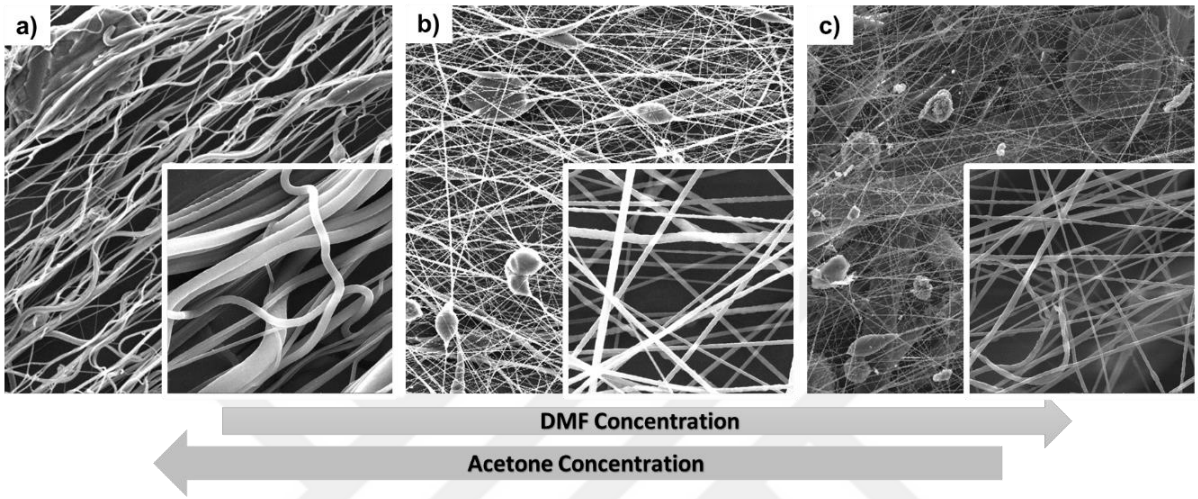

Figure 3.18 : SEM images of the TPU nanofibrous mats according to effect of different DMF:Acetone ratio a) 1:1, b) 2:1, and c) 3:1.

3.4.3 Needle (gauge) optimization

In order to obtain completely bead-free fibers, we reduced the diameter of the needle, that is, we used large gauge needles. With the decrease in the needle diameter, the beads completely changed into fiber form. However, there was no significant change in fiber diameters. There was only an increase of 75 nm between the fibers produced with the 23G needle and the fibers produced with the 30G needle. This increase in fiber diameter can be neglected as the overall production efficiency is higher with 30G needles [123]. The fiber diameter distribution of the samples can be seen in Figure 3.25.

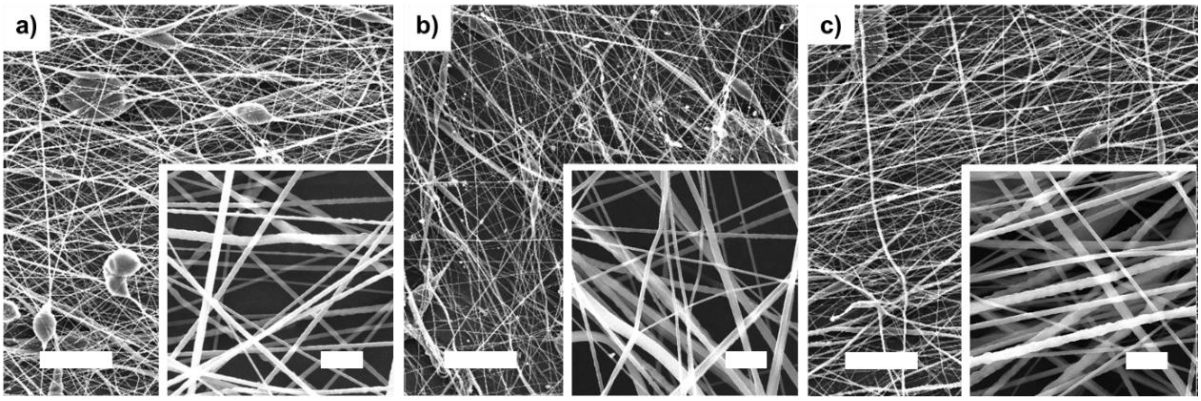

Figure 3.19 : SEM images of the TPU nanofibrous mats according to effect of needle gauge, a) 23G, b) 25G, c) 30G, and d) fiber diameter distribution.

3.4.4 Rotating speed

As the nozzle rotation speed increases, the air friction force also increases, resulting in a more thinning of the polymer jet coming out of the needle tip [124]. For this reason, increasing the nozzle rotation speed from 8000 rpm to 13000 rpm in the study provided the finest bead-free fibers with a diameter of 305 nm. Figure 3.20 shows the fibers obtained with different rotating speeds.

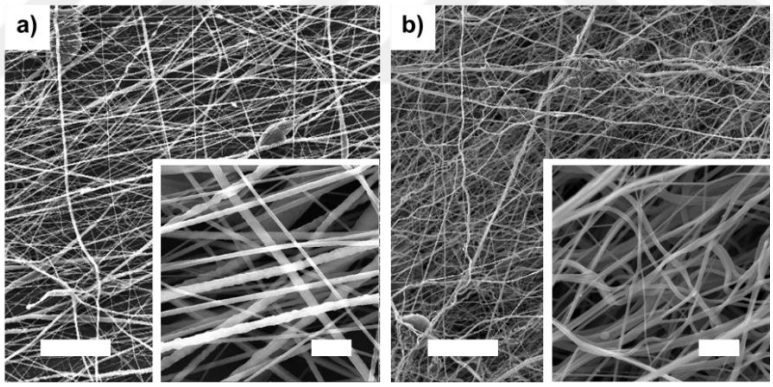

Figure 3.20 : SEM images of the TPU nanofibrous mats according to effect of rotational speed a) 8000 rpm, and b) 13000 rpm.

3.4.5 Alginate treatment

CA coating was applied to the produced optimum TPU nanofibrous mat by using different ratios of SA. 0.5%, 2%, and 5% were tried. As the SA ratio increased, the space between the fibers began to close. On the other hand, more SA ratio formed a film closing the pores, so the 5wt.% SA ratio was not reported. The best rate in which small pores were formed was chosen as 2wt.%. With the SA coating, the fibers became almost 3 times thicker. In this way, the pores

became smaller (Figure 3.21 : SEM images of the TPU nanofibrous mats according to effect of SA concentration a) 0wt.%, b) 0.5wt.%, c) 2wt.% and d) fiber diameter distribution.Figure 3.21).

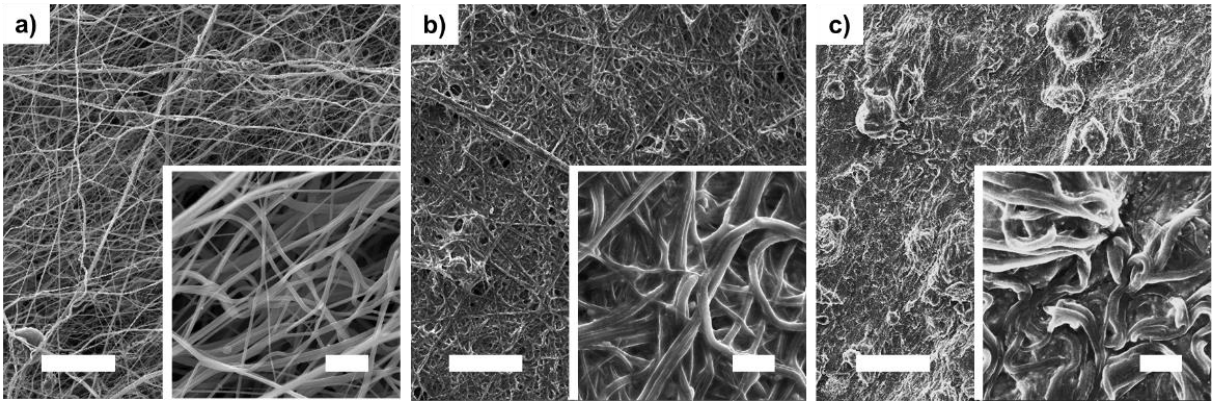

Figure 3.21 : SEM images of the TPU nanofibrous mats according to effect of SA concentration a) 0wt.%, b) 0.5wt.%, c) 2wt.% and d) fiber diameter distribution.

3.4.6 Hot press

Treated and non-treated samples were exposed to a hot-pressing machine. Variation of temperature was applied and the final samples were examined. Duration of pressing was varied between 2 and 5 minutes. Temperature of pressing set between 60, 100, and 120℃. The force was held constant at 8 tons.

Firstly, while holding time constant at 2 minutes, samples were pressed with 60, 100, 120℃. Figure 3.22 shows the SEM images of the samples. It can be seen that the sample pressed at 60℃ only showed fiber bonding due to the force applied leading to pore closure without any melting due to the heat applied. The sample pressed at 100℃ showed a better fiber structure with few poins starting to melt. At 120℃, the showed some film formatin and more bonding of the nanofibers.

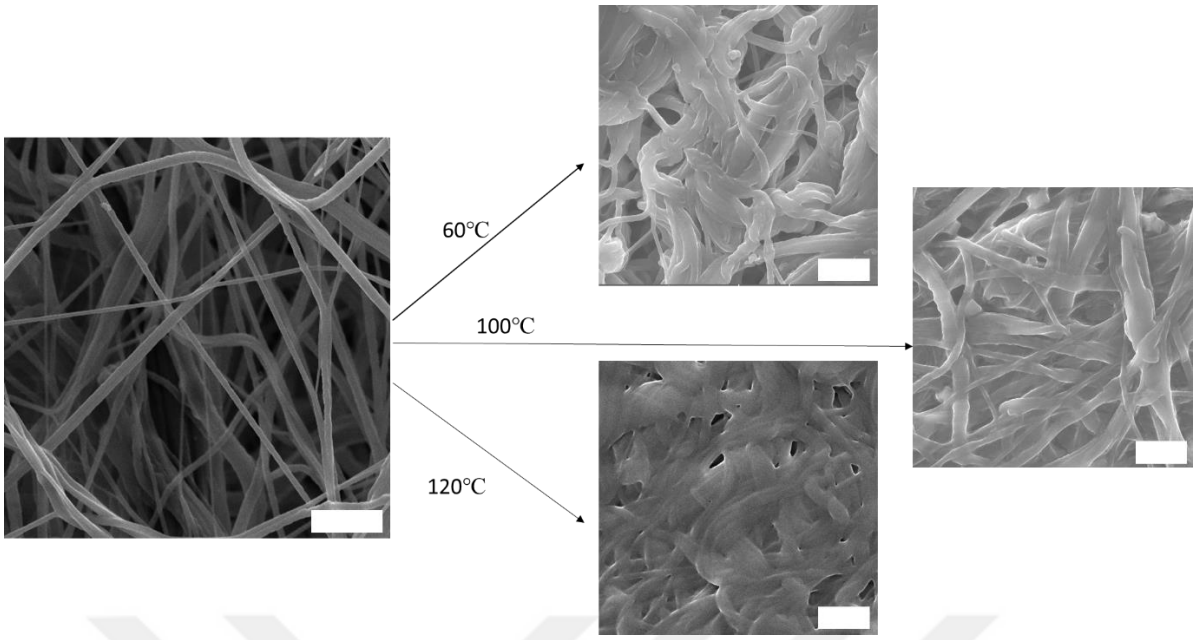

Figure 3.22 : Hot press temperature optimization.

After that, the duration was increased to be 5 minutes and the samples were pressed at 100, and 120°C. As showin in Figure 3.23, the samples pressed at 120°C showed a film structure in comparison to the samples pressed at 100°C.

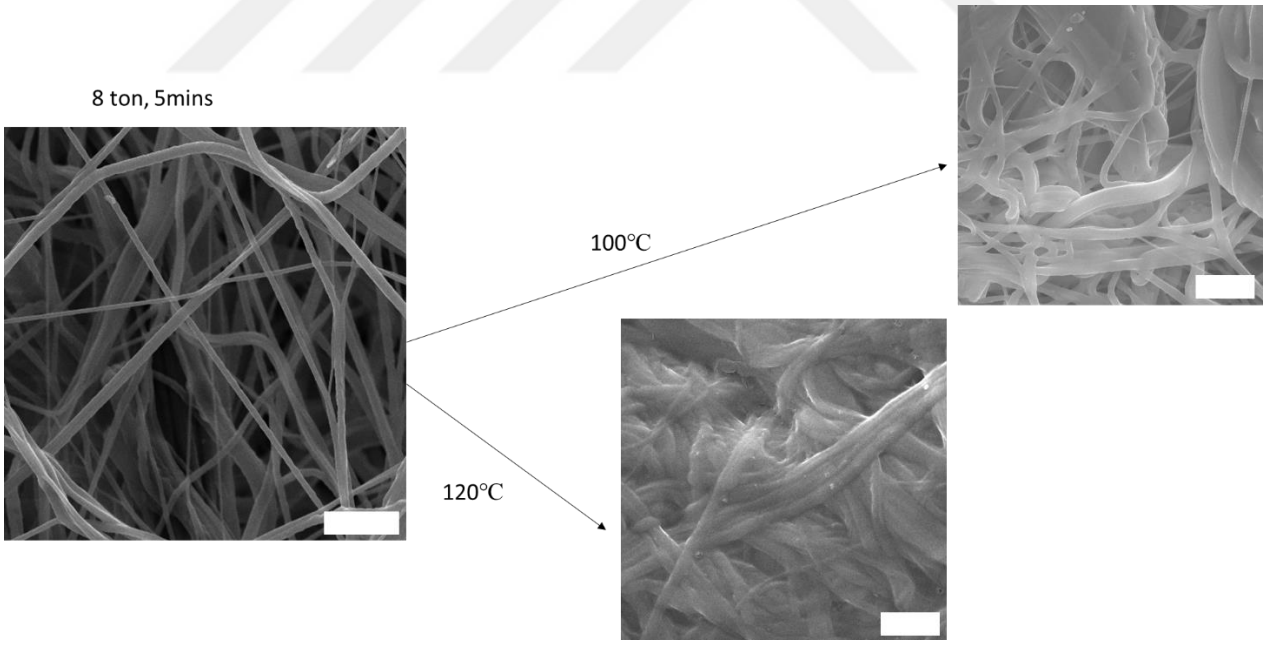

Figure 3.23 : Hot press duration optimization.

The samples are then hot pressed after treatment with CA (Figure 3.24), and later on samples were all carried at 120°C for 2 minutes and 8 tonn of force.

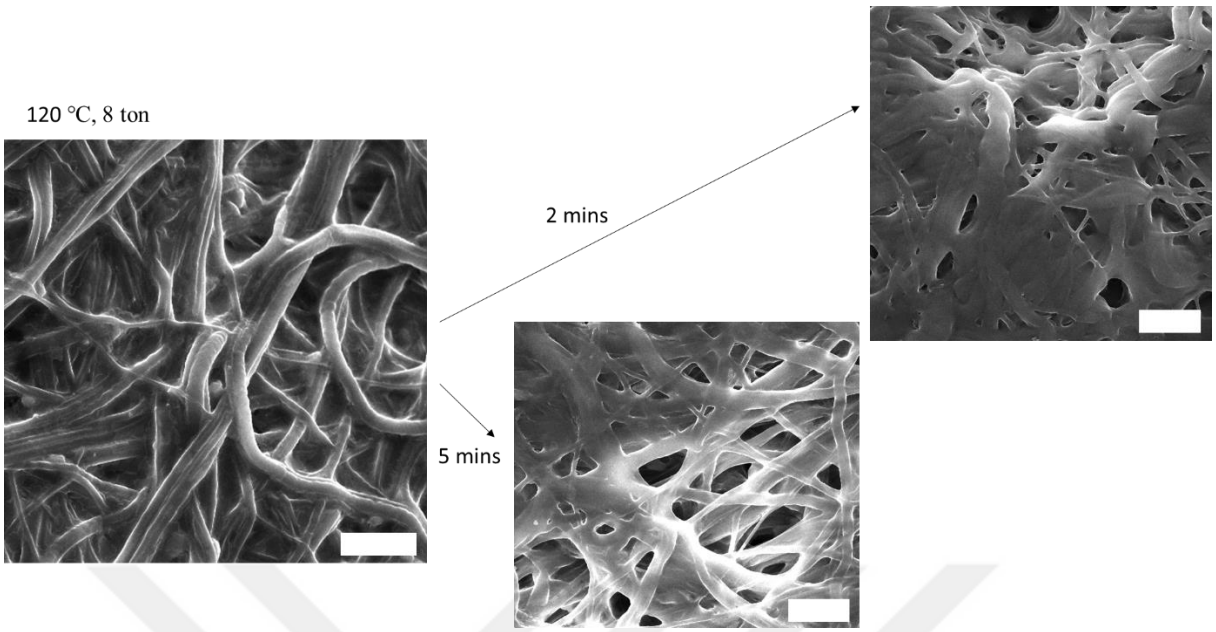

Figure 3.24 : Treated sample hot press.

If we make a comparison between the hot press SEM images of the treated and non-treated samples, observable thermal enhancement can be seen. Non-treated fibers pressed at 120℃, 8 ton for 2 and 5mins almost got stick to each other closing any observable existed pores. While treated fibers sustained better shape under the heated press and exhibited better thermal stability preserving its porous structure.

An overall comparison of all produced samples with the fiber diameter range obtained is shown in Figure 3.25. The fiber diameter of 10wt.% concentration sample, which is the concentration that the work was carried on, was about 300nm. After doing a full optimization proces, almost the same fiber diameter range was preserved while eliminating all kind of beads formed on the nanofibers. That was done by altering the rotation speeds, the solvent ratio and the needle gauge.

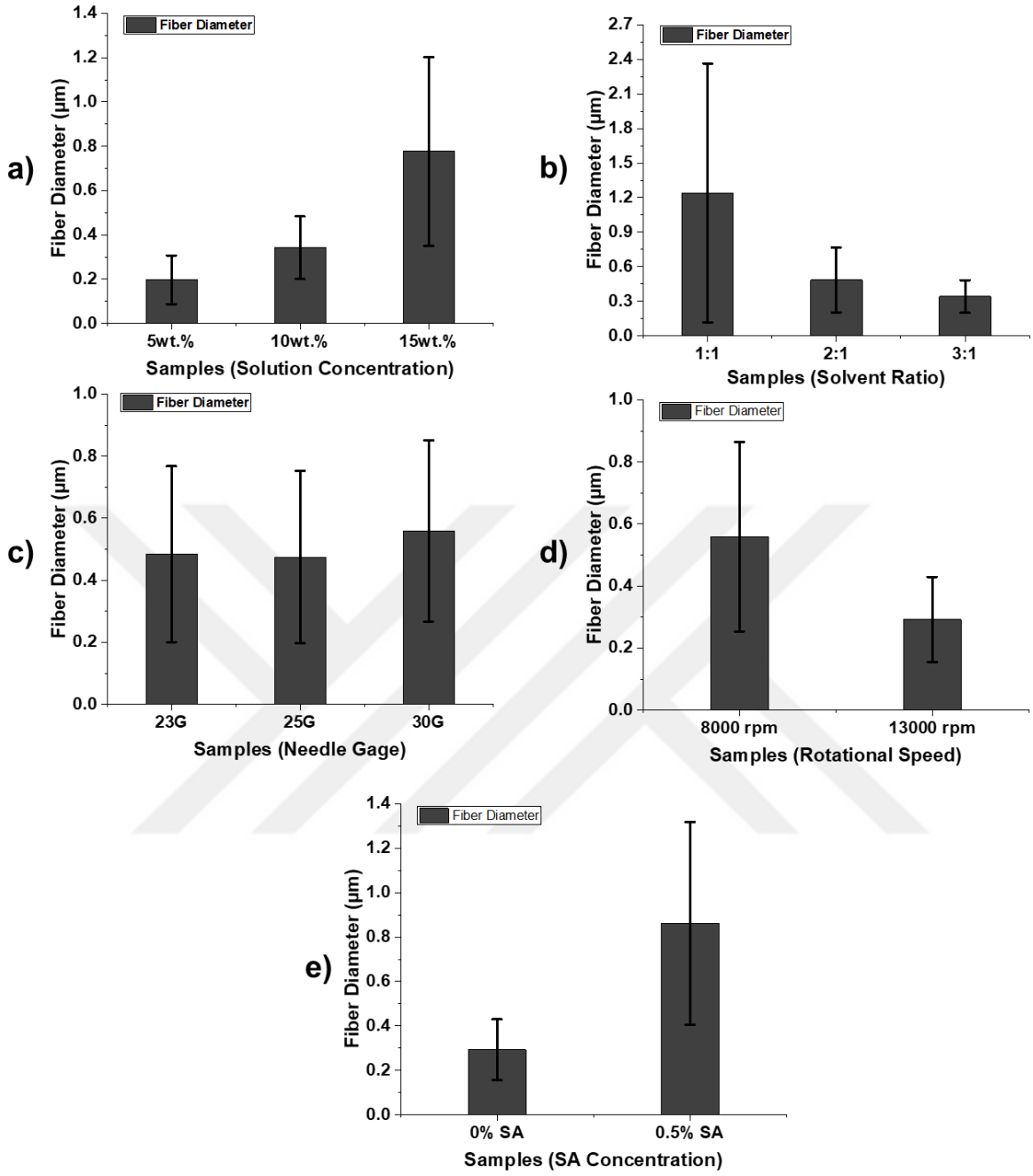

Figure 3.25 : Fiber diameter distributions of the optimization study; (a) solution, (b) solvent, (c) needle gauge, (d) rpm, (e) SA coating.

3.4.7 Contact angle

Neat as produced TPU nanofibers have a contact angle of 94º similar to the degree reported in other works [116]. After pressing the nanofibers at 120°C for 2 minutes using hot pressing machine, the contact angle showed an increment up to 150º. This significant increase is due to

the reduce of the pore size inhibiting water droplets from passing. Samples of membranes treated with 0.5, and 2% cross-linked calcium alginate showed observable drop of the contact angle to 31º and reached zero degree after 5 minutes. These results showed that calcium alginate can provide notable raise the hydrophilicity of the treated surface.

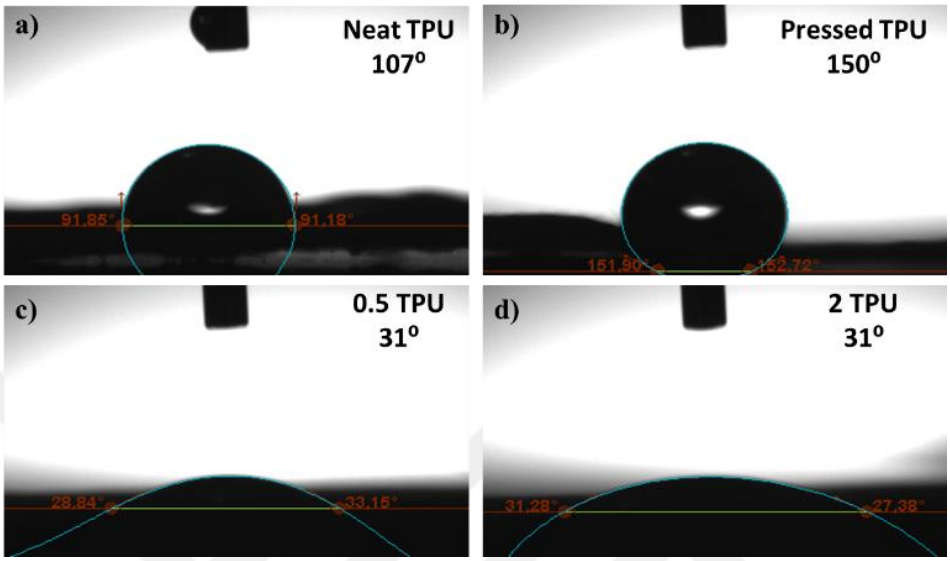

Figure 3.26 : Contact angle of TPU samples, a) Neat TPU, b) pressed TPU, c) 0.5 TPU, d) 2 TPU.

3.4.8 Porosity

Porosity measurement were taken for samples before and after pressing, different concentration treatments. As expected, porous structure with large pore size is found in neat TPU nanofiber. The mean pore size was found to be 5.4 µm with maximum pore of 11.5 µm. The mean pore size dropped to 2.7 µm after pressing the sample in the hot press machine at 120℃ for 2 minutes. The drop in pore size is anticipated as the nanofibers will be partially melted and softened which leads to bonding of nanofibers, reducing the porosity of the membrane [125]. Sodium alginate treated samples shows a smaller pore size distribution. The reason for that is that calcium alginate coats the nanofibers increasing its initial diameter as shown in previous SEM images. While %0.5 alginate didn't show a significant drop in the pore size, %2 showed more uniform pore size structure with mean pore size of 2.3 µm.

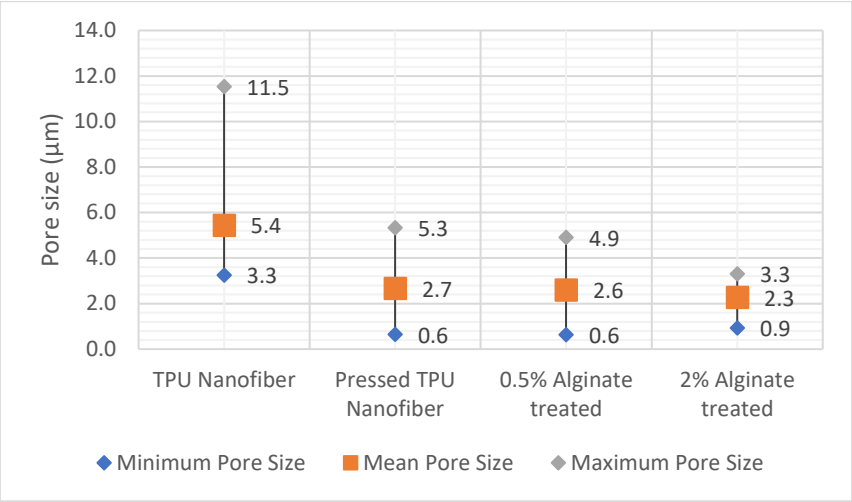

Figure 3.27 : Porosity of TPU membranes.

3.4.9 Electrochemical performance

The electrochemical analysis carried demonstrates the performance difference between the samples. The Nyquist plot of the impedance for the separators along Celgard PP separators is shown in figure asds. The Intercept of the curves with x-axis on the Nyquist plot shown, denote the bulk resistance (R_b) of the separators or membranes [126]. The equivalent circuit used is shown in the graph which consists of a constant phase element, a Warburg impedance element, and resistances. The absence of the semi-circle and exhibition of straight lines indicates that capacitive behavior is dominant and ion transfer is happening through diffusion phenomena which means less charge transfer resistance is occurring [127]. The summary of the values obtained for each sample is shown in table asddsa. It can be seen that neat TPU sample exhibited an ionic conductivity of 0.23 mS/cm^2 which tripled after hot pressing the sample. This increment could be referred to the fact that the thickness of the membrane dropped after hot press which led to a significant drop in the resistance. Also, hot pressing the sample lead to a more uniform thickness throughout the sample.

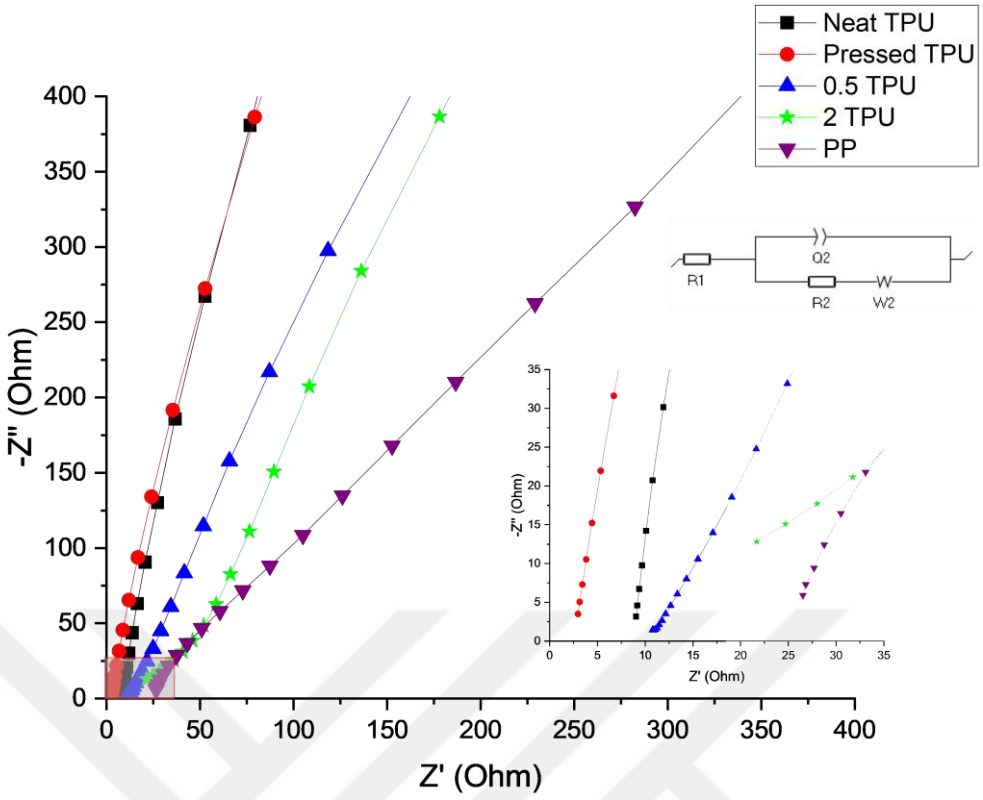

Figure 3.28 : EIS of SS/separator/SS system in 1M $NaClO_4$ electrolyte.

Table 3.2 : Ionic conductivities of different TPU samples in symmetric Na-ion cell.

Sample	Thickness (μm)	Bulk resistance (ohm)	Ionic Conductivity (mS/cm^2)
Neat TPU	40	8.479	0.23
Pressed TPU	35	2.59	0.67
0.5 TPU	60	16.8	0.17
2 TPU	70	21.7	0.16
PP	25	21.84	0.05

The full cell configuration results are shown in Table 3.3. While the nyquist plot obtained from AC impedance measurment along the proposed equivalent circuit is shown in Figure 3.29. The proposed circuit was explained in the previous chapter.

Table 3.3 : Ionic conductivities of different TPU samples in full Na-ion cell.

Sample	Thickness (μm)	Bulk resistance (ohm)	Ionic Conductivity (mS/cm^2)
Neat TPU	40	2.107	1.53
Pressed TPU	35	14.43	0.19
0.5 TPU	60	71.01	0.05
2 TPU	70	73.77	0.03

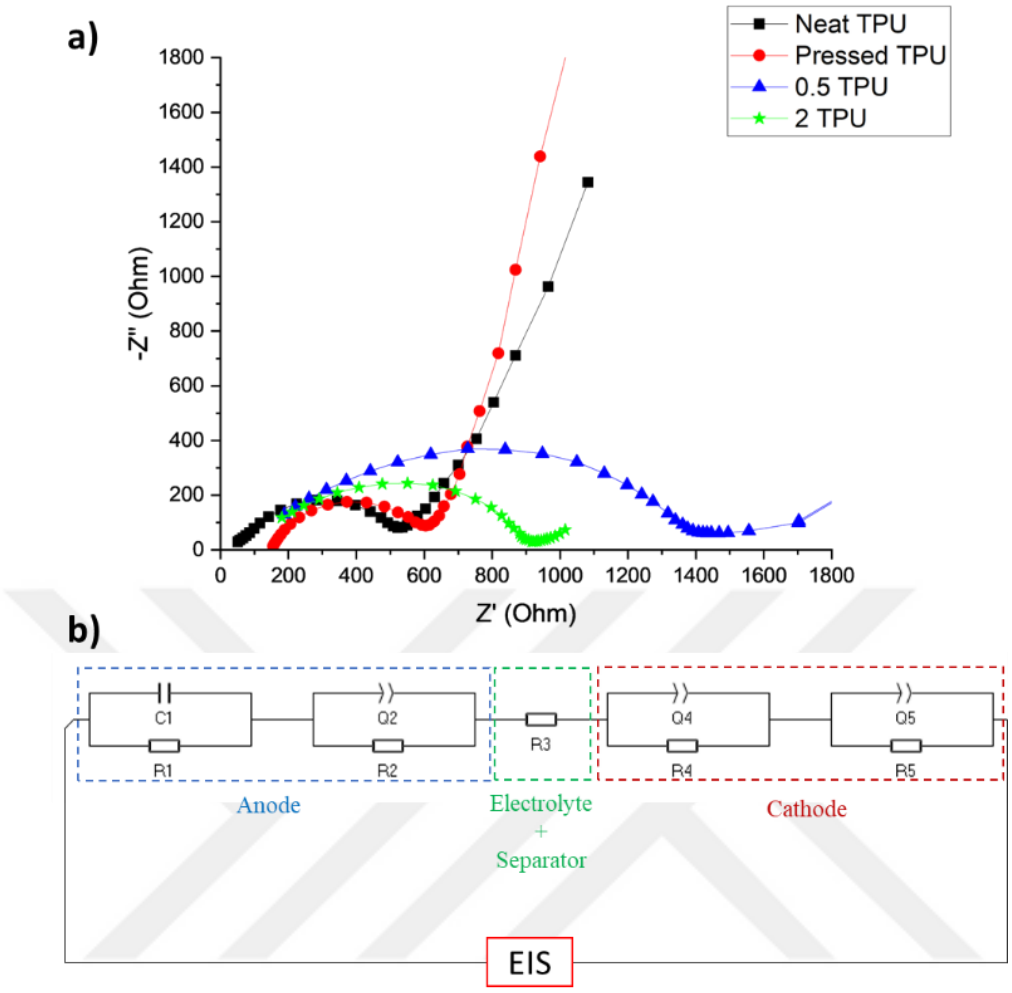

Figure 3.29 : EIS of Anode/separator/cathode system, a) nyquist plot, b) equivalent circuit.

TPU samples show a significance performance in the sodium ion battery. This could be referred to the fact that neat TPU membranes showed a small fiber diameters with high porosity which facilitate higher electrolyte uptake easing the movement of the sodium ions and in the same time causing less ion resistance. While whenm the samples are pressed, the nanofibers are fused together and bonded making them having better stability but in the same time significantly dropping the porosity which led to the drop in the ionic conductivity. Coated samples with calcium alginate exhibited higher observable resistance. Since the pore size is of great importance for ion transportation and due to the bigger diameter size of Na-ions, the coated samples showed this jump. Since the diameter of the semicircle is known to be as the charge trasfer resistance (R_{ct}), the depressing of the semi-cricle for 2 TPU sample could be referred to

the effect of higher calcium alginate presence decrewasing the overall charge transfer resistance.

Table 3.4 summarizes the results obtained from Li-ion coin cell analysis. The Neat TPU sample showed better ionic conductivity (0.1mS/cm^2) than the commercial separator (0.07 mS/cm^2) although its bulk resistance is higher. The reason lies in the fact that it had bigger thickness which in turn lead to better electrolyte retention ability. 0.5 TPU sample exhibited the higher ionic conductivity performance among the samples with 0.21 mS/cm^2 and the least bulk resistance even though it has the largest thickness. This difference could be explained by the fact that thicker separators holds better electrolyte increasing the ionic conductivity, but in the same time drop of the bulk resistance signifies that calcium alginate in small concentration facilitates easier movement of the ions.

Table 3.4: Ionic conductivities of different TPU samples in symmetric Na-ion cell.

Sample	Thickness (μm)	Bulk resistance (ohm)	Ionic Conductivity (mS/cm^2)
Neat TPU	40	20	0.10
0.5 TPU	70	16.75	0.21
2 TPU	65	35.57	0.09
PP	25	16.75	0.07

3.4.10 Thermal shrinkage

Thermal shrinkage of the samples was measured to simulate the how the separator would act under high heat condition. Dimensional thermal stability was conducted by putting the samples inside the oven at 200°C for 2h. It was found that neat TPU nanofibers showed a 63% shrinkage as shown in Figure 3.30a. Since the melting point of TPU is around 145°C, the shrinkage occurred is considered to be normal. Hot pressing of the samples significantly enhanced the dimensional stability performance. This is due to the fact that upon hot press, melted nanofibers partially melt leading to bonding of the nanofibers which eventually lead to better integrity of the membrane against harsh thermal conditions [125]. For the CA treated sample, 0% shrinkage happened. That emphasize the huge role CA plays in enhancing the thermal performance of the membrane as proposed. CA coating gives the fibers higher crystal structure which make their mechanical performance under high state of heat way better than neat TPU nanofibrous membranes. Commercial Celgard 2400 separator totally collapsed after conducting the tests.

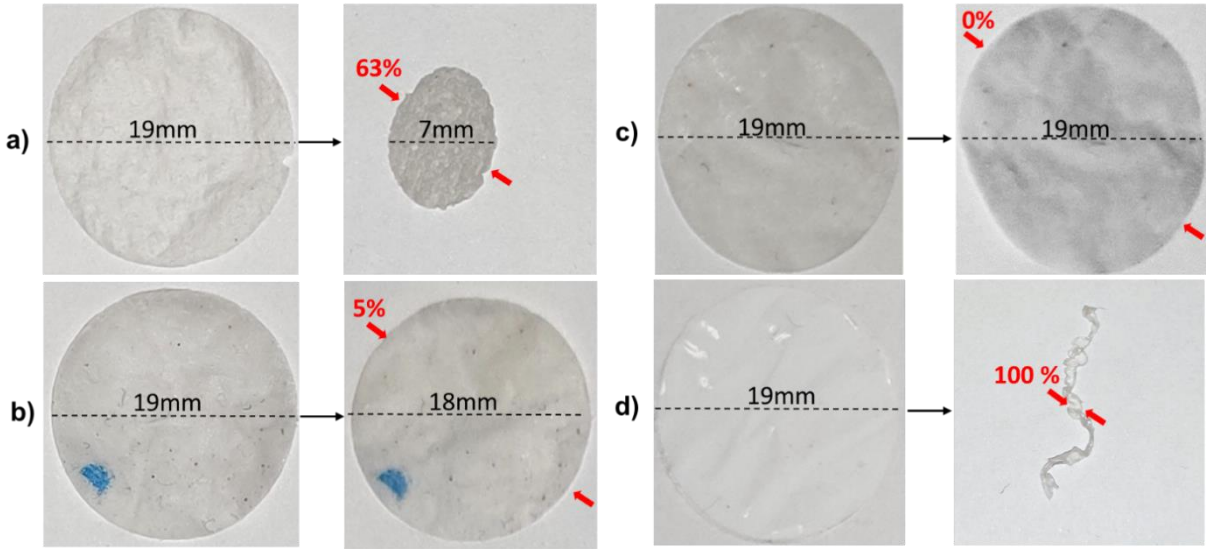

Figure 3.30 : Dimensional stability tests, (a) Neat TPU, (b) 0.5 TPU, (c) 2 TPU, (d) commercial.

3.4.11 Flammability

The possibility of the sample to catch fire was measure by flame test according to the setup explained previously. Figure assaas shows the sample structure after 1 and 10 seconds of exposing to heat. It can be seen that neat TPU (figure asd a) directly shrinked and melted which is expected due to its low melting point. The hot-pressed sample, although it had better mechanical integrity when it was exposed to heat in the dimensional stability, it acts as neat TPU and melts in the same manner. CA treated sample (figure c and d) shows better performance against the hot flames. 0.5CA treated sample started to burn after 10 seconds without starting to melt while for the 2CA sample, no flame or color change occurred. The sample showed significant resistance to the flames. That shows that CA coating had accomplished its intended purpose by suppressing the flames.

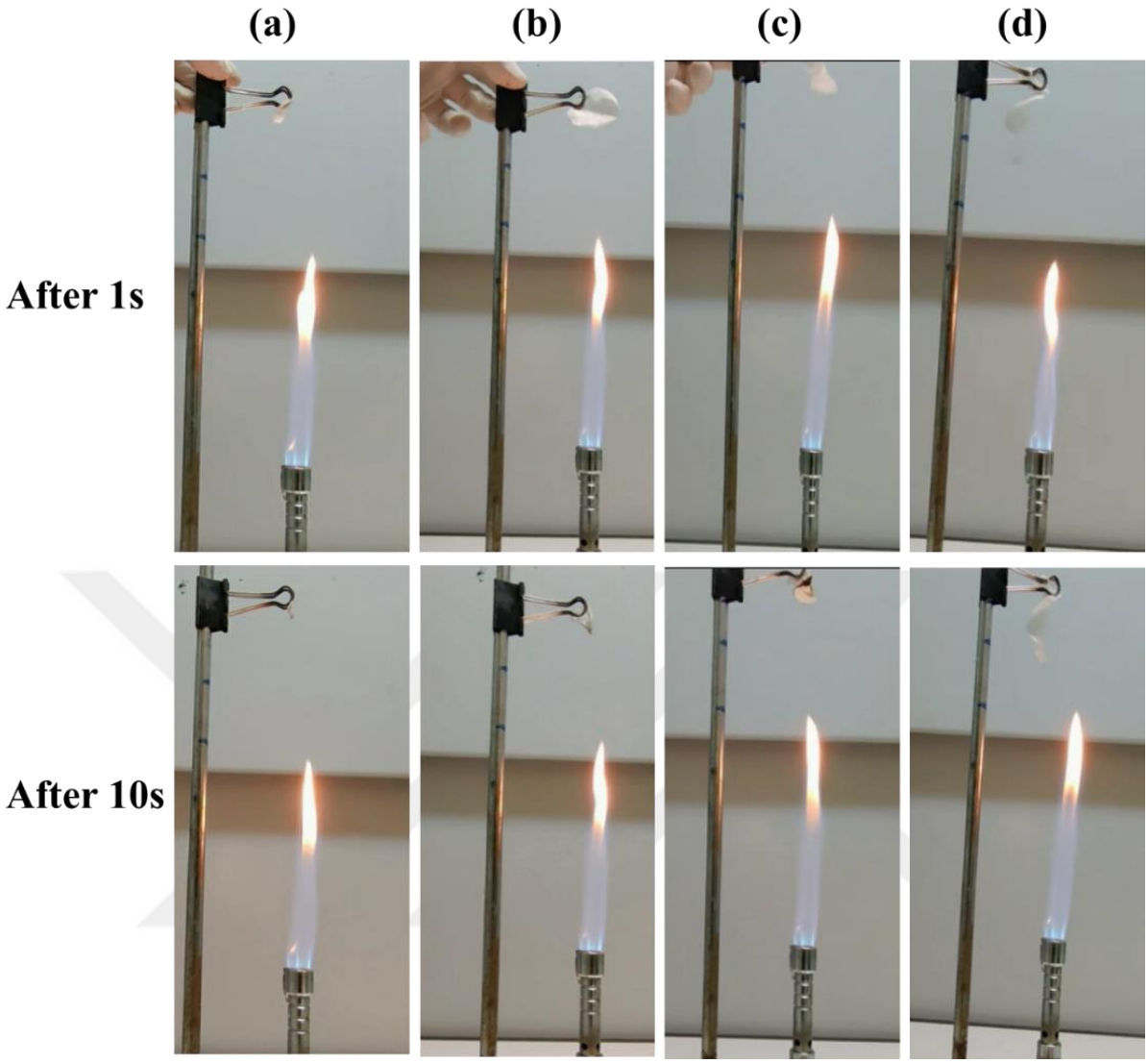

Figure 3.31 : Flammability tests after 1 and 10 seconds, (a) Neat TPU, (b) Pressed TPU, (c) 0.5 TPU, (d) 2 TPU.

4. CONCLUSIONS AND RECOMMENDATIONS

UHMWPE membranes were successfully fabricated. The results of the full cell prepared showed that fabrication of UHMWPE with the proposed method is achievable. Since UHMWPE's viscosity is very high, processing the polymer through the available film die (0.1-0.5mm lips) was unproductive. Lubricants and processing aids were used yet the issue continued to happen. It's recommended to use coat hanger die with adjustable lips that could ease the flow of the viscous polymer through the film die. A mold could be used in the hot press stage to obtain a film with uniform thickness which will definitely lead to a more precise control of the membrane and gain mor homogeneous structure. Closed system heating is advisable in the stage of uniaxial stretching, where the thermal heat can be controlled precisely and any heat loss can be avoided.

The TPU nanofibrous membrane gained remarkable thermal properties when coated with calcium alginate. It exhibited outstanding performance in both dimensional stability and flammability tests. This shows that coating TPU nanofiber with inherently flame-retardant biopolymers have the potential in enhancing the thermal properties of nanofibers. On the other hand, in the electrochemical tests, neat TPU nanofibers exhibited better performance in comparison to the coated samples. While higher calcium alginate showed smaller charge transfer resistance with the 0.5% sample. The interaction mechanism between sodium-based electrolyte and alginates needs to be further investigated. A comparison study in the performance of TPU nanofibers for both sodium and lithium ions could be done. Electrospraying of SA could be done to mitigate the effect of pore closure happens due to dip coating on the drop of TPU electrochemical performance. the Usage of commercial electrodes and cycling the battery would help in examining the exact electrochemical performance of the membranes and their cycling capacity. If the samples hold high cycle life, TPU nanofibers and alginate coatings holds the potential for a marked performance in metal-ion battery applications. The obtained results showed the high potential calcium

alginate carries in battery applications. Studies to enhance the ionic conductivities of the calcium alginate can be conducted and better integrating methods can be proposed.

REFERENCES

[1] **Ibrahim, H., Ilinca, A., and Perron, J.** (2008). Energy storage systems Characteristics and comparisons. *Renew. Sustain. Energy Rev.*, *12*,1221–1250.

[2] (2022). Trends in electric light-duty vehicles – Global EV Outlook. *IEA*. Retrieved March 3, 2023 From https://www.iea.org/reports/global-ev outlook-2022/trends-in-electric-light-duty-vehicles.

[3] **Babiker, D.M.D., Wan, C., Mansoor, B., Usha, Z.R., Yu, R., Habumugisha, J.C., ..., Li, L.** (2021). Superior lithium battery separator with extraordinary electrochemical performance and thermal stability based on hybrid UHMWPE/SiO2 nanocomposites via the scalable biaxial stretching process. *Compos. Part B Eng.*, *211*, 108658.

[4] **Carmichael, R.S.** (1988). *Practical Handbook of Physical Properties of Rocks and Minerals*. Boca Raton, CRC Press.

[5] **Goodenough, J.B. and Park, K.-S.** (2013). The Li-Ion Rechargeable Battery: A Perspective. *J. Am. Chem. Soc.*, *135*, 1167–1176.

[6] **Robeson, L.M.** (2012). 8.13 - Polymer Membranes. in: K. Matyjaszewski, M. Möller (Eds.), Polym. Sci. Compr. Ref., Elsevier, Amsterdampp. 325 347.

[7] **Francis, C.F.J., Kyratzis, I.L., and Best, A.S.** (2020). Lithium-Ion Battery Separators for Ionic-Liquid Electrolytes: A Review. *Adv. Mater.*, *32*, 1904205.

[8] **Li, Y., Fu, X., Wang, Y., Zhong, W.-H., and Li, R.** (2019). "See" the invisibles: Inspecting battery separator defects via pressure drop. *Energy Storage Mater.*, *16*, 589–596.

[9] **Lee, H., Yanilmaz, M., Toprakci, O., Fu, K., and Zhang, X.** (2014). A review of recent developments in membrane separators for rechargeable lithium-ion batteries. *Energy Environ. Sci.*, *7*, 3857–3886.

[10] **Ren, W., Ding, C., Fu, X., and Huang, Y.** (2021). Advanced gel polymer electrolytes for safe and durable lithium metal batteries: Challenges, strategies, and perspectives. *Energy Storage Mater.*, *34*, 515–535.

[11] **Mun, S.C. and Won, J.H.** (2021). Manufacturing Processes of Microporous Polyolefin Separators for Lithium-Ion Batteries and Correlations between Mechanical and Physical Properties. *Crystals*, *11*, 1013.

[12] **Hwang, K., Kwon, B., and Byun, H.** (2011). Preparation of PVdF nanofiber membranes by electrospinning and their use as secondary battery separators. *J. Membr. Sci.*, *378*, 111–116.

[13] **Gogia, A., Wang, Y., Rai, A.K., Bhattacharya, R., Subramanyam, G., and Kumar, J.** (2021). Binder-Free, Thin-Film Ceramic-Coated Separators for Improved Safety of Lithium-Ion Batteries. *ACS Omega*, *6*, 4204 4211.

[14] **Luo, X., Pan, W., Liu, H., Gong, J., and Wu, H.** (2015). Glass fiber fabric mat as the separator for lithium-ion battery with high safety performance. *Ionics*, *21*, 3135–3139.

[15] **Tan and Rodrigue** (2019). A Review on Porous Polymeric Membrane Preparation. Part II: Production Techniques with Polyethylene, Polydimethylsiloxane, Polypropylene, Polyimide, and Polytetrafluoroethylene. *Polymers*, *11*, 1310.

[16] **Zhang, S.S.** (2007). A review on the separators of liquid electrolyte Li-ion batteries. *J. Power Sources*, *164*, 351–364.

[17] **Yang, S., Gu, J., and Yin, Y.** (2018). A biaxial stretched β-isotactic polypropylene microporous membrane for lithium-ion batteries. *J. Appl. Polym. Sci.*, *135*, 45825.

[18] **Khayet, M., Feng, C.Y., Khulbe, K.C., and Matsuura, T.** (2002). Preparation and characterization of polyvinylidene fluoride hollow fiber membranes for ultrafiltration. *Polymer*, *43*, 3879–3890.

[19] **Das, B., Chakrabarty, B., and Barkakati, P.** (2016). Preparation and characterization of novel ceramic membranes for micro-filtration applications. *Ceram. Int.*, *42*, 14326–14333.

[20] **Petersen, R.J.** (1993). Composite reverse osmosis and nanofiltration membranes. *J. Membr. Sci.*, *83*, 81–150.

[21] **Bicy, K., Gueye, A.B., Rouxel, D., Kalarikkal, N., and Thomas, S.** (2022). Lithium-ion battery separators based on electrospun PVDF: A review. *Surf. Interfaces*, *31*, 101977.

[22] **Stojanovska, E., Kurtulus, M., Abdelgawad, A., Candan, Z., and Kilic, A.** (2018). Developing lignin-based bio-nanofibers by centrifugal spinning technique. *Int. J. Biol. Macromol.*, *113*, 98–105.

[23] **Zhong, D., Zhou, J., and Wang, Y.** (2021). Hollow-fiber membranes of block copolymers by melt spinning and selective swelling. *J. Membr. Sci.*, *632*, 119374.

[24] **Sanchez, J.-Y., Chabert, F., Iojoiu, C., Salomon, J., El Kissi, ..., Mercier, R.** (2007). Extrusion: An environmentally friendly process for PEMFC membrane elaboration. *Electrochimica Acta*, *53*, 1584–1595.

[25] **Patil, H., Tiwari, R.V., and Repka, M.A.** (2015). Hot-Melt Extrusion: from Theory to Application in Pharmaceutical Formulation. *AAPS PharmSciTech*, *17*, 20–42.

[26] **Maniruzzaman, M., Boateng, J.S., Snowden, M.J., and Douroumis, D.** (2012). A Review of Hot-Melt Extrusion: Process Technology to Pharmaceutical Products. *ISRN Pharm.*, *2012*, 1–9.

[27] **Harper, J.M. and Clark, J.P.** (1979). Food extrusion. *C R C Crit. Rev. Food Sci. Nutr.*, 11, 155–215.

[28] **Giles, H.F., Wagner, J.R., and Mount, E.M.** (2014). *Extrusion: the definitive processing guide and handbook.* Amesterdam, William Andrew Publications.

[29] (2017). An Introduction to Single Screw Extrusion. *AZoM.Com*. Retrieved March 12, 2022 From https://www.azom.com/article.aspx?ArticleID=13566.

[30] **Kimura, Y., Chaudhary, A.K., and Spalding, M.A**. (2017). *Handbook of Industrial Polyethylene and Technology: Definitive Guide to Manufacturing, Properties, Processing, Applications and Markets*. Hoboken, NJ, USA, Wiley & Sons, Inc.

[31] **Vlachopoulos, J. and Polychronopoulos, N.** (2019). *Understanding Rheology and Technology of Polymer Extrusion.* Dundas, ON, Canada, Polydynamics Inc.
[32] **Ashter, S.A.** (2014). *Thermoforming of Single and Multilayer Laminates*. Amesterdam, William Andrew Publications.
[33] **Rosato, D.V.** (1998). Extruding Plastics: A practical processing handbook. Boston, US, Springer.
[34] **Lloyd, D.R., Kinzer, K.E., and Tseng, H.S.** (1990). Microporous membrane formation via thermally induced phase separation. I. Solid-liquid phase separation. *J. Membr. Sci.*, *52*, 239–261.
[35] **Dayyoub, T., Olifirov, L.K., Chukov, D.I., Kaloshkin, S.D., Kolesnikov, E., and Nematulloev, S.** (2020). The Structural and Mechanical Properties of the UHMWPE Films Mixed with the PE-Wax. *Materials*, *13*, 3422.
[36] **Qiao, G.** (2021). *Superstrong Ultrahigh Molecular Weight Polyethylene Membrane with Tunable Pore Structure for Separation Processes — Seawater Desalination and Air Purification* (PhD thesis). The Hong Kong University of Science and Technology.
[37] **Rahman, M.M., Biswas, Md.A.S., and Hoque, K.N.** (2022). Recent development on micro-texturing of UHMWPE surfaces for orthopedic bearings: A review. *Biotribology*, *31*, 100216.
[38] **Lucas, A. de A., Ambrósio, J.D., Otaguro, H., Costa, L.C., and Agnelli, J.A.M.** (2011). Abrasive wear of HDPE/UHMWPE blends. *Wear*, *270*, 576–583.
[39] **Chen, S., Bao, X., Wang, Z., Rong, X., Zhang, X., Li, C., ... Wei, L.** (2022). Comparative study on the effects of water pressure on water absorption of ultra-high molecular weight polyethylene and polyformaldehyde. *J. Appl. Polym. Sci.*, *139*, e52783.
[40] **Kurtz, S.M., Mazzucco, D., Rimnac, C.M., and Schroeder, D.** (2006). Anisotropy and oxidative resistance of highly crosslinked UHMWPE after deformation processing by solid-state ram extrusion. *Biomaterials*, *27*, 24–34.
[41] **Smith, P. and Lemstra, P.J.** (1980). Ultra-high-strength polyethylene filaments by solution spinning/drawing. *J. Mater. Sci.*, *15*, 505–514.
[42] **Fang, L., Leng, Y., and Gao, P.** (2006). Processing and mechanical properties of HA/UHMWPE nanocomposites. *Biomaterials*, *27*, 3701–3707.
[43] **Pan, C. and Radosz, M.** (1999). Modeling of solid–liquid equilibria in naphthalene, normal-alkane and polyethylene solutions. *Fluid Phase Equilibria*, *155*, 57–73.
[44] **Basko, A. and Pochivalov, K.** (2022). Current State-of-the-Art in Membrane Formation from Ultra-High Molecular Weight Polyethylene. *Membranes*, *12*, 1137.
[45] **Li, N., Xiao, C., Wang, R., and Zhang, S.** (2012). The effect of binary diluents on the performance of ultrahigh molecular weight polyethylene/SiO2 hybrid hollow fiber membrane. *J. Appl. Polym. Sci.*, *124*, E169–E176.
[46] **Pluyter, P.B., Smith, P., Unen, L.H.T. van, and Rutten, H.J.J.** (1993). U.S. Patent No. 5248461A, 1993.
[47] **Sbriglia, G.A.** (2018). U.S. Patent No. S9926416B2.
[48] **Simmons, D.K. and Yaritz, J.G.** (2020). U.S. Patent No. 10615388B2.
[49] **Wu, B., Cai, Y., Zhao, X., and Ye, L.** (2021). Fabrication of well-miscible and highly enhanced polyethylene/ultrahigh molecular weight polyethylene

blends by facile construction of interfacial intermolecular entanglement. *Polym. Test.*, *93*, 106973.

[50] **Cao, X., Li, Y., and He, G.** (2020). Fabrication of Self-Lubricating Porous UHMWPE with Excellent Mechanical Properties and Friction Performance via Rotary Sintering. *Polymers*, *12*, 1335.

[51] **Fang, W., Liang, G., Li, J., and Guo, S.** (2022). Microporous Formation Mechanism of Biaxial Stretching PA6/PP Membranes with High Porosity and Uniform Pore Size Distribution. *Polymers*, *14*, 2291.

[52] **Backer, J.A.D., Kranz, B.C., and Slager, B.** (2011). U.S. Patent No. 20110028671A1.

[53] **Harding, K.C., Weedon, G.C., and Owen, L.** (2011). U.S. Patent No. 7964266B2.

[54] **Uehara, H., Tamura, T., Hashidume, K., Tanaka, H., and Yamanobe, T.** (2014). Non-solvent processing for robust but thin membranes of ultra-high molecular weight polyethylene. *J Mater Chem A*, *2*, 5252–5257.

[55] **Arzhakova, O.V., Nazarov, A.I., Solovei, A.R., Dolgova, A.A., Kopnov, A.Y., Chaplygin, D.K., ..., Yarysheva, A.Y.** (2021)**.** Mesoporous Membrane Materials Based on Ultra-High-Molecular-Weight Polyethylene: From Synthesis to Applied Aspects. *Membranes*, *11*, 834.

[56] **Jeon, M.Y. and Kim, C.K.** (2007). Phase behavior of polymer/diluent/diluent mixtures and their application to control microporous membrane structure. *J. Membr. Sci.*, *300*, 172–181.

[57] **Zhao, C., He, J., Li, J., Tong, J., and Xiong, J.** (2018). Preparation and properties of UHMWPE microporous membrane for lithium ion battery diaphragm. *IOP Conf. Ser. Mater. Sci. Eng.*, *324*, 012089.

[58] **Sheng, L., Zhang, Y., Xie, X., Yang, L., Bai, Y., Liu, G.,....., He, J.** (2022). Morphology of porous UHMWPE originating from the S–L phase separation in UHMWPE/liquid paraffin (LP) blends. *Iran. Polym. J.*, *31*, 1047–1056.

[59] **Babiker, D.M.D., Wan, C., Mansoor, B., Usha, Z.R., Yu, R., Habumugisha, J.C., ..., Li, L.** (2021). Superior lithium battery separator with extraordinary electrochemical performance and thermal stability based on hybrid UHMWPE/SiO2 nanocomposites via the scalable biaxial stretching process. *Compos. Part B Eng.*, *211*, 108658.

[60] **Ding, L., Li, D., Du, F., Zhang, D., Zhang, S., and Wu, T.** (2022). Novel preparation of lithium-ion battery wet-processed separator based on the synergistic effect of porous skeleton nano-Al2O3 in situ blending and synchro-draw. *Polym. Int.*, *n/a*,.

[61] **Habumugisha, J.C., Usha, Z.R., Rui Yu, M.D.Babiker, D., Wan, C., Chen, X., ..., Li, L.** (2021). Thermally stable and high electrochemical performance ultra-high molecular weight polyethylene/poly(4-methyl-1-pentene) blend film used as Li-ion battery separator. *Applied Materials Today*, *24*, 101136.

[62] **Magar, H.S., Hassan, R.Y.A., and Mulchandani, A.** (2021). Electrochemical Impedance Spectroscopy (EIS): Principles, Construction, and Biosensing Applications. *Sensors*, *21*, 6578.

[63] **Hashimoto, Y., Nishitsuji, S., Kurose, T., and Ito, H.** (2018). Structural Formation of UHMWPE Film Tracked by Real-Time Retardation Measurements during Uniaxial/Biaxial Stretching. *Materials*, *11*, 2292.

[64] **Ihm, D., Noh, J., and Kim, J.** (2002). Effect of polymer blending and drawing conditions on properties of polyethylene separator prepared for Li-ion secondary battery. *J. Power Sources*, *109*, 388–393.

[65] **Wang, X.N., Mu, Y., Zhao, G.Q., Gao, J.C., Zhou, Y.L., and Cheng, Z.H.** (2020). The Effect of Stretching on UHWMPE Microporous Film by Thermally Induced Phase Separation Method. *Mater. Sci. Forum*, *993*, 906–914.

[66] **Chen, L., Deng, B., Li, X., and Wang, Z.** (2022). Structural evolution of UHMWPE gel fibers as high degree plasticized system during stretching: An in-situ wide and small angle X-ray scattering study. *Polymer*, *255*, 125149.

[67] **Zhang, C., Lv, W., Zhou, G., Huang, Z., Zhang, Y., Lyu, R., ...,Yang, Q**. (2018). Vertically Aligned Lithiophilic CuO Nanosheets on a Cu Collector to Stabilize Lithium Deposition for Lithium Metal Batteries. *Adv. Energy Mater.*, *8*, 1703404.

[68] **Sheng, L., Xu, R., Zhang, H., Bai, Y., Song, S., Liu, G., ..., He, J.** (2020). The morphology of polyethylene (PE) separator for lithium-ion battery tuned by the extracting process. *J. Electroanal. Chem.*, *873*, 114391.

[69] **Nasrollahzadeh, M., Sajadi, S.M., Sajjadi, M., and Issaabadi, Z.** (2019). Applications of Nanotechnology in Daily Life. in: Interface Sci. Technol., Elsevier, pp. 113–143.

[70] **Lian, H. and Meng, Z.** (2017). Melt electrospinning vs. solution electrospinning: A comparative study of drug-loaded poly (ε-caprolactone) fibres. *Mater. Sci. Eng. C*, *74*, 117–123.

[71] **Lu, X., Wang, C., and Wei, Y.** (2009). One-Dimensional Composite Nanomaterials: Synthesis by Electrospinning and Their Applications. *Small*, *5*, 2349–2370.

[72] **Wang, H., Lu, Y.** (2012). Morphological control of self-assembly polyaniline micronano-structures using dichloroacetic acid. *Synthetic Metals*, *162*, 1369-1374.

[73] **Donmez, I., Kayaci, F., Ozgit-Akgun, C., Uyar, T., Biyikli, T.** (2013). Fabrication of hafnia hollow nanofibers by atomic. *Journal of Alloys and Compounds*, 559, 146-151,

[74] **Xia, X., Dong, X.J., Wei, Q.F., Cai, Y.B., and Lu, K.Y.** (2012). Formation mechanism of porous hollow SnO2 nanofibers prepared by one-step electrospinning. *Express Polym. Lett.*, *6*, 169–176.

[75] **Silva, V.D., Ferreira, L.S., Simões, T.A., Medeiros, E.S., and Macedo, D.A.** (2019). 1D hollow MFe2O4 (M = Cu, Co, Ni) fibers by Solution Blow Spinning for oxygen evolution reaction. *J. Colloid Interface Sci.*, *540*, 59–65.

[76] **Islam, M.S., Ang, B.C., Andriyana, A., and Afifi, A.M.** (2019). A review on fabrication of nanofibers via electrospinning and their applications. *SN Appl. Sci.*, *1*, 1248.

[77] **Asmatulu, R.** (2016). Highly Hydrophilic Electrospun Polyacrylonitrile/ Polyvinypyrrolidone Nanofibers Incorporated with Gentamicin as Filter Medium for Dam Water and Wastewater Treatment. *J. Membr. Sep. Technol.*, *5*, 38–56.

[78] **Gahan, R. and Zguris, G.C.** (2000). A review of the melt blown process. in: Fifteenth Annu. Battery Conf. Appl. Adv. Cat No00TH8490, pp. 145–149.

[79] **Zuo, F., Tan, D.H., Wang, Z., Jeung, S., Macosko, C.W., and Bates, F.S.** (2013). Nanofibers from Melt Blown Fiber-in-Fiber Polymer Blends. *ACS Macro Lett.*, *2*, 301–305.

[80] **Gupta, B.S. and Edwards, J.V.** (2019). 3 - Textile materials and structures for topical management of wounds. in: S. Rajendran (Ed.), Adv. Text. Wound Care Second Ed., Woodhead Publishing, pp. 55–104.

[81] **Polat, Y., Pampal, E.S., Stojanovska, E., Simsek, R., Hassanin, A., Kilic, A., ..., Yilmaz. S.** (2016). Solution blowing of thermoplastic polyurethane nanofibers: A facile method to produce flexible porous materials. *J. Appl. Polym. Sci.*, *133*, 43025.

[82] **Zhang, Z. and Sun, J.** (2017). Research on the development of the centrifugal spinning. *the 3rd International Conference on Mechatronics and Mechanical Engineering MATEC* Web Conference, October 21-23.

[83] **Yanilmaz, M. and Zhang, X.** (2015). Polymethylmethacrylate/polyacrylonitrile membranes via centrifugal spinning as separator in Li-ion batteries. *Polymers*, *7*, 629–643.

[84] **Alghoraibi, I. and Alomari, S.** (2018). Different Methods for Nanofiber Design and Fabrication. in: A. Barhoum, M. Bechelany, A. Makhlouf (Eds.), Handb. Nanofibers, Springer International Publishing, Champp. 1–46.

[85] **Beachley, V. and Wen, X.** (2010). Polymer nanofibrous structures: Fabrication, biofunctionalization, and cell interactions. *Prog. Polym. Sci.*, *35*, 868–892.

[86] **Salas, C.** (2017). Solution electrospinning of nanofibers. Electrospun Nanofibers, Woodhead Publishing, pp. 73–108.

[87] **Zhang, Z. and Sun, J.** (2017). Research on the development of the centrifugal spinning. *MATEC Web Conf.*, *95*, 07003.

[88] **Zou, W., Chen, R.Y., Zhang, G.Z., Zhang, H.C., and Qu, J.P.** (2014). Recent Advances in Centrifugal Spinning Preparation of Nanofibers. *Adv. Mater. Res.*, *1015*, 170–176.

[89] **Badrossamay, M.R., Balachandran, K., Capulli, A.K., Golecki, H.M., Agarwal, A., Goss, J.A., ..., Parker, K.** (2014). Engineering hybrid polymer-protein super-aligned nanofibers via rotary jet spinning. *Biomaterials*, *35*, 3188–3197.

[90] **Tepekiran, B.N., Calisir, M.D., Polat, Y., Akgul, Y., and Kilic, A.** (2019). Centrifugally spun silica (SiO2) nanofibers for high-temperature air filtration. *Aerosol Sci. Technol.*, *53*, 921–932.

[91] **Gholipour-Kanani, A. and Daneshi, P.** (2022). A Review on Centrifugal and Electro-Centrifugal Spinning as New Methods of Nanofibers Fabrication. *10*, 41–55.

[92] **Thavasi, V., Singh, G., and Ramakrishna, S.** (2008). Electrospun nanofibers in energy and environmental applications. *Energy Environ. Sci.*, *1*, 205–221.

[93] **Zhang, Y., Yang, J., Li, Q., and Cao, X.** (2007). Preparation of Ga2O3 nanoribbons and tubes by electrospinning. *J. Cryst. Growth*, *308*, 180–184.

[94] **Ramaseshan, R., Sundarrajan, S., Liu, Y., Barhate, R.S., Lala, N.L., and Ramakrishna, S.** (2006). Functionalized polymer nanofibre membranes for protection from chemical warfare stimulants. *Nanotechnology*, *17*, 2947.

[95] **Thavasi, V., Singh, G., and Ramakrishna, S.** (2008). Electrospun nanofibers in energy and environmental applications. 205–221.

[96] **Kaur, S., Ma, Z., Gopal, R., Singh, G., Ramakrishna, S., and Matsuura, T.** (2007). Plasma-Induced Graft Copolymerization of Poly(methacrylic acid) on Electrospun Poly(vinylidene fluoride) Nanofiber Membrane. *Langmuir*, *23*, 13085–13092.

[97] **Selling, G.W. and Woods, K.K**. (2008). Improved Isolation of Zein from Corn Gluten Meal Using Acetic Acid and Isolate Characterization as Solvent. *Cereal Chem.*, *85*, 202–206.

[98] **Gouma, P.I.** (2003). Nanostructured polymorphic oxides for advanced chemosensors. *Rev. Adv. Mater. Sci.*, *5*, 147–154.

[99] **Zupančič, Š., Preem, L., Kristl, J., Putrinš, M., Tenson, T., Kocbek, P., ..., Kogermann K. (**2018). Impact of PCL nanofiber mat structural properties on hydrophilic drug release and antibacterial activity on periodontal pathogens. *Eur. J. Pharm. Sci.*, *122*, 347–358.

[100] **Kim, C., Yang, K.S., Kojima, M., Yoshida, K., Kim, Y.J., Kim, Y.A., and Endo, M..** (2006). Fabrication of Electrospinning-Derived Carbon Nanofiber Webs for the Anode Material of Lithium-Ion Secondary Batteries. *Adv. Funct. Mater.*, *16*, 2393–2397.

[101] **Wang, P., Zhang, D., Ma, F., Ou, Y., Chen, Q.N., Xie, S., ..., Li, J.** (2012). Mesoporous carbon nanofibers with a high surface area electrospun from thermoplastic polyvinylpyrrolidone. *Nanoscale*, *4*, 7199.

[102] **Yanilmaz, M., Lu, Y., Dirican, M., Fu, K., and Zhang, X.** (2014). Nanoparticle-on-nanofiber hybrid membrane separators for lithium-ion batteries via combining electrospraying and electrospinning techniques. *J. Membr. Sci.*, *456*, 57–65.

[103] **Jung, J.-W., Lee, C.-L., Yu, S., and Kim, I.-D.** (2016). Electrospun nanofibers as a platform for advanced secondary batteries: a comprehensive review. *J. Mater. Chem. A*, *4*, 703–750.

[104] **Li, B., Liu, Y., Wei, S., Huang, Y., Yang, S., Xue, Y., ..., Yuan, H.** (2020). A Solvent System Involved Fabricating Electrospun Polyurethane Nanofibers for Biomedical Applications. *Polymers*, *12*, 3038.

[105] **Hattig, J. and Drube, W.** (2003). Wide area of applications: Upward trend for thermoplastic polyurethanes. *Kunststoffe-Plast Eur.*, *93*, 28.

[106] **Choi, J., Moon, D.S., Jang, J.U., Yin, W.B., Lee, B., and Lee, K.J.** (2017). Synthesis of highly functionalized thermoplastic polyurethanes and their potential applications. *Polymer*, *116*, 287–294.

[107] **Kharbas, H.A., Ellingham, T., Manitiu, M., Scholz, G., and Turng, L.-S.** (2017). Effect of a cross-linking agent on the foamability of microcellular injection molded thermoplastic polyurethane. *J. Cell. Plast.*, *53*, 407–423.

[108] **Mistry, P., Chhabra, R., Muke, S., Narvekar, A., Sathaye, S., Jain, R., ..., Hassanin, A.** (2021). Fabrication and characterization of starch-TPU based nanofibers for wound healing applications. *Mater. Sci. Eng. C*, *119*, 111316.

[109] **Shehata, N., Nair, R., Boualayan, R., Kandas, I., Masrani, A., Elnabawy, E., ..., Hassanin, A**. (2022). Stretchable nanofibers of polyvinylidenefluoride (PVDF)/thermoplastic polyurethane (TPU) nanocomposite to support piezoelectric response via mechanical elasticity. *Sci. Rep.*, *12*, 8335.

[110] **Tang, L., Wu, Y., He, D., Lei, Z., Liu, N., He, Y., ..., Chen, J.** (2023). Electrospun PAN membranes toughened and strengthened by TPU/SHNT for high-performance lithium-ion batteries. *J. Electroanal. Chem.*, *931*, 117181.

[111] **Han, L., Liao, C., Liu, Y., Yu, H., Zhang, S., Zhu, Y., ..., Hu, Y.** (2022). Non-flammable sandwich-structured TPU gel polymer electrolyte without flame retardant addition for high performance lithium ion batteries. *Energy Storage Mater.*, *52*, 562–572.

[112] **Liu, K., Liu, M., Cheng, J., Dong, S., Wang, C., Wang, Q., ..., Cui, G.** (2016). Novel cellulose/polyurethane composite gel polymer electrolyte for high performance lithium batteries. *Electrochimica Acta*, *215*, 261–266.

[113] **Wang, X., Lu, Y., Geng, D., Li, L., Zhou, D., Ye, H., ..., Wang, R**. (2020). Planar Fully Stretchable Lithium-Ion Batteries Based on a Lamellar Conductive Elastomer. *ACS Appl. Mater. Interfaces*, *12*, 53774–53780.

[114] **Shi, C., Zhang, L., Wang, X., Sun, T., Jiang, Z., and Zhao, J.** (2022). Ion Flux Self-Regulation Strategy with a Volume-Responsive Separator for Lithium Metal Batteries. *ACS Appl. Mater. Interfaces*, *14*, 51931–51940.

[115] **Yu, S., Ling, Y., Sun, S., Wang, Y., Yu, Z., Zheng, J., ..., Zhou, H. (2022**). Flexible self-charging lithium battery for storing low-frequency mechanical energy. *Nano Energy*, *94*, 106911.

[116] **Douglas, T. and Haugen, H.J.** (2008). Coating of polyurethane scaffolds with collagen: comparison of coating and cross-linking techniques. *J. Mater. Sci. Mater. Med.*, *19*, 2713–2719.

[117] **Gheorghita Puscaselu, R., Lobiuc, A., Dimian, M., and Covasa, M.** (2020). Alginate: From Food Industry to Biomedical Applications and Management of Metabolic Disorders. *Polymers*, *12*, 2417.

[118] **Lee, K.Y. and Mooney, D.J.** (2012). Alginate: properties and biomedical applications. *Prog. Polym. Sci.*, *37*, 106–126.

[119] **Jadach, B., Świetlik, W., and Froelich, A.** (2022). Sodium Alginate as a Pharmaceutical Excipient: Novel Applications of a Well-known Polymer. *J. Pharm. Sci.*, *111*, 1250–1261.

[120] **Url-120** <https://www.dharmatrading.com/information/sodium-alginate.html>, access date 30.09.2022.

[121] **Kong, Q., Wang, B., Ji, Q., Xia, Y., Guo, Z., and Yu, J.** (2009). Thermal degradation and flame retardancy of calcium alginate fibers. *Chin. J. Polym. Sci.*, *27*, 807–812.

[122] **Xu, Y.-J., Qu, L.-Y., Liu, Y., and Zhu, P.** (2021). An overview of alginates as flame-retardant materials: Pyrolysis behaviors, flame retardancy, and applications. *Carbohydr. Polym.*, *260*, 117827.

[123] **Wray, L.S. and Orwin, E.J.** (2009). Recreating the microenvironment of the native cornea for tissue engineering applications. *Tissue Eng. Part A*, *15*, 1463–1472.

[124] **Zhmayev, Y., Divvela, M.J., Ruo, A.-C., Huang, T., and Joo, Y.L.** (2015). The jetting behavior of viscoelastic Boger fluids during centrifugal spinning. *Phys. Fluids*, *27*, 123101.

[125] **Wang, Z., Sahadevan, R., Crandall, C., Menkhaus, T.J., and Fong, H.** (2020). Hot-pressed PAN/PVDF hybrid electrospun nanofiber membranes for ultrafiltration. *J. Membr. Sci.*, *611*, 118327.

[126] **Dong, G., Liu, B., Kong, L., Wang, Y., Tian, G., Qi, S., ..., Wu, D.** (2019). Neoteric Polyimide Nanofiber Encapsulated by the TiO2 Armor As the Tough, Highly Wettable, and Flame-Retardant Separator for Advanced Lithium-Ion Batteries. *ACS Sustain. Chem. Eng.*, *7*, 17643–17652.

[127] **Xu, R., Guo, F., Cui, X., Zhang, L., Wang, K., and Wei, J.** (2015). High performance carbon nanotube based fiber-shaped supercapacitors using redox additives of polypyrrole and hydroquinone. *J Mater Chem A*, *3*,.

CURRICULUM VITAE

Name Surname : Ubey Ahmetoglu

EDUCATION :

- **B.Sc. :** 2019, Yildiz Technical University, Faculty of Chemistry and Metallurgy, Department of Chemical Engineering

PROFESSIONAL EXPERIENCE AND REWARDS:

- 2021-2023 R&D Engineer at Areka Group ltd.

PUBLICATIONS, PRESENTATIONS AND PATENTS ON THE THESIS:

- **Ahmetoglu U., Gungor M., Kilic, A.** 2022. Production of TPU Nanofibrous Membrane via Centrifugal Spinning Method for Li-Ion Battery Application. Proceedings of International Fiber and Polymer Research Symposium. November 4-5, 2022 Gebze, Turkey pp. 281-285

OTHER PUBLICATIONS, PRESENTATIONS AND PATENTS:

- **Ahmetoglu U., Toptas A., Sohag, M., Kilic, A.** 2021: Improvement of Filtration Properties of PVDF Nanofibers Produced by Electro-assisted Solution Blowing. Proceedings of International Fiber and Polymer Research Symposium. November 19-20, 2021 Usak, Turkey pp. 112